2016-06-01

Investigation of Structural Capacity of Geogrid-Reinforced Aggregate Base Materials in Flexible Pavements

Eric J. Sweat
Brigham Young University

Investigation of Structural Capacity of Geogrid-Reinforced Aggregate Base Materials in Flexible Pavements

Eric J Sweat

A thesis submitted to the faculty of
Brigham Young University
in partial fulfillment of the requirements for the degree of

Master of Science

W. Spencer Guthrie, Chair
Grant G. Schultz
Kevin W. Franke

Department of Civil and Environmental Engineering

Brigham Young University

June 2016

ABSTRACT

Investigation of Structural Capacity of Geogrid-Reinforced Aggregate Base Materials in Flexible Pavements

Eric J Sweat
Department of Civil and Environmental Engineering, BYU
Master of Science

The installation of geogrid as a means of extending the service life of a roadway or reducing the required base course thickness of a pavement structure has become increasingly popular. The realization of these benefits depends largely on the degree to which the geogrid reinforcement leads to an increase in the stiffness of the aggregate base course layer. The objective of this research was to investigate the structural capacity of geogrid-reinforced aggregate base materials in flexible pavements through full-scale testing. The scope involved field testing at two sites in northern Utah that each included five different geogrid-reinforced sections and five accompanying unreinforced control sections.

Five different geogrid types were utilized to ensure that the experimentation was representative of the geogrid products available in the industry at the time of the study. At each of the two field sites, 10 test sections were established, and several field tests were conducted during and following construction of the two pavements to characterize the in-situ structural properties of the subgrade, base, and hot mix asphalt layers of each geogrid-reinforced and unreinforced test section. The procedures involved nuclear density gauge, soil stiffness gauge, Clegg impact soil tester, dynamic cone penetrometer (DCP), portable falling-weight deflectometer, and falling-weight deflectometer testing of each test section. Samples of the subgrade and base materials were also obtained from both field sites for laboratory testing, which included dry and washed sieve analyses, Atterberg limits testing, and material classification. An analysis of covariance (ANOCOVA) was conducted on the results of each field test to determine if the structural capacity of the geogrid-reinforced sections was different than that of the accompanying unreinforced control sections.

Among the 24 ANOCOVA models developed for the two field sites, only four indicated that geogrid presence was statistically significant. Of these four models, three indicated that the presence of geogrid reinforcement led to higher values of the given measurement of structural capacity compared to the unreinforced condition; however, in none of the cases was the difference practically important as defined in this research and would therefore not result in a different input in the pavement design process. Notably, in all three of these models, the same testing procedure, namely the DCP, was used for the testing.

A measurable increase in the structural capacity of the reinforced layer may not be immediately observable using standard pavement testing procedures. Further field research is recommended to investigate the duration of the required conditioning period and also the extent of the zone of influence of geogrid reinforcement in aggregate base courses.

Key words: aggregate, conditioning period, geogrid, structural capacity, zone of influence

ACKNOWLEDGEMENTS

This research was funded by the Utah Department of Transportation. Orem City and Granite Construction facilitated testing at the Orem site, and The Church of Jesus Christ of Latter-day Saints and Geneva Rock Products facilitated testing at the Springville site. I acknowledge the assistance of Brigham Young University students Jaren Knighton, Aaron Smith, Scoot Flannery, Callie Vogel, Katri Clay, Elizabeth Smith, Danielle Nixon, Tenli Waters, Hannah Polanco, Joseph Eixenberger, Brian Peterson, and Zachary Steele with the field and laboratory testing and data analysis required for this research. I also acknowledge Tensar International Corporation, Hanes Geo Components, and Alliance Geosynthetics for their donations of geogrid products for this research. I appreciate Dr. Grant G. Schultz and Dr. Kevin W. Franke for participating on my graduate advisory committee. I am especially grateful to Dr. W. Spencer Guthrie for his mentorship, example, and friendship; I have become a better student and person while working with him. Most importantly, I thank my wife, Rebekah, for her support and encouragement throughout my education; my success and accomplishments are because of her.

TABLE OF CONTENTS

LIST OF TABLES

LIST OF FIGURES

1 INTRODUCTION

1.1 Problem Statement

As road construction and rehabilitation costs continue to rise, the use of geosynthetic reinforcing materials in pavement structures has received increasing attention in the transportation industry. In particular, the installation of geogrid as a means of extending the service life of a roadway or reducing the required base course thickness of a pavement structure has become increasingly popular (Chen and Abu-Farsakh 2012, Collin et al. 1996, Huntington and Ksaibati 2000, Joshi 2010, Kwon and Tutumluer 2009). The realization of these benefits depends largely on the degree to which the geogrid reinforcement leads to an increase in the stiffness of the aggregate base course layer (Al-Qadi et al. 2008, Erickson and Drescher 2001, Henry et al. 2011, Kwon et al. 2008).

Increases in the stiffness of the aggregate base material are possible when the geogrid facilitates increased aggregate interlock, which is manifest as greater inter-particle friction and reduced lateral and rotational movement of the base course aggregate particles (Al-Qadi et al. 2008, Aran 2006, Kwon and Tutumluer 2009, Maubeuge and Klompmaker 2011, Moayedi et al. 2009). Because a stiffer base layer offers greater support to the overlying surface layer and greater protection of the underlying subgrade, pavement performance under traffic loading may therefore be improved (Henry et al. 2009, Moghaddas-Nejad and Small 1996).

Predicting the degree of improvement in pavement performance during the design process requires a means of evaluating the potential effect of geogrid reinforcement on the stiffness of the aggregate base material. Although several laboratory and field studies have documented the performance of specific geogrid products with specific aggregate base materials under specific conditions (Al-Qadi et al. 2008, Aran 2006, Hall et al. 2004, Hufenus et al. 2006, Knighton 2015, Kwon and Tutumluer 2009, Reck 2009), the Federal Highway Administration (FHWA) has stated that developing a generic specification for geogrid reinforcement for use in pavements has been difficult because of "the proprietary nature (i.e., current product patents) of biaxial geogrids and geocomposites; a lack of a thorough understanding of the mechanistic benefits of geosynthetic reinforcement; lack of performance documentation; and inability to measure contribution of geosynthetic reinforcement to pavement structure with non-destructive testing methods" (FHWA 2008, p. 5-80). Given the current availability of several geogrid products, including both biaxial and triaxial geogrids, in the industry and their potential value in pavement construction, the Utah Department of Transportation (UDOT) needed new research to quantify the effectiveness of geogrid reinforcement of locally sourced aggregate base materials in pavement structures in Utah. UDOT specifically requested full-scale field testing with both reinforced and unreinforced, or control, sections to supplement previous studies performed in other locations.

1.2 Research Objective and Scope

The objective of this research, as commissioned by UDOT, was to investigate the structural capacity of geogrid-reinforced aggregate base materials in flexible pavements through full-scale testing. The scope of this research involved field testing at two sites that each included five different geogrid-reinforced sections and five accompanying unreinforced control sections.

One site was located in Orem, Utah, and the other was located in Springville, Utah, as shown in Figure 1-1. Both sites experience wintertime freeze-thaw cycling typical of northern Utah.

Field testing was performed at both sites to measure the structural capacity of each test section. Field instruments used for this purpose included the nuclear density gauge (NDG), soil stiffness gauge (SSG), heavy Clegg impact soil tester (CIST), dynamic cone penetrometer (DCP), portable falling-weight deflectometer (PFWD), and truck-mounted falling-weight deflectometer (FWD). Subsurface temperatures and moisture contents were also measured using in-situ sensors installed at the time of construction at the Orem field site. The Orem and Springville field sites were monitored for 15 and 7 months, respectively, including one winter season.

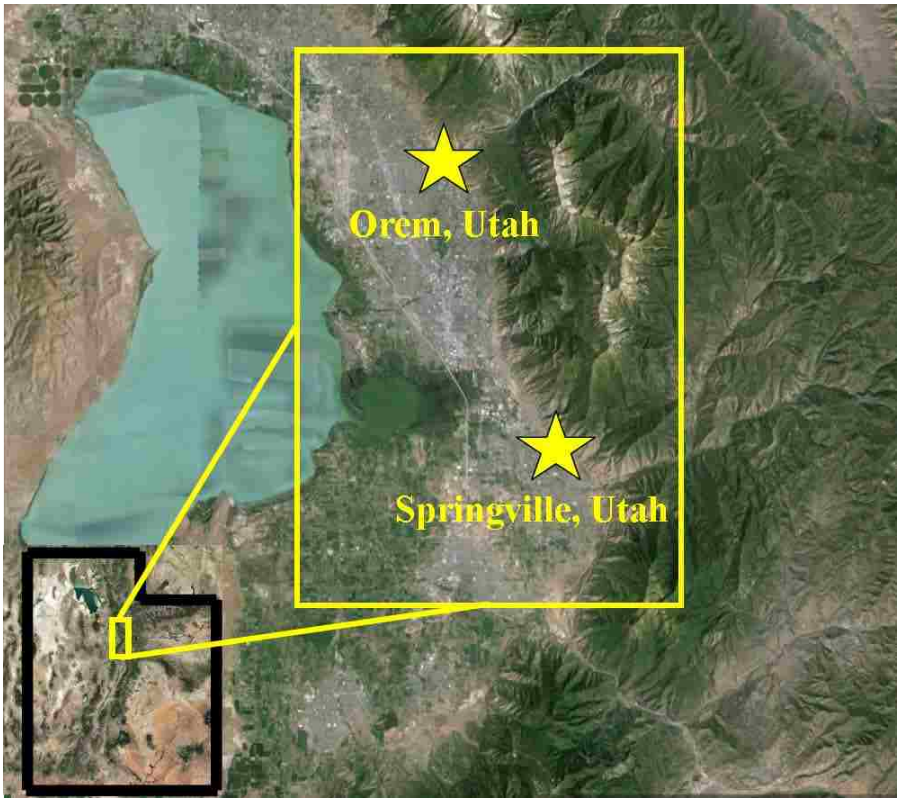

Figure 1-1: Field site locations.

1.3 Outline of Report

This report contains five chapters. This chapter introduces the research, defines the problem statement, and states the research objectives and scope. Chapter 2 provides background information obtained from a literature review about the use of geogrid-reinforced aggregate base materials in flexible pavements. Chapters 3 and 4 detail the procedures and results of this research, respectively. Chapter 5 provides a summary together with conclusions and recommendations resulting from this research.

2 BACKGROUND

2.1 Overview

This chapter provides background information obtained from a literature review about the use of geogrid-reinforced aggregate base materials in flexible pavements. A brief description of geogrids and a discussion of their use are presented in the following sections.

2.2 Geogrid Description

Geogrid is a high-strength extruded geosynthetic material consisting of connected sets of tensile ribs with apertures that can be penetrated by surrounding aggregate particles (Aran 2006, Reck 2009). Characteristics of geogrid differ due to varying geometric, mechanical, and durability properties (Hanes Geo Components 2015, Tensar International Corporation 2015). Geometric properties include aperture shapes and sizes along with rib spacing, depth, width, length, and shape. Biaxial geogrids, which have rectangular aperture shapes, provide tensile strength in two directions, while triaxial geogrids, which have triangular aperture shapes, provide tensile strength in three directions. The aperture size directly determines the degree to which aggregate particles can penetrate the geogrid. A general recommendation is that the minimum aperture size of the geogrid should be at least equal to the particle size corresponding to 50 percent passing (D_{50}) of the aggregate being placed on the geogrid, but not less than 0.5 in., and the maximum aperture size should be less than twice the particle diameter corresponding to 85

percent passing (D_{85}), but not greater than 3 in. (FHWA 2008). Mechanical properties include tensile strength, radial stiffness, aperture stability, and flexural rigidity of the geogrid. Durability is a measure of the resistance of geogrid to ultraviolet degradation, installation damage, and chemical damage (Hanes Geo Components 2015, Tensar International Corporation 2015).

2.3 Geogrid Use in Pavement Structures

Many field and laboratory studies regarding geogrid reinforcement and pavement performance have been conducted to investigate the benefits of geogrid-reinforced aggregate base materials in flexible pavements (Al-Qadi et al. 2008, Haas et al. 1988, Huntington and Ksaibati 2000, Kwon and Tutumluer 2009, Tingle and Jersey 2009). Although the general consensus is that geogrid can be beneficial, quantifying the effect of including geogrid reinforcement in pavement structures has proven to be difficult (Aran 2006, Hall et al. 2004). Because laboratory evaluations of geogrid reinforcement do not usually account for environmental, trafficking, and subgrade capacity variations associated with actual pavement structures in the field, full-scale field studies of geogrid-reinforced pavement structures are often preferred for evaluating potential benefits of geogrid (Al-Qadi et al. 2008, Barksdale et al. 1989, Brandon et. al 1996, Helstrom et al. 2006, Joshi and Zomberg 2011). Furthermore, the use of control, or unreinforced, sections is critical in such investigations (Holder and Andrae 2004).

As discussed in the following sections, previous studies have incorporated full-scale experimentation and testing to evaluate performance, stiffness, and strength improvements in geogrid-reinforced aggregate base materials. Specifically, the possible requirement for a conditioning period has been explored, a zone of influence resulting from the reinforcement has been identified, and the effects of different geogrid positions within the pavement structure have been investigated.

2.3.1 Conditioning Period

Research suggests that a sufficient conditioning period may be required before the full effects of geogrid reinforcement on pavement performance can be observed (Kwon and Tutumluer 2009). A sufficient conditioning period has been defined as the time required for the geogrid and surrounding aggregate to fully interlock (Tingle and Jersey 2009). For a given geogrid and aggregate, the length of the conditioning period is presumed to vary depending on the amount of trafficking, where higher traffic loads and/or volumes are expected to aid in the densification of the aggregates and their interlock with the geogrid (Hall et al. 2004, Helstrom et al. 2006).

In full-scale pavement testing conducted in Mississippi (Tingle and Jersey 2009), researchers showed that an adequate trafficking and densification period was required before optimal geogrid performance was achieved. As summarized in Table 2-1, eight 12-ft by 24-ft full-scale pavement sections were constructed for testing. Each pavement section was constructed on native silty clay subgrade material that was surfaced with a 24-in. layer of high-plasticity clay and an unsurfaced 6-in. base layer comprised of crushed aggregate, crushed limestone, or clay gravel. The high-plasticity clay layer was specified to ensure consistency in

Table 2-1: Experimental Design for Mississippi Study

Test Section	Base Material	Base Thickness (in.)	Geogrid Reinforcement Present	Geotextile Present
1	Crushed Aggregate	6	No	No
2	Clay Gravel	6	No	No
3	Crushed Limestone	6	No	No
4	Crushed Limestone	6	No	Yes
5	Crushed Limestone	6	Yes	Yes
6	Crushed Limestone	6	Yes	No
7	Clay Gravel	6	Yes	No
8	Crushed Aggregate	6	Yes	No

the underlying base layer support across all eight pavement sections. Each test section was trafficked with a dual-wheel tandem-axle truck loaded to 21.8 tons, and FWD deflection data were measured after different numbers of total truck passes, specifically 0, 1,000, 5,500, and 10,000, to quantify the structural capacity for each section. The highest backcalculated modulus values of the base layer were observed at 5,500 passes of the truck, and the increase in stiffness was attributed to the development of progressively greater aggregate interlock with the geogrid. In this study, the modulus values of the geogrid-reinforced base layers were generally lower than those of the unreinforced base layers in two of the comparisons for which FWD data were presented in this study; however, three of the four geogrid-reinforced sections did not exhibit rutting failure, which was defined as more than 3 in. of permanent deformation after 10,000 truck passes, while only two of the unreinforced sections, including one with a geotextile, did not fail. Overall, despite having lower average base layer stiffness, the geogrid-reinforced test sections demonstrated an improved resistance to rutting in comparison to the unreinforced sections.

Research performed in Wyoming compared the performance of two pavement sections, an unreinforced section with a 17-in. conventional granular base layer and a geogrid-reinforced section with an 11-in. base layer (Huntington and Ksaibati 2000). Testing consisting of FWD measurements, rutting evaluations, and pavement condition surveys was performed shortly after construction of the roadway and again after three years of trafficking to evaluate the performance of the sections. The results of the FWD testing indicated that the stiffness of the geogrid-reinforced section was initially lower than that of the unreinforced section but increased during the three-year period to a level equal to or surpassing that of the unreinforced section by the end of the study. The rutting evaluations indicated that the unreinforced and geogrid-reinforced test sections were equivalent after three years of service. In the pavement condition surveys, no other

distresses were identified in either section of the pavement. The researchers concluded that a 6-in. reduction in base thickness, in this case from 17 in. to 11 in., was possible with the inclusion of geogrid (Huntington and Ksaibati 2000).

These field studies substantiate the idea that quantifying the benefit of geogrid reinforcement in a pavement section requires an adequate conditioning period, allowing the geogrid and surrounding aggregate to fully interlock. Although exact predictions of the length of the conditioning period are probably not possible, several months or even a few years may be required in some cases.

2.3.2 Zone of Influence

The spatial extent of increased stiffness in the immediate vicinity of geogrid reinforcement can be quantified in terms of a zone of influence. The zone of influence may or may not extend through the entire base course layer, depending on the degree of interlock between the geogrid and aggregate and the thickness of the base layer (Edil et al. 2007, Tutumluer et al. 2009). Therefore, when the degree of interlock is lower and/or the base layer is thicker, increases in stiffness can be more difficult to detect (Schuettpelz et al. 2009).

In a study performed in California (Kwon and Tutumluer 2009), researchers investigated aggregate interlock associated with geogrid-reinforced base layers in pavements along with the increase in stiffness in the vicinity of the geogrid. Geogrid was placed at the base-subgrade interface in pavements with varying cross sections and trafficked for five years. Two geogrid-reinforced sections included a base layer of 6 in. and 11 in. of hot mix asphalt (HMA), while two unreinforced sections consisted of either 18 in. or 19 in. of base and 9 in. of HMA. The study lacked a proper control section, such that the higher stiffness of the 6 in. of base material in the reinforced section compared to the upper 6 in. of base material in the unreinforced section could

not be clearly attributed to only the presence of geogrid; however, the results of the DCP testing indicated a uniform stiffness throughout the full depth of the reinforced 6-in. base layers. This result suggests that the zone of influence of the geogrid may have extended 6 in. above the geogrid in the reinforced sections.

In a study performed in Illinois (Kwon et al. 2008), nine full-scale pavement test sections were constructed with varying pavement sections, reinforcement positions, and base layer thicknesses, as shown in Table 2-2, to evaluate the effectiveness of geogrid reinforcement. The pavement sections were subjected to accelerated loading using a dual-tire assembly with an applied load of 9,000 lb, a tire inflation pressure of 100 psi, and a traverse speed of 5 mph. Numbers of passes ranging from 3,300 to 89,000 were applied to the test sections until failure, which was defined as 1 in. of rutting, or until a terminal number of passes was reached. Although the exact spatial extent was not quantified, the researchers cited a region of increased stiffness immediately above the geogrid reinforcement that was attributed to aggregate interlock with the geogrid; this conclusion was supported by rutting profiles observed through open trenches excavated after the testing was complete. The reinforced sections exhibited less rutting in the

Table 2-2: Experimental Design for Illinois Study

Section	HMA Thickness (in.)	Base Thickness (in.)	Geogrid or Control	Position of Reinforcement
A-1	3	8	Geogrid	Base-subgrade interface
A-2	3	8	Geogrid	Base-subgrade interface
A-3	3	8	Control	-
B-1	3	12	Control	-
B-2	3	12	Geogrid	Base-subgrade interface
C-1	5	12	Control	-
D-1	3	18	Geogrid	6 in. below HMA
D-2	3	18	Geogrid	6 in. below HMA and at base-subgrade interface
D-3	3	18	Control	-

base layers and/or sustained greater numbers of load repetitions to failure than the unreinforced sections (Kwon et al. 2008).

Laboratory testing performed in Montana addressed the presence of a zone of influence in geogrid-reinforced aggregate base material specimens (Perkins et al. 2004). In this testing, a circle of geogrid was positioned horizontally at the center of 12-in. by 24-in. specimens during the compaction process. Results from repeated load permanent deformation testing showed that the geogrid reinforcement restrained radial movement of the aggregate within a region that extended approximately one radius of the laboratory specimen being tested, or 6 in. in this case, above and below the reinforcement (Perkins et al. 2004).

The field and laboratory studies presented in this section demonstrate the occurrence of a zone of influence in the immediate vicinity of geogrid reinforcement. Although exact measurements of the extent of the zone of influence have not been commonly reported, values approaching 6 in. may be possible in some cases.

2.3.3 Optimal Geogrid Position

Several studies have been performed to identify the optimal position for geogrid reinforcement in a pavement structure. Researchers in Illinois (Al-Qadi et al. 2008) tested pavement sections, previously shown in Table 2-2, to evaluate the effects of geogrid reinforcement with respect to geogrid position in a pavement structure. Results from performance testing under accelerated trafficking, including rutting, cracking, and visual observation, indicated that the optimal geogrid reinforcement position in thin base layers is at the base-subgrade interface. Thin base layers for this research consisted of layers in the range of 8 in. to 18 in. thick. For thicker base layers, greater than 18 in., the researchers suggested installing geogrid at the base-subgrade interface and an additional geogrid in the upper one-third of the

layer. Pavement sections were constructed over a weak subgrade with a California bearing ratio (CBR) value of 4.

Laboratory testing performed in Canada (Haas et al. 1988) on full-scale pavement sections involved varying subgrade strengths (CBR values ranging from 1 to 8), thicknesses of reinforced and unreinforced granular base layers (4 in. to 12 in.), and HMA thicknesses (2 in. to 4 in.) in order to evaluate different geogrid positions in pavement structures. Single layers of geogrid reinforcement were placed in the upper, middle, or bottom portions of the base layers, and a single test section including two layers of geogrid reinforcement placed at the middle and bottom of the base layer was also evaluated. Based on stress, strain, and deflection data obtained in the testing, the conclusion of this work was that the optimum geogrid position was at the base-subgrade interface. However, for very thick base layers, the researchers stated that the use of two layers of geogrid reinforcement, one placed at the base-subgrade interface and the other at the middle of the base layer, may help delay permanent deformation within the pavement.

In one laboratory study in Louisiana (Chen and Abu-Farsakh 2012), geogrid reinforcement was placed at one of three positions, including the base-subgrade interface, the middle of the base layer, or the upper one-third position within the base layer, in full-scale pavement sections constructed in a 6.5-ft by 6.5-ft by 5.5-ft test box. The aggregate base layer was 12 in. thick and was surfaced with a 0.75-in.-thick HMA layer. A 9,000-lb load was applied through a single wheel with a tire pressure of 80 psi. The number of load cycles recorded for each pavement section was used in backcalculating effective base resilient modulus values using Mechanistic-Empirical Pavement Design Guide software with a failure criterion of 0.75 in. of rutting. The backcalculated effective base resilient modulus values were compared to base resilient modulus values obtained through DCP testing of the corresponding unreinforced

sections to quantify the effect of the geogrid reinforcement. The researchers showed that geogrid reinforcement placed at the upper one-third position within the base layer performed best in increasing the effective base resilient modulus values in this case, followed by geogrid reinforcement placed at the base-subgrade interface and, after that, geogrid reinforcement placed at the middle of the base layer (Chen and Abu-Farsakh 2012).

In a laboratory study in Montana (Perkins 1999), geogrid reinforcement was placed at either the base-subgrade interface or the lower one-third position of the base layer in pavement sections constructed in a 6.5-ft by 6.5-ft by 5.0-ft test box. The base layer varied from 8 in. to 15 in., and the HMA layer was 3 in. thick. In conjunction with stress and strain measurements obtained from instrumentation embedded in the pavement layers, the results of cyclic plate load testing indicated that geogrid reinforcement placed at the base-subgrade interface limits the amount of lateral spreading that occurs in both the bottom of the base layer and the top of the subgrade. In this study, pavement performance was defined by surface rutting, which was lower in the sections where reinforcement was placed in the lower one-third position than in the sections where reinforcement was placed at the base-subgrade interface, although both performed better than unreinforced sections (Perkins 1999).

These field and laboratory studies confirm that geogrid reinforcement position within a pavement section can affect the ability of the reinforcement to provide improved pavement performance. Several studies have been completed to investigate the effects of different geogrid positions, and the optimal position appears to vary based on many factors. However, the general consensus is that, for thin base layers, placing geogrid reinforcement at the base-subgrade interface is a good approach, while thick base layers may warrant placing a second layer of geogrid reinforcement at the middle or upper one-third position within the base layer.

2.4 Summary

This chapter provides background information obtained from a literature review about the use of geogrid-reinforced aggregate base materials in flexible pavements. A brief description of geogrids and a discussion of their use are presented. Many field and laboratory studies regarding geogrid reinforcement and pavement performance have been conducted to investigate the benefits of geogrid-reinforced aggregate base materials in flexible pavements. Previous studies have incorporated full-scale experimentation and testing to evaluate performance, stiffness, and strength improvements in geogrid-reinforced aggregate base materials. Specifically, the possible requirement for a conditioning period has been explored, a zone of influence resulting from the reinforcement has been identified, and the effects of different geogrid positions within the pavement structure have been investigated.

Field studies substantiate the idea that quantifying the benefit of geogrid reinforcement in a pavement section requires an adequate conditioning period, allowing the geogrid and surrounding aggregate to fully interlock. Although exact predictions of the length of the conditioning period are probably not possible, several months or even a few years may be required in some cases.

Field and laboratory studies demonstrate the occurrence of a zone of influence in the immediate vicinity of geogrid reinforcement. Although exact measurements of the extent of the zone of influence have not been commonly reported, values approaching 6 in. may be possible in some cases.

Both field and laboratory studies confirm that geogrid reinforcement position within a pavement section can affect the ability of the reinforcement to provide improved pavement performance. The optimal position appears to vary based on many factors. However, the general

consensus is that, for thin base layers, placing geogrid reinforcement at the base-subgrade interface is a good approach, while thick base layers may warrant placing a second layer of geogrid reinforcement at the middle or upper one-third position within the base layer.

3 PROCEDURES

3.1 Overview

In this research, various field tests, including several non-destructive tests, were used to evaluate the structural capacity of unreinforced and geogrid-reinforced aggregate base layers in flexible pavements. Field testing at two full-scale pavement sites in northern Utah was the main focus of this work. The following sections describe the geogrid selection, site characterization and pavement construction, field and laboratory testing, and statistical analyses performed for this research. The procedures and results associated with a separate investigation of geogrid reinforcement with the inclusion of a geotextile are presented in Appendix A.

3.2 Geogrid Selection

Five different geogrid types, each categorized as either biaxial or triaxial, were utilized in this research to ensure that the experimentation was representative of the geogrid products available in the industry at the time of the study. The objective of this research was not to compare geogrid types but rather to compare geogrid-reinforced aggregate base layers to unreinforced aggregate base layers for multiple geogrid types. All major suppliers of geogrid products in the United States were contacted about their products and manufacturing processes. The suppliers were informed of the planned experimentation, given details about the expected aggregate base material characteristics, and asked to provide an approximately 1-ft by 1-ft

sample for evaluation. In consultation with UDOT, the researchers chose geogrid products from three independent manufacturers for inclusion in the study, and the suppliers of these products were subsequently asked to provide full-width rolls with a minimum length of 50 ft. Four biaxial geogrids and one triaxial geogrid, shown in Figure 3-1 and hereafter referred to as geogrids A, B, C, D, and E, respectively, were used in this research.

3.3 Field Sites

The researchers selected sites in Orem and Springville based on the scope of work, construction scheduling, and willingness of the project owners and contractors to incorporate the proposed research experiments into the pavement construction process. Of particular importance were the requirements to construct control sections in the experimental pavements and to permit testing both during and after construction.

Because the sites were comparatively close to each other, approximately 11 miles apart, their typical climates were similar. Annual climatological data provided by the United States Department of Commerce National Oceanic and Atmospheric Administration and the United States Climate Data user websites (NOAA 2016, USCD 2016) for three weather stations close to the two research sites are shown in Table 3-1. Data from a fourth weather station in Lehi indicate that the 10-year air freezing index is approximately 800°F-days in this area.

At each of the two field sites, 10 test sections were established end to end or side by side in a line within the designated test area. Each test section had lateral dimensions of 12 ft by 12 ft, and the test sections were consistently labeled from 1 to 10 with increasing numbers from north to south. Geogrids A, B, C, D, and E were consistently placed in sections 2, 4, 6, 8, and 10, respectively, and an accompanying unreinforced control section was immediately adjacent to each geogrid-reinforced section. This experimental layout minimized the possibility of

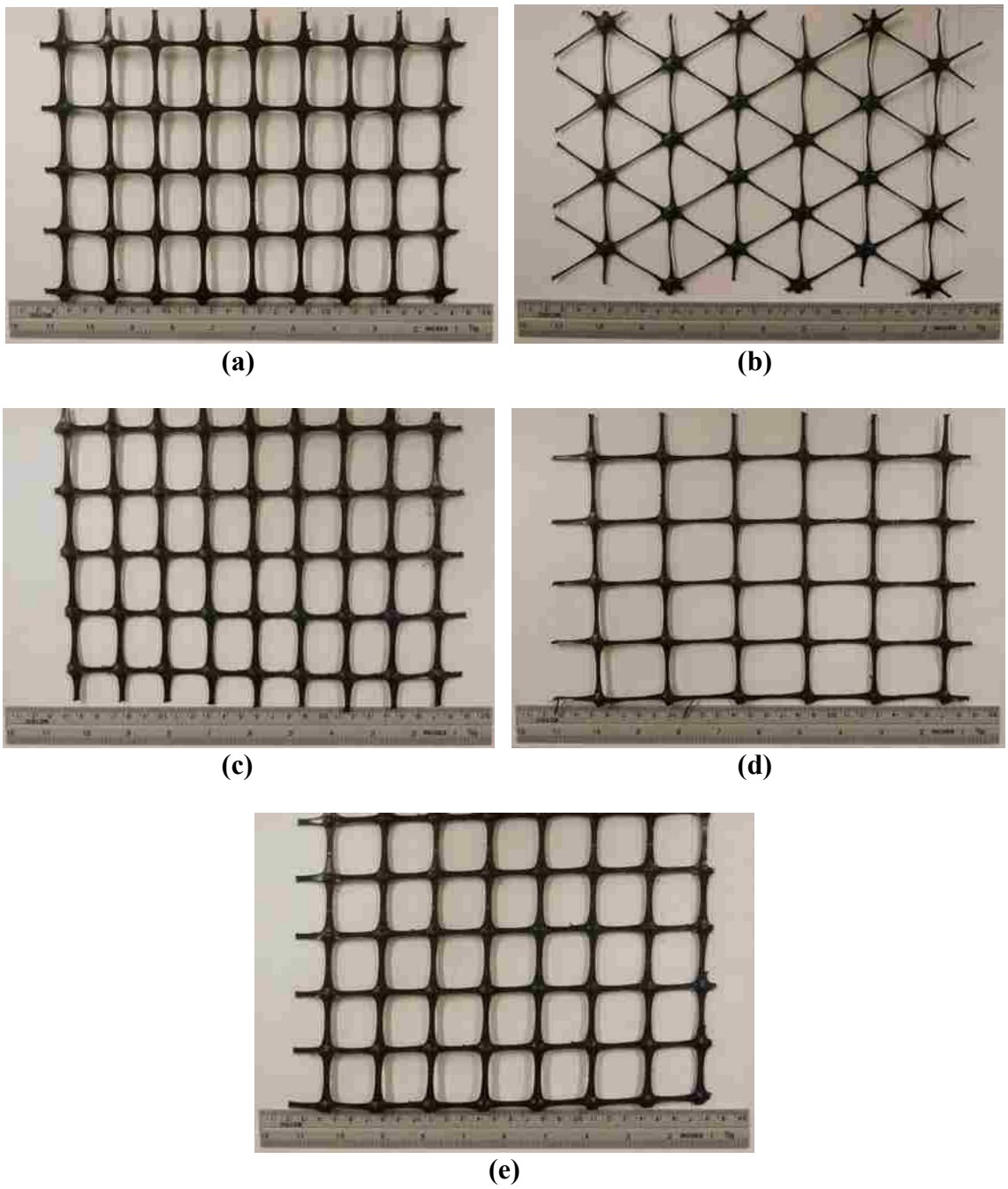

Figure 3-1: Geogrid products used in this research: (a) A, (b) B, (c) C, (d) D, and (e) E.

significant variability in subgrade conditions, for example, between the geogrid-reinforced sections and the corresponding control sections. Details regarding construction of the Orem and Springville sites are given in the following sections.

Table 3-1: Climate Data for Weather Stations near Field Sites

Site Characteristic	Weather Station		
	Provo, Utah	Pleasant Grove, Utah	Spanish Fork, Utah
Elevation (ft)	4570	4712	4720
Latititude	40.246° N	40.368° N	40.080° N
Longitutde	111.651° W	111.734° W	111.604° W
2014-2015 Highest Temperature (°F)	103	105	102
2014-2015 Lowest Temperature (°F)	0	0	-1
2014 Annual Mean Temperature (°F)	55.7	55.4	54.0
2015 Annual Mean Temperature (°F)	56.7	56.4	54.9
2014 Total Precipitation (in.)	16.9	8.8	19.9
2015 Total Precipitation (in.)	15.7	11.1	14.9

3.3.1 Orem Field Site

The first field site established for this research comprised the southbound lane of 800 East in Orem, Utah, just south of the intersection with 1200 North as shown in Figure 3-2. The average daily traffic at this location is approximately 11,000 (UDOT 2014). At this location, the roadway width is approximately 48 ft as needed to accommodate one 12-ft lane in each direction, a 12-ft two-way turning lane, and 6-ft shoulders. The previous pavement, which had failed prematurely, was removed, and the subgrade was then over-excavated prior to reconstruction. The new pavement was constructed under the direction of Orem City by Granite Construction in the summer of 2014. The pavement design applied to the reconstruction included 6 in. of HMA as the surface course and 12 in. of slag aggregate as the base course, as shown in Figure 3-3. Orem City specified the materials for this project prior to its selection for this research.

After the subgrade was graded and proof-rolled, the test site was instrumented with subsurface temperature, moisture, and electrical conductivity sensors. The sensors were embedded in the subgrade directly beneath the base-subgrade interface at five locations throughout the test site corresponding to the midpoints of the boundaries between the pairs of

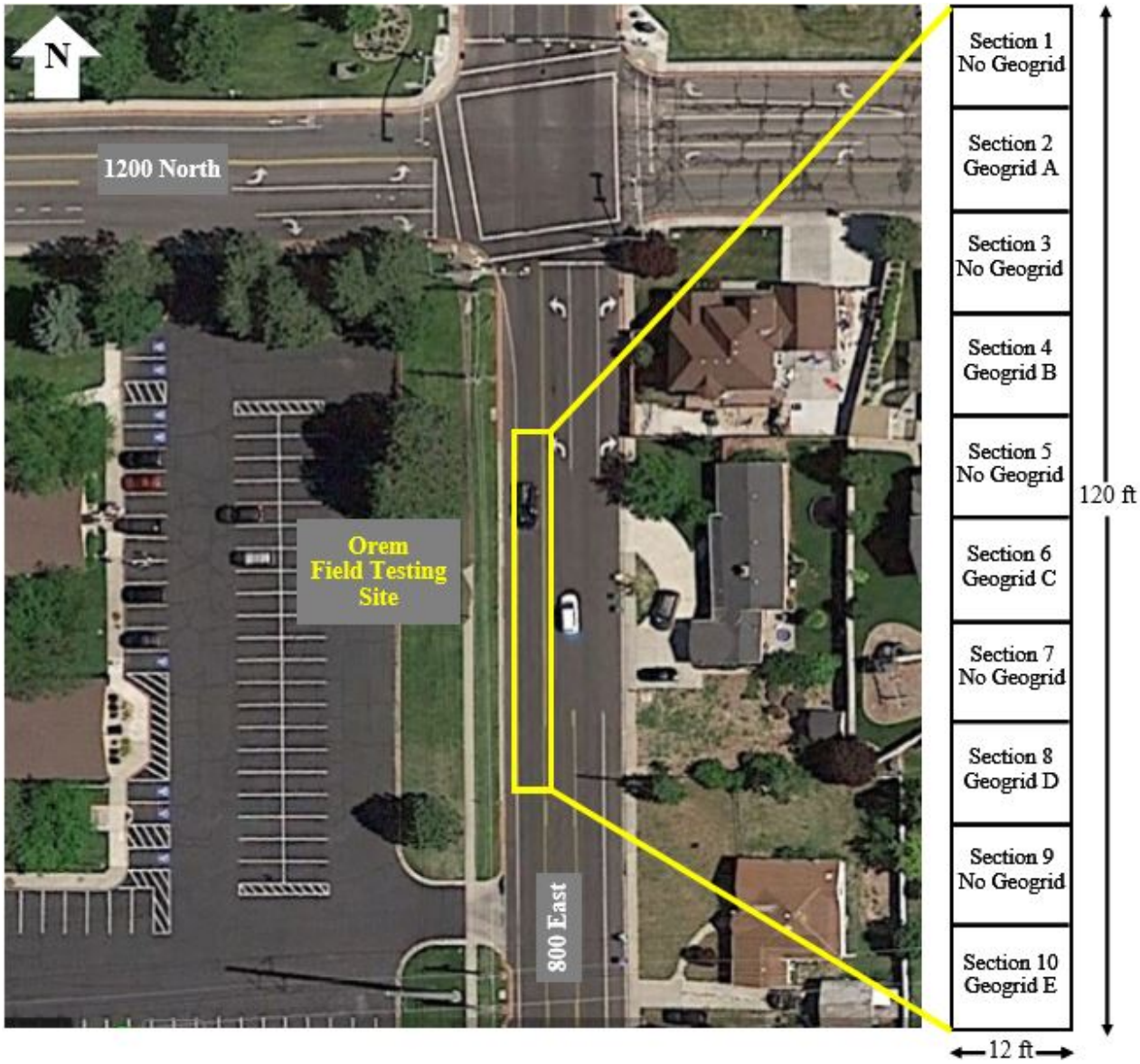

Figure 3-2: Layout of Orem site.

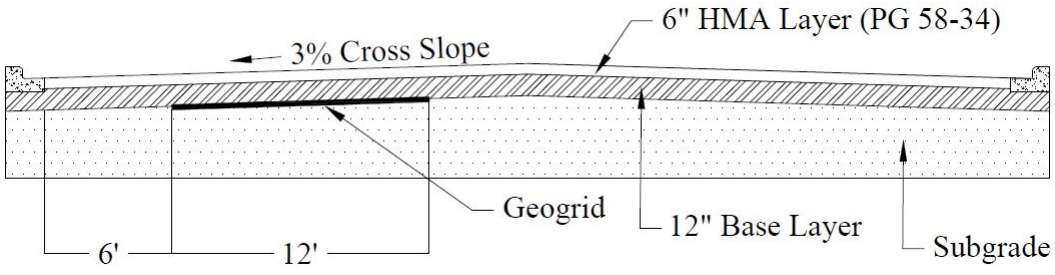

Figure 3-3: Typical pavement cross section for Orem site.

geogrid-reinforced and unreinforced sections. The sensor type used in this research is depicted in Figure 3-4. The sensor data were used in the statistical analyses performed in this research to account for variability in subsurface conditions across the site; in particular, differences in subgrade moisture content were visually apparent across the site during construction and may have led to changes in pavement performance (Guthrie et al. 2010).

After the sensors were installed, 12-ft by 12-ft geogrid squares were installed at the base-subgrade interface within the designated test sections. Care was taken by the researchers to ensure that the geogrid squares were installed according to the manufacturer's recommendations and UDOT guidelines (UDOT 2012) by minimizing wrinkling and movement of the geogrid squares during placement of the overlying base material; a representative from one of the geogrid manufacturers was present to oversee the installation process. The researchers manually flattened the geogrid squares against the subgrade and then shoveled small amounts of base material on top of each one, as shown in Figure 3-5. The contractor then used a front loader to place a large load of base material in the middle of each geogrid square to ensure that no further movement occurred during the remaining grading and compaction activities. The base layer was compacted in two 6-in. lifts to a total thickness of 12 in. with a smooth-drum vibratory compactor, shown in Figure 3-6, and the HMA was then also compacted in two lifts, the lower being 4 in. thick and the upper being 2 in. thick. Following standard practices, each HMA lift was compacted using both a double-drum vibratory roller and a finish roller as shown in Figure 3-7. To determine pavement layer thicknesses and surface slopes, the researchers used a rod and level and a global positioning system to perform elevation surveys on the subgrade, base, and HMA layers at the four corners of each test section during pavement construction.

Figure 3-4: Soil moisture, temperature, and electrical conductivity sensor.

Figure 3-5: Installation of geogrid reinforcement at Orem site.

Figure 3-6: Vibratory roller for compaction of base layer at Orem site.

Figure 3-7: Vibratory and finish rollers for compaction of HMA at Orem site.

3.3.2 Springville Field Site

The second field site established for this research comprised an area within a parking lot at a meetinghouse owned by The Church of Jesus Christ of Latter-day Saints and located on the

southwest corner of the intersection of 200 North and 900 East in Springville, Utah, as shown in Figure 3-8. The average daily traffic at this location is estimated to be approximately 100. The previous pavement, which had failed after decades of use, was removed, and the subgrade was then over-excavated prior to reconstruction. The parking lot was reconstructed by Geneva Rock under the direction of the Church in the fall of 2014. The research area was located on the east side of the meetinghouse. The pavement design applied to the reconstruction included 3 in. of fiber-reinforced HMA as the surface course and 9 in. of crushed aggregate as the base course, as shown in Figure 3-9. The Church specified the materials for this project prior to its selection for this research.

After the subgrade was graded and proof-rolled, geogrid squares were installed as shown in Figure 3-10 at the base-subgrade interface in a manner similar to that previously described for the Orem field site. The base layer was then compacted in a single 9-in. lift with a smooth-drum vibratory roller, as depicted in Figure 3-11, and the HMA layer was compacted in a single 3-in. lift using both a double-drum vibratory roller and a finish roller, as shown in Figure 3-12. To determine pavement layer thicknesses and surface slopes, the researchers used a rod and level to perform elevation surveys on the subgrade, base, and HMA layers at the four corners of each test section during pavement construction. The Springville field site was not instrumented with subsurface sensors due to the accelerated construction schedule at this site.

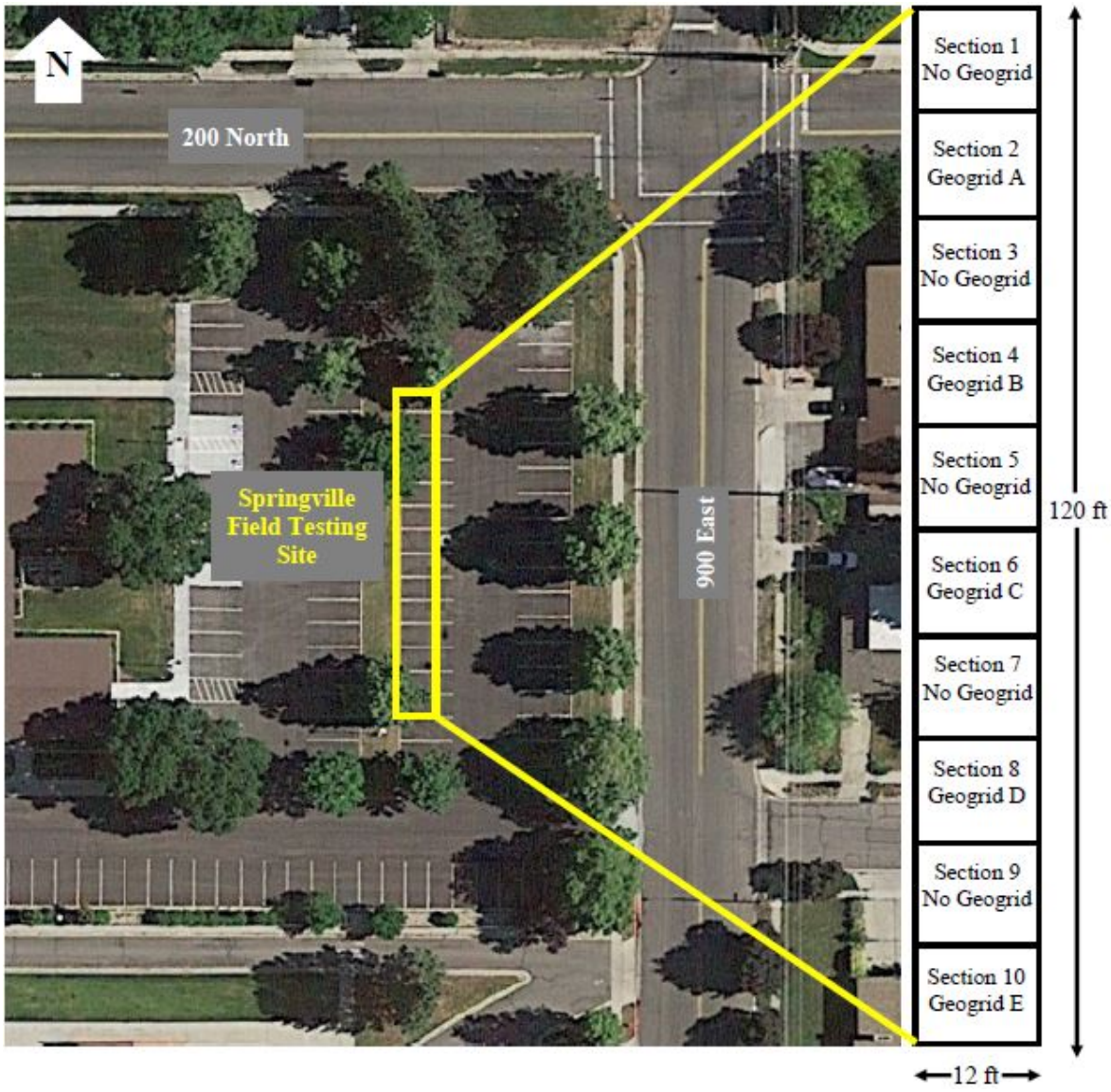

Figure 3-8: Layout of Springville site.

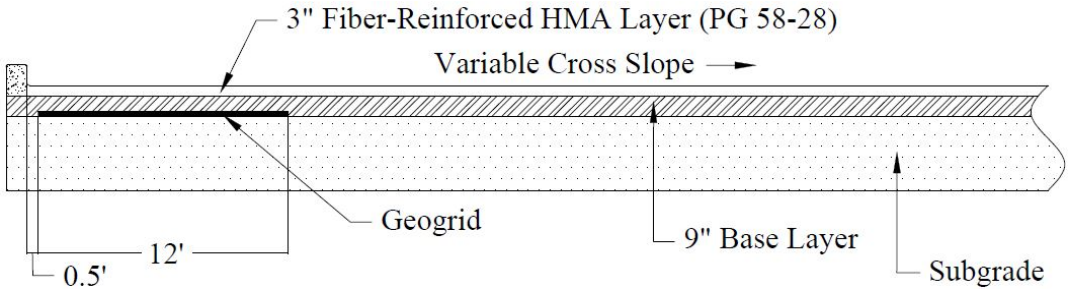

Figure 3-9: Typical pavement cross section for Springville site.

Figure 3-10: Installation of geogrid reinforcement at Springville site.

Figure 3-11: Vibratory roller for compaction of base layer at Springville site.

Figure 3-12: Vibratory and finish rollers for compaction of HMA at Springville site.

3.4 Field Procedures

Field testing was performed between July 2014 and October 2015 for the Orem field site and from October 2014 to May 2015 for the Springville field site to characterize the in-situ structural properties of the subgrade, base, and HMA layers of each geogrid-reinforced and unreinforced test section. Several field tests were conducted during and following construction of the two pavements as outlined in Tables 3-2 and 3-3. The Orem and Springville field sites were monitored for 15 and 7 months, respectively, including one winter season.

A testing pattern was established that included two testing locations for NDG, SSG, CIST, and PFWD testing in each test section and one location at the center of each test section for DCP and FWD testing. This pattern, shown in Figure 3-13, was consistently followed at each of the 10

test sections at each field site. To facilitate repeated PFWD testing over time, survey nails were hammered into the surface of the HMA layer to mark the PFWD testing locations.

Table 3-2: Testing Schedule for Orem Site

Date	Type of Testing						
	Sensors	NDG	SSG	CIST	DCP	PFWD	FWD
July 15, 2014	x	x	x	x			
August 7, 2014	x	x	x	x	x		
September 19, 2014	x	x				x	
November 26, 2014	x					x	
December 10, 2014	x						x
May 7, 2015	x					x	
October 29, 2015	x				x		

Table 3-3: Testing Schedule for Springville Site

Date	Type of Testing					
	NDG	SSG	CIST	DCP	PFWD	FWD
October 13, 2014	x	x	x			
October 14, 2014	x	x	x	x		
November 20, 2014	x					
November 26, 2014					x	
December 10, 2014						x
May 5, 2015					x	

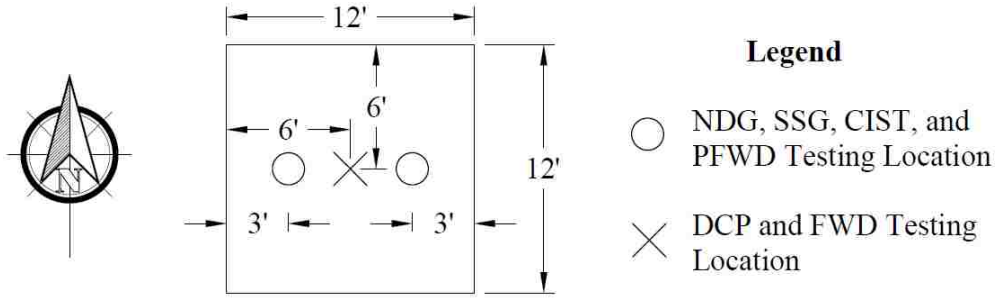

Figure 3-13: Typical testing locations for each test section.

NDG tests were performed in general accordance with American Society for Testing and Materials (ASTM) D6938 (Standard Test Methods for In-Place Density and Water Content of Soil and Soil-Aggregate by Nuclear Methods (Shallow Depth)). The NDG was utilized to measure in-situ wet density, dry density, and moisture content of the subgrade and base layer and the asphalt content and density of the HMA layer. The NDG rod was inserted 6 in. into the subgrade and base layers during testing in the direct transmission mode. The backscatter mode was used for testing the HMA layer. One test was consistently performed at each of two testing locations in each section, as shown in Figure 3-13. Figures 3-14 and 3-15 show NDG tests being performed on the subgrade at the Orem site and on the HMA layer at the Springville site, respectively.

SSG tests were performed in general accordance with ASTM D6758 (Standard Test Method for Measuring Stiffness and Apparent Modulus of Soil and Soil-Aggregate In-Place by Electro-Mechanical Method). The SSG is a compact cylinder weighing 22 lb that imparts very small displacements, using a harmonic oscillator, to the soil through a ring-shaped foot. Stiffness is measured as a function of the deflections of the soil caused by the vibrations from the gauge. The SSG measures the stiffness of the underlying soil to an average depth of 9 in. to 12 in. from the surface. Following standard procedures, a thin layer of moist sand was placed between the SSG and the surface of the layer being tested to ensure good contact with the surface. The SSG was utilized to evaluate the stiffness of the subgrade and base layers of the pavement structures. One SSG test was consistently performed at each of two testing locations in each section, as shown in Figure 3-13. Figure 3-16 shows an SSG test being performed at the Orem site.

CIST tests were performed in general accordance with ASTM D5874 (Standard Test Methods for Determination of the Impact Value (IV) of a Soil). A Clegg hammer, consisting of a

Figure 3-14: NDG testing of subgrade.

Figure 3-15: NDG testing of HMA layer.

44-lb weight dropped from a height of 12 in. through a guide tube, returns a deceleration value as a Clegg impact value (CIV). The highest deceleration value measured in four consecutive drops at a testing location is recorded. The CIST was utilized to evaluate the stiffness of the subgrade

Figure 3-16: SSG testing of base layer.

and base layers of the pavement structures. Modulus values were calculated from the recorded CIV values using Equation 3-1 (CHM 1999):

$$MR = 33.56 \times CIV^2 \quad (3\text{-}1)$$

where $MR =$ resilient modulus, psi

$CIV =$ Clegg impact value

One CIST test was consistently performed at each of two testing locations in each section, as shown in Figure 3-13. Figure 3-17 shows a CIST test being performed at the Orem site.

DCP tests were performed in general accordance with ASTM D6951 (Standard Test Method for Use of the Dynamic Cone Penetrometer in Shallow Pavement Applications). The DCP consists of a 0.47-in.-diameter metal rod fitted with a standard metal cone at the end. A 10-lb slide hammer is repeatedly dropped 22.5 in., and the penetration rate, measured in mm/blow, of the DCP into the tested layers is recorded. For the DCP testing performed in Orem in August 2014 and October 2015, the average depth of penetration into the subgrade layer was

Figure 3-17: CIST testing of base layer.

approximately 5 in. and 9 in., respectively. In Springville, the average depth of penetration into the subgrade layer was approximately 19 in. Average penetration rates within the respective layers were used to assess pavement layer thickness and estimate CBR values for both the base and subgrade layers, which were then correlated to modulus values. Equations 3-2 and 3-3 were used for CBR and modulus value calculations, respectively, for both the base and subgrade layers:

$$CBR = \frac{292}{DCP^{1.12}} \tag{3-2}$$

where CBR = California bearing ratio, %

DCP = penetration rate, mm/blow

$$MR = 2550 \times CBR^{0.64} \tag{3-3}$$

where MR = resilient modulus, psi

CBR = California bearing ratio, %

One DCP test was consistently performed at one test location in each section, as shown in Figure 3-13. Figure 3-18 shows DCP testing being performed at the Orem site before the HMA layer was placed. For testing in October 2015, DCP testing was performed through 1.5-in.-diameter holes drilled in advance through the HMA layer at the specified test locations; the holes were subsequently filled with cold-mix asphalt, which was compacted into place using a handheld tool designed for this purpose.

PFWD tests were performed in general accordance with ASTM E2583 (Standard Test Method for Measuring Deflections with a Light Weight Deflectometer (LWD)). The PFWD consists of a 44.1-lb weight that is dropped approximately 30 in. onto a 7.87-in.-diameter load plate. Three sensors were used to measure the pavement deflection at radial distances of 0 in., 12 in., and 24 in. from the point of impact. A seating load was applied before deflection

Figure 3-18: DCP testing of base layer.

measurements were recorded to ensure that the load plate was properly situated on the surface of the HMA layer, and data for three drops were then recorded at each testing location. The deflections measured by the PFWD were used to backcalculate modulus values for all three layers in the pavement system using the backcalculation software program BAKFAA. Three PFWD tests were consistently performed at each of two testing locations in each section, as shown in Figure 3-13. Figure 3-19 shows PFWD testing being performed at the Orem site.

FWD tests were performed in general accordance with ASTM D4694 (Standard Test Method for Deflections with a Falling-Weight-Type Impulse Load Device). The FWD was provided and operated at both sites by UDOT personnel. The FWD consists of a set of weights mounted on a truck or trailer that are dropped from various heights onto a 12-in.-diameter load plate to achieve a desired load up to 16,000 lb in this research. Seven sensors were used to measure the pavement deflection at radial distances of 0 in., 8 in., 12 in., 18 in., 24 in., 36 in., and 60 in. from the point of impact. A seating load was applied before deflection measurements were recorded to ensure that the load plate was properly situated on the surface of the HMA layer, and data for three drops were then recorded at each testing location. Deflections measured by the FWD were used to backcalculate modulus values for all three layers in the pavement system using BAKFAA. A range of loads was applied to each field site. In Orem, loads of 8,000 lb, 10,000 lb, 12,000 lb, 14,000 lb, and 16,000 lb were applied to the pavement, while in Springville loads of 8,000 lb and 10,000 lb were applied to the pavement. The higher loads applied at the Orem site were possible due to the greater thickness of the layers used at that site compared to the Springville site. Three FWD tests were consistently performed at one testing location in each section, as shown in Figure 3-13. Figure 3-20 shows an FWD test being performed at the Springville site.

Figure 3-19: PFWD testing of pavement.

Figure 3-20: FWD testing of pavement.

The backcalculation process applicable to the PFWD and FWD data required multiple input values. Specifically, data required to perform the backcalculations in BAKFAA include deflection measurements recorded by the PFWD or FWD, the applied load, the load plate radius, seed modulus values, Poisson's ratios, and layer thicknesses for each layer in the pavement structure. Seed modulus values varied depending on the temperature at the time of testing. For example, testing conducted in colder temperatures would be expected to yield higher modulus values for each pavement layer as a result of the effects of temperature on asphalt viscosity and water surface tension (Mamlouk and Zaniewski 2011, Marshall and Holmes 1988). A Poisson's ratio of 0.35 was used for all pavement layers, with the exception of the subgrade layer at the Springville test site, where a Poisson's ratio of 0.40 was used due to the clayey composition of that layer (Huang 2004). Layer thicknesses for the HMA and base layers, determined for each test section from elevation survey results, were used in the backcalculations. Separate backcalculations were performed for each individual drop of the PFWD and FWD.

A two-step backcalculation process was used to analyze the PFWD and FWD deflection data (Rogers 2013). The first step involved an analysis of a modified two-layer pavement system, in which the HMA and base layers were combined into a single layer. This first analysis yielded a subgrade modulus value that was then held constant in the second step, in which the actual thicknesses of the HMA and base layers were entered. The second analysis yielded modulus values for the HMA and base layers. Use of this two-step process was necessary to generate reasonable modulus values for the individual layers.

3.5 Laboratory Procedures

Samples of the subgrade and base materials were obtained from both field sites for laboratory testing as part of this research. During construction, the materials were sampled from

the grade using shovels and transported in buckets to the Brigham Young University Highway Materials Laboratory for characterization. Testing included dry and washed sieve analyses, Atterberg limits testing, and material classification.

The bulk materials were dried and sieved in general accordance with ASTM D6913 (Standard Test Methods for Particle-Size Distribution (Gradation) of Soils Using Sieve Analysis) to produce master gradations. Based on the master gradations, samples of each material were prepared for further testing. Washed sieve analyses were performed on both the subgrade and base materials in general accordance with ASTM D6913. A hydrometer analysis was performed in general accordance with ASTM D422 (Standard Test Method for Particle-Size Analysis of Soils) for both subgrade materials due to their comparatively high fines contents. Atterberg limits for the materials were measured according to ASTM D4318 (Standard Test Methods for Liquid Limit, Plastic Limit, and Plasticity Index of Soils). Following this testing, the aggregates were classified according to the Unified Soil Classification System (USCS) and the American Association of State Highway and Transportation Officials (AASHTO) methods in general accordance with ASTM D2487 (Standard Practice for Classification of Soils for Engineering Purposes (Unified Soil Classification System)) and AASHTO M 145 (Classification of Soils and Soil-Aggregate Mixtures for Highway Construction Purposes), respectively. In addition, values for the optimum moisture content and maximum dry density of both base materials were obtained from the suppliers.

3.6 Statistical Analyses

An analysis of covariance (ANOCOVA) was conducted on the results of each field test performed on the subgrade, base, and HMA materials. The statistical analyses were performed to determine if the structural capacity of the geogrid-reinforced sections was different than that of

the accompanying unreinforced control sections. The Orem and Springville field sites were evaluated separately.

In each ANOCOVA model, the dependent variable was the given measurement of structural capacity, and the independent variable was the presence of geogrid reinforcement. Several potentially relevant covariates were also considered in the analyses. In each analysis, a full model, with factors including the independent variable and all relevant covariates, was first produced. The *p*-values computed for the factors were examined, and a reduced model was then created by sequentially deleting covariates with a *p*-value greater than 0.15 so that all remaining covariates had a *p*-value less than or equal to 0.15. The coefficient of determination, or R^2 value, was computed for each reduced model. In addition, least squares means were computed for the main effect of the independent variable for all models in which it was statistically significant, as indicated by a *p*-value less than or equal to 0.05 in the reduced ANOCOVA model.

In addition to statistical significance, practical importance was also evaluated. For determining the magnitude of a practically important difference in structural capacity, a correlation chart showing relationships among multiple measurements of structural capacity for untreated base course materials was consulted (Huang 2004). The correlation chart indicated that a change in the AASHTO structural coefficient of 0.01, which is the smallest increment used in practice, would change the base modulus value by about 2 ksi, for example. Therefore, because a difference in base modulus of less than 2 ksi would not result in a different input in the pavement design process, it was selected as a minimum threshold for identifying practically important differences for modulus measurements. An equivalent threshold for other measurements of structural capacity could then be readily determined from the correlation chart.

3.7 Summary

This chapter provides a detailed description of the various field tests that were used in this research to evaluate the structural capacity of unreinforced and geogrid-reinforced aggregate base layers in flexible pavements. Field testing at two full-scale pavement sites in northern Utah was the main focus of this work. Five different geogrid types, each categorized as either biaxial or triaxial, were utilized in this research to ensure that the experimentation was representative of the geogrid products available in the industry at the time of the study. The researchers selected sites in Orem and Springville based on the scope of work, construction scheduling, and willingness of the project owners and contractors to incorporate the proposed research experiments into the pavement construction process.

At each of the two field sites, 10 test sections were established end to end or side by side in a line within the designated test area. Several field tests were conducted during and following construction of the two pavements to characterize the in-situ structural properties of the subgrade, base, and HMA layers of each geogrid-reinforced and unreinforced test section. A testing pattern was established that included two testing locations for NDG, SSG, CIST, and PFWD testing in each test section and one location at the center of each test section for DCP and FWD testing.

Samples of the subgrade and base materials were obtained from both field sites for laboratory testing as part of this research. Testing included dry and washed sieve analyses, Atterberg limits testing, and material classification.

An ANOCOVA was conducted on the results of each field test performed on the subgrade, base, and HMA materials at the Orem and Springville field sites. The statistical analyses were performed to determine if the structural capacity of the geogrid-reinforced sections was different than that of the accompanying unreinforced control sections. In each ANOCOVA

model, the dependent variable was the given measurement of structural capacity, and the independent variable was the presence of geogrid reinforcement. Several potentially relevant covariates were also considered in the analyses. In addition to statistical significance, practical importance was also evaluated.

4 RESULTS AND ANALYSIS

4.1 Overview

This chapter presents the results of laboratory and field testing, as well as the results of statistical analyses performed for this research. All results presented in this chapter are limited in their application to the material types, pavement designs, construction techniques, environmental conditions, and trafficking levels associated with this study.

4.2 Laboratory Results

Laboratory results included dry and washed sieve analyses for both the subgrade and base materials, hydrometer analyses and Atterberg limits testing on the subgrade material, and soil classification of the subgrade and base materials obtained from each field site. The results of the washed sieve analyses for the subgrade and base materials are shown in Figure 4-1 and Figure 4-2, respectively. Numerical values for the particle-size distributions are provided in Appendix B.

Regarding the base materials, the D_{50} values were determined to be approximately 0.2 in. and 0.3 in. for the Orem and Springville sites, respectively, and the corresponding D_{85} values were determined to be approximately 0.5 in. and 0.8 in. Therefore, based on FHWA recommendations (FHWA 2008), the minimum geogrid aperture size for the Orem and

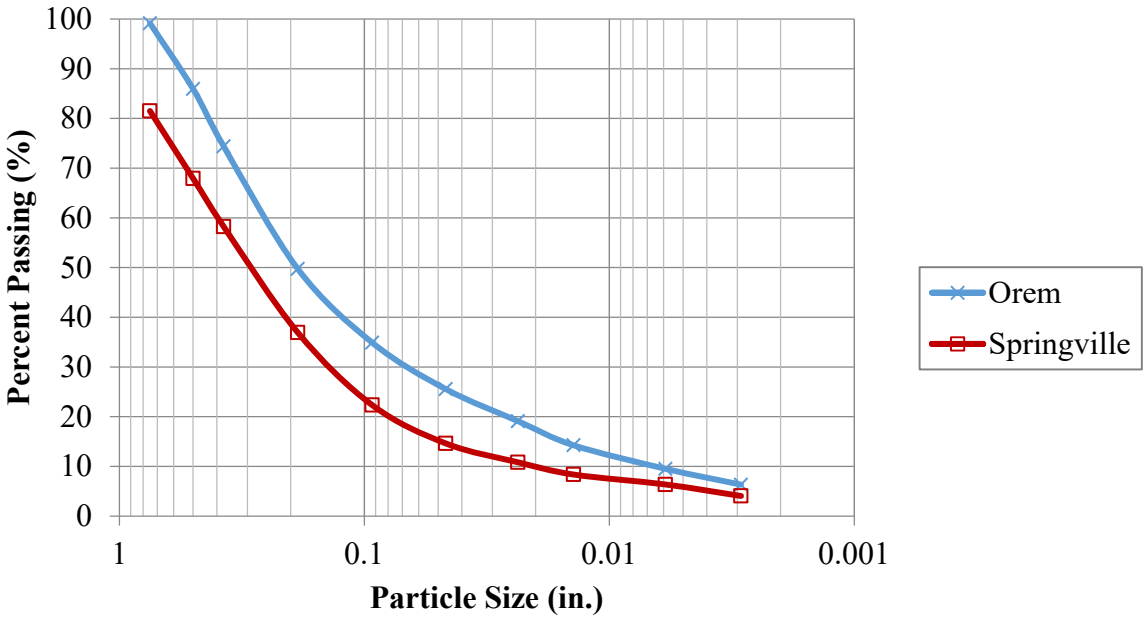

Figure 4-1: Particle-size distributions for base materials.

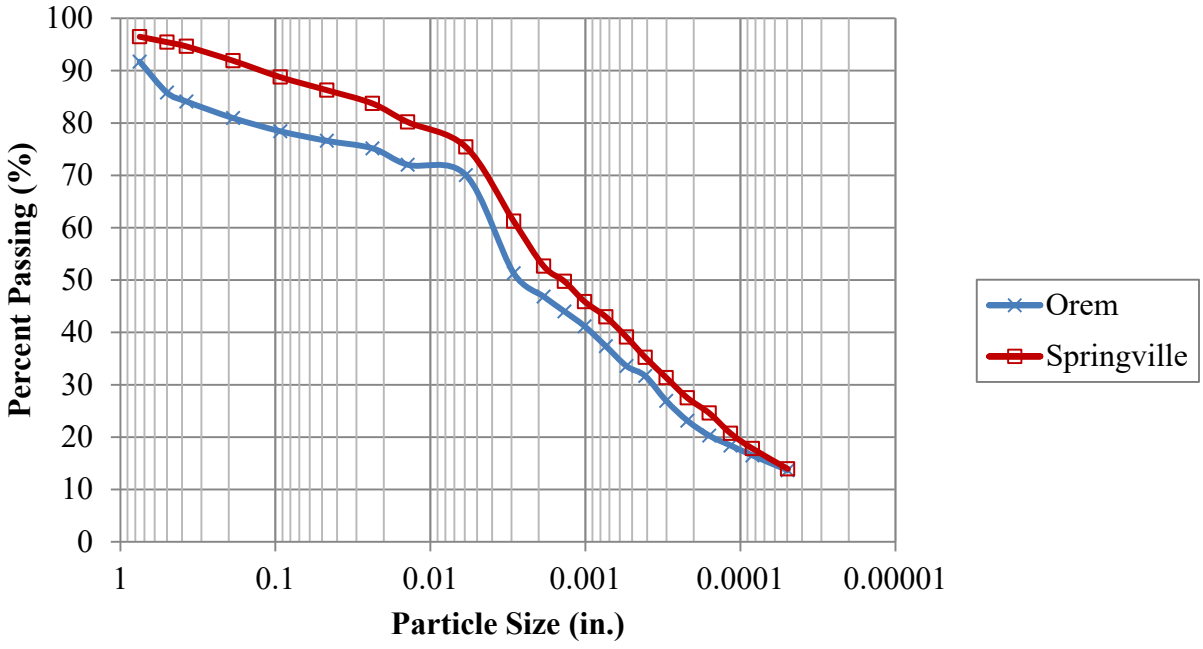

Figure 4-2: Particle-size distributions for subgrade materials.

Springville base materials was 0.5 in., and the maximum geogrid aperture size was 1.0 in. for the Orem base material and 1.6 in. for the Springville base material. Among the geogrids selected for use in this research, all of the geogrids except B and D met the recommendations for the Orem base material, and all of the selected geogrids met the recommendations for the Springville base material. Geogrid B, in particular, was not available in a size that met the recommendations for the Orem base material, but, like geogrid D, it is commonly used with similar base materials according to the manufacturer. As stated previously, the aggregate base materials were already specified for both projects prior to their selection for this research.

The results of the Atterberg limits testing for the subgrade materials are shown in Table 4-1. According to the USCS and AASHTO classification methods, respectively, the Orem subgrade material was classified as lean clay with sand (CL) and A-6, and the Springville subgrade material was classified as lean clay (CL) and A-6. Atterberg limits testing indicated that the base materials at both sites were non-plastic. According to USCS and AASHTO classification methods, the Orem base material was classified as well-graded gravel with silt and sand (GW-GM) and A-1-a, and the Springville base material was classified as well-graded gravel with sand (GW) and A-1-a. The moisture-density information obtained from the supplier of each base material is listed in Table 4-2.

Table 4-1: Atterberg Limits and Soil Classifications for Subgrade Materials

Property	Orem	Springville
Plastic Limit	20	16
Liquid Limit	35	31
Plasticity Index	15	16

Table 4-2: Moisture-Density Relationships for Base Materials

Property	Orem	Springville
Optimum Moisture Content (%)	12.1	12.4
Maximum Dry Density (pcf)	127.6	116.3

4.3 Field Results

Field results included measurements obtained using the NDG, SSG, CIST, DCP, PFWD, and FWD. Individual test values for each section at each field site are provided in Appendix C and were the basis for statistical analyses performed to compare the geogrid-reinforced sections and accompanying unreinforced control sections evaluated in this research. Example BAKFAA screen shots and detailed inputs for the two-step process that applied to the PFWD and FWD data analyses are presented in Appendix D. As exhibited by the data, modulus values measured at the same time on the same layer can differ due to the different methods of interrogation associated with different testing instruments; in this research, the different results were examined independently to address the stated research objective.

4.4 Statistical Analyses

The results of the statistical analyses performed for this research are presented in Tables 4-3 through 4-6. The independent variable of geogrid presence, as well as all covariates considered in each ANOCOVA model, are shown in the tables for each given measurement of structural capacity. All listed covariates except those marked as not applicable (N/A) were included in the analyses. A hyphen in the tables indicates that the given covariate had a *p*-value exceeding 0.15 and was therefore excluded in development of the reduced ANOCOVA model. A *p*-value less than or equal to 0.05 indicates that a given factor was statistically significant. While

Table 4-3: ANOCOVA Results for SSG, CIST, and DCP Testing at Orem Site

Factor	*p* -value						
	SSG Base Modulus	CIST Base CIV	CIST Base Modulus	DCP Base CBR for Varying Times		DCP Base Modulus for Varying Times	
				Aug. 2014	Oct. 2015	Aug. 2014	Oct. 2015
Geogrid Presence	0.793	0.224	0.226	0.003	0.613	0.004	0.260
Subgrade Dry Density at Time of Construction	<0.001	0.086	0.051	-	0.003	-	0.014
Subgrade Wet Density at Time of Construction	-	0.085	0.05	-	-	-	-
Subgrade Moisture Content at Time of Construction	-	0.121	0.073	-	-	-	-
Subgrade Modulus from SSG	0.005	0.014	0.051	-	0.003	-	0.012
Subgrade CIV from CIST	-	-	-	-	-	-	-
Subgrade Modulus from CIST	-	0.101	0.091	-	-	-	-
Subgrade CBR from DCP	N/A	N/A	N/A	N/A	-	N/A	0.084
Subgrade Modulus from DCP	N/A	N/A	N/A	N/A	<0.001	N/A	0.045
Subgrade Temperature at Time of Testing	-	0.001	0.002	-	-	-	-
Subgrade Electrical Conductivity at Time of Testing	-	-	-	0.132	-	0.122	-
Subgrade Moisture Content at Time of Testing	0.008	0.002	0.003	<0.001	0.006	<0.001	0.008
Base Thickness	-	-	-	-	-	-	-
Base Dry Density at Time of Construction	0.011	0.005	0.006	-	-	-	-
Base Wet Density at Time of Construction	-	0.005	0.007	-	-	-	-
Base Moisture Content at Time of Construction	-	0.01	0.012	0.041	-	0.044	-
R^2	0.702	0.906	0.891	0.876	0.780	0.873	0.833

Table 4-4: ANOCOVA Results for PFWD and FWD Testing at Orem Site

Factor	*p* -value							
	PFWD Base Modulus for Varying Times			FWD Base Modulus for Varying Loads (lb)				
	Nov. 2014	Sept. 2014	May 2015	16,000	14,000	12,000	10,000	8,000
Geogrid Presence	0.561	0.997	0.941	0.622	0.745	0.361	0.054	0.011
Subgrade Modulus at Time of Testing	0.001	-	0.001	<0.001	<0.001	0.005	<0.001	<0.001
Subgrade Temperature at Time of Testing	0.002	-	0.005	-	0.002	0.032	0.005	<0.001
Subgrade Electrical Conductivity at Time of Testing	0.034	-	-	-	0.008	0.022	0.005	0.001
Subgrade Moisture Content at Time of Testing	-	-	-	0.009	0.093	-	0.024	<0.001
Base Thickness	-	-	-	-	-	0.063	0.004	0.005
Base Dry Density at Time of Construction	-	0.028	-	-	-	-	-	-
HMA Thickness	0.043	-	-	0.053	0.004	0.053	0.011	<0.001
HMA Modulus at Time of Testing	0.001	0.001	0.023	0.037	-	0.096	0.026	<0.001
HMA Wet Density at Time of Construction	-	-	-	-	-	-	-	-
HMA Asphalt Content	0.093	-	-	-	-	-	-	-
R^2	0.832	0.571	0.706	0.927	0.942	0.859	0.971	0.979

Table 4-5: ANOCOVA Results for SSG, CIST, and DCP Testing at Springville Site

Factor	*p* -value				
	SSG Base Modulus	CIST Base CIV	CIST Base Modulus	DCP Base CBR	DCP Base Modulus
Geogrid Presence	0.764	0.432	0.575	0.528	0.032
Subgrade Dry Density at Time of Construction	0.068	0.075	-	0.076	-
Subgrade Wet Density at Time of Construction	0.070	0.074	-	0.050	0.051
Subgrade Moisture Content at Time of Construction	0.067	0.083	-	-	-
Subgrade Modulus from SSG	-	-	-	-	0.014
Subgrade CIV from CIST	-	0.009	0.010	-	-
Subgrade Modulus from CIST	0.064	0.011	0.014	0.001	0.001
Subgrade CBR from DCP	0.068	-	0.113	-	0.029
Subgrade Modulus from DCP	0.070	-	0.132	0.001	0.019
Base Thickness	-	-	-	<0.001	<0.001
Base Dry Density at Time of Construction	-	0.046	0.111	0.015	-
Base Wet Density at Time of Construction	-	0.104	0.119	0.013	0.005
Base Moisture Conent at Time of Construction	0.015	-	0.143	0.015	-
R^2	0.394	0.628	0.710	0.966	0.968

Table 4-6: ANOCOVA Results for PFWD and FWD Testing at Springville Site

Factor	*p* -value			
	PFWD Base Modulus for Varying Times		FWD Base Modulus for Varying Loads (lb)	
	Nov. 2014	May 2015	10,000	8,000
Geogrid Presence	0.824	0.411	0.351	0.989
Subgrade Modulus at Time of Testing	-	0.009	<0.001	<0.001
Base Thickness	-	0.002	<0.001	<0.001
HMA Modulus at Time of Testing	<0.001	<0.001	<0.001	<0.001
HMA Wet Density at Time of Construction	-	-	-	-
HMA Thickness	0.004	0.002	<0.001	<0.001
R^2	0.639	0.917	0.982	0.978

not all factors that potentially influenced geogrid performance could be measured and accounted for in this study, the inclusion of a high number of covariates produced comparatively high R^2 values for the reduced models. Thus, a high percentage of variation in the dependent variables is explained by variation in the independent variable and covariates included in the models.

Consistent with the objective of this research, the independent variable of geogrid presence was included in every ANOCOVA model evaluated in this research. The *p*-value resulting from each analysis specifically indicated whether or not geogrid presence had a statistically significant effect on the given measurement of structural capacity after all of the included covariates were accounted for in the model. Among the 15 ANOCOVA models developed for the Orem site, only three indicated that geogrid presence was statistically significant. These included the models developed for base CBR from DCP testing performed in August 2014, base modulus from DCP testing performed in August 2014, and base modulus from FWD testing under an 8,000-lb load. Among the nine ANOCOVA models developed for the Springville site, only one indicated that geogrid presence was statistically significant, which was the model developed for base modulus from DCP testing.

Tables 4-7 and 4-8 display the least squares means for the main effect of geogrid presence for the four reduced ANOCOVA models in which geogrid presence was statistically significant, and Figures 4-3 through 4-6 present graphs of the same data. The least squares means computed for three of the four models indicate that the presence of geogrid reinforcement led to higher values of the given measurement of structural capacity compared to the unreinforced condition. These included the models developed for base CBR from DCP testing performed in August 2014 at the Orem site, base modulus from DCP testing performed in August 2014 at the Orem site, and base modulus from DCP testing performed at the Springville

Table 4-7: Least Squares Means for Main Effect of Geogrid Presence at Orem Site

Factor	Level	DCP		FWD
		Base CBR (%)	Base Modulus (ksi)	Base Modulus (ksi) at 8,000 lb
Geogrid Presence	With Geogrid	53.7	32.6	82.2
	Without Geogrid	51.9	31.9	85.9

Table 4-8: Least Squares Means for Main Effect of Geogrid Presence at Springville Site

Factor	Level	DCP
		Base Modulus (ksi)
Geogrid Presence	With Geogrid	11.1
	Without Geogrid	10.3

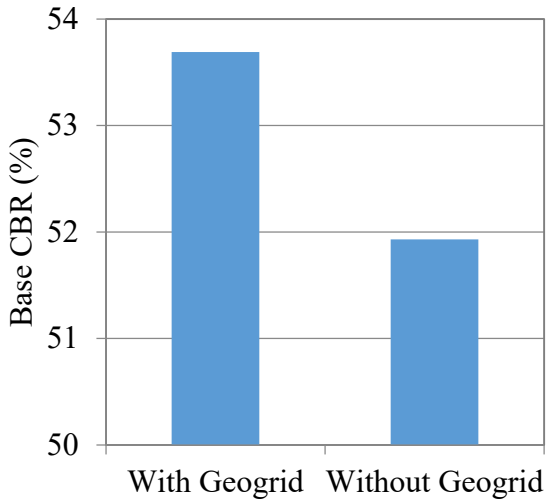

Figure 4-3: Main effect of geogrid presence on base CBR measured with DCP at Orem site.

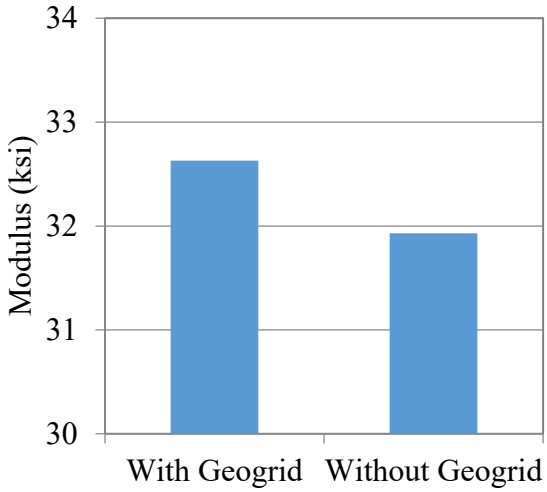

Figure 4-4: Main effect of geogrid presence on base modulus measured with DCP at Orem site.

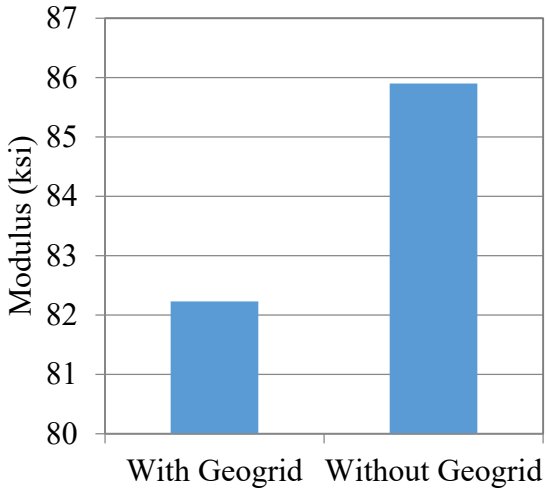

Figure 4-5: Main effect of geogrid presence on base modulus measured with FWD at 8,000 lb at Orem Site.

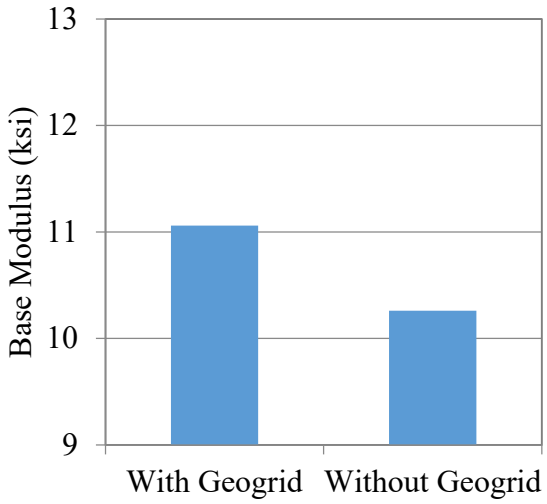

Figure 4-6: Main effect of geogrid presence on base modulus measured with DCP at Springville site.

site. However, in none of the cases was the difference practically important, which was defined in this research as greater than or equal to 2 ksi for modulus, or greater than or equal to 10 for CBR, which is an equivalent threshold for the range of measured CBR values; therefore, these differences would not result in a different input in the pavement design process. The least squares means for the remaining model, which was developed for base modulus from FWD testing under an 8,000-lb load at the Orem site, indicate that the presence of geogrid reinforcement led to a lower value of the given measurement of structural capacity compared to the unreinforced condition. In this case, the difference in modulus exceeded 2 ksi and was therefore considered to be practically important. A reason for this result, which was consistent in some respects with the results of other research (Aran 2006, Hall et al. 2004,Tingle and Jersey 2009), was not identified.

For the three models for which the least squares means indicate that the presence of geogrid reinforcement led to higher values of the given measurement of structural capacity, the same testing procedure, namely the DCP, was used for the testing. Therefore, use of the DCP

may be more likely than other testing procedures to show structural improvements associated with geogrid reinforcement, especially in the absence of an HMA surface course as in these cases.

As previously described, quantifying the benefit of geogrid reinforcement in a pavement section requires an adequate conditioning period, allowing the geogrid and surrounding aggregate to fully interlock. Although exact predictions of the length of the conditioning period are probably not possible, several months or even a few years may be required in some cases. Therefore, results more favorable than those reported in this study may have been obtained after a longer conditioning period at each site. Also, to the extent that the benefit of geogrid reinforcement is limited to a zone of influence that extends only partially into the base layer, calculating average values of structural properties for the full depth of the tested base layers, as reported in this study, may have masked localized improvements associated with the use of geogrid reinforcement.

4.5 Summary

This chapter presents the results of laboratory and field testing, as well as the results of statistical analyses performed for this research. Laboratory results included dry and washed sieve analyses for both the subgrade and base materials, Atterberg limits testing on the subgrade material, and soil classification of the subgrade and base materials obtained from each field site. Field results included measurements obtained using the NDG, SSG, CIST, DCP, PFWD, and FWD.

Among the 15 ANOCOVA models developed for the Orem site, only three indicated that geogrid presence was statistically significant. These included the models developed for base modulus from FWD testing under an 8,000-lb load, base CBR from DCP testing performed in August 2014, and base modulus from DCP testing performed in August 2014. Among the nine

ANOCOVA models developed for the Springville site, only one indicated that geogrid presence was statistically significant, which was the model developed for base modulus from DCP testing.

Among the four models that indicated that geogrid presence was statistically significant, three indicated that the presence of geogrid reinforcement led to higher values of the given measurement of structural capacity compared to the unreinforced condition; however, in none of the cases was the difference practically important as defined in this research and would therefore not result in a different input in the pavement design process. Notably, in all three of these models, the same testing procedure, namely the DCP, was used for the testing. Therefore, use of the DCP may be more likely than other testing procedures to show structural improvements associated with geogrid reinforcement, especially in the absence of an HMA surface course as in these cases.

Results more favorable than those reported in this study may have been obtained after a longer conditioning period at each site. Also, to the extent that the benefit of geogrid reinforcement is limited to a zone of influence that extends only partially into the base layer, calculating average values of structural properties for the full depth of the tested base layers, as reported in this study, may have masked localized improvements associated with the use of geogrid reinforcement.

5 CONCLUSION

5.1 Summary

The installation of geogrid as a means of extending the service life of a roadway or reducing the required base course thickness of a pavement structure has become increasingly popular. The realization of these benefits depends largely on the degree to which the geogrid reinforcement leads to an increase in the stiffness of the aggregate base course layer. The objective of this research, as commissioned by UDOT, was to investigate the structural capacity of geogrid-reinforced aggregate base materials in flexible pavements through full-scale testing. The scope of this research involved field testing at two sites that each included five different geogrid-reinforced sections and five accompanying unreinforced control sections. One site was located in Orem, Utah, and the other was located in Springville, Utah.

In this research, various field tests were used to evaluate the structural capacity of unreinforced and geogrid-reinforced aggregate base layers in flexible pavements. Five different geogrid types, each categorized as either biaxial or triaxial, were utilized to ensure that the experimentation was representative of the geogrid products available in the industry at the time of the study. At each of the two field sites, 10 test sections were established within the designated test area. Several field tests were conducted during and following construction of the two pavements to characterize the in-situ structural properties of the subgrade, base, and HMA layers of each geogrid-reinforced and unreinforced test section. The procedures involved NDG,

SSG, CIST, DCP, PFWD, and FWD testing of each test section. Samples of the subgrade and base materials were also obtained from both field sites for laboratory testing, which included dry and washed sieve analyses, Atterberg limits testing, and material classification. An ANOCOVA was conducted on the results of each field test to determine if the structural capacity of the geogrid-reinforced sections was different than that of the accompanying unreinforced control sections. In addition to statistical significance, practical importance was also evaluated.

5.2 Findings

All results from this research are limited in their application to the material types, pavement designs, construction techniques, environmental conditions, and trafficking levels associated with this study. Among the 15 ANOCOVA models developed for the Orem site, only three indicated that geogrid presence was statistically significant. Among the nine ANOCOVA models developed for the Springville site, only one indicated that geogrid presence was statistically significant. Of these four models, three indicated that the presence of geogrid reinforcement led to higher values of the given measurement of structural capacity compared to the unreinforced condition; however, in none of the cases was the difference practically important as defined in this research and would therefore not result in a different input in the pavement design process. Notably, in all three of these models, the same testing procedure, namely the DCP, was used for the testing. Therefore, use of the DCP may be more likely than other testing procedures to show structural improvements associated with geogrid reinforcement, especially in the absence of an HMA surface course as in these cases.

Results more favorable than those reported in this study may have been obtained after a longer conditioning period at each site. Also, to the extent that the benefit of geogrid reinforcement is limited to a zone of influence that extends only partially into the base layer,

calculating average values of structural properties for the full depth of the tested base layers, as reported in this study, may have masked localized improvements associated with the use of geogrid reinforcement.

5.3 Recommendations

Although the primary purpose of installing geogrid in aggregate base course layers is to improve pavement performance under traffic loading, a measurable increase in the structural capacity of the reinforced layer may not be immediately observable using standard pavement testing procedures. In this situation, engineers who specify installation of geogrid as a means of extending the service life of a roadway or reducing the required base course thickness of a pavement structure may be unable to readily verify their assumptions. Further field research is recommended to investigate the duration of the required conditioning period and also the extent of the zone of influence of geogrid reinforcement in aggregate base courses. Specifically, long-term monitoring of the sites established for this research may be particularly useful; use of the DCP is recommended for future testing.

REFERENCES

Al-Qadi, I. L., Dessouky, S. H., Kwon, J., and Tutumluer, E. (2008). "Geogrid in flexible pavements: validated mechanism." *Transportation Research Record: Journal of the Transportation Research Board*, 2045, 102-109.

Aran, S. (2006). "Base reinforcement with biaxial geogrid: long-term performance." *Transportation Research Record: Journal of the Transportation Research Board*, 1975, 115-123.

Barksdale, R. D., Brown, S. F., and Chan, F. (1989). "Potential benefits of geosynthetics in flexible pavement systems." National Cooperative Highway Research Program Report 315. Transportation Research Board, Washington, DC.

Brandon, T. L., Al-Qadi, I. L., Lacina, B. A., and Bhutta, S. A. (1996). "Construction and instrumentation of geosynthetically stabilized secondary road test sections." *Transportation Research Record: Journal of the Transportation Board*, 1534, 50-57.

Clegg Hammer Modulus (CHM). (1999). Newsletter 14. <http://www.clegg.com.au /information_list3.asp> (August 30, 2014).

Chen, Q., and Abu-Farsakh, M. (2012). "Structural contribution of geogrid reinforcement in pavement." *GeoCongress 2012: State of the Art and Practice in Geotechnical Engineering*, American Society of Civil Engineers, Reston, VA, 1468-1475.

Collin, J. G., Kinney, T. C., and Fu, X. (1996). "Full scale highway load test of flexible pavement systems with geogrid reinforced base courses." *Geosynthetics International*, 3(4), 537-549.

Edil, T., Kim, W., Benson, C., and Tanyu, B. (2007). "Contribution of geosynthetic reinforcement to granular layer stiffness." *Soil and Stiffness Material Inputs for Mechanistic-Empirical Pavement Design*, *Proceedings of Geo-Denver 2007*, American Society of Civil Engineers, Reston, VA, 1-10.

Erickson, H., and Drescher, A. (2001). "The use of geosynthetics to reinforce low volume roads." Report No. MN/RC-2001-15. Office of Research Services, Minnesota Department of Transportation, St. Paul, MN.

Federal Highway Administration (FHWA). (2008). "Geosynthetic design and construction guidelines." Report No. FHWA NHI-07-092. FHWA, United States Department of Transportation, McLean, VA.

Guthrie, W. S., Rogers, T., and Ellis, P. M. (2010). "Variability in construction of cement-treated base layers: probabilistic analysis of pavement life using mechanistic-empirical approach." *Proceedings of the 89th Transportation Research Board Annual Meeting*, Washington, DC.

Haas, R., Walls, J., and Carroll, R. G. (1988). "Geogrid reinforcement of granular bases in flexible pavements." *Transportation Research Record: Journal of the Transportation Research Board*, 1188, 19-27.

Hall, K. D., Warren, K. A., and Howard, I. L. (2004). "Low volume flexible pavement roads reinforced with geosynthetics." Final Report AHTD TRC-0406. Planning and Research Division, Arkansas State Highway and Transportation Department, Little Rock, AR.

Hanes Geo Components. (2015). "Terragrid RX 1200 product data sheet." <http://hanesgeo.com/Catalog/Product?id=1704> (December 15, 2015).

Helstrom, C. L., Humphrey, D. N., and Hayden, S. A. (2006). "Geogrid reinforced pavement structure in a cold region." *Proceedings of the American Society of Civil Engineers Thirteenth International Conference on Cold Regions Engineering*, Orono, ME, 1-12.

Henry, K. S., Clapp, J., Davids, W. G., and Barna, L. (2011). "Back-calculated pavement layer modulus values of geogrid reinforced test sections." *Proceedings of Geo-Frontiers: Advances in Geotechnical Engineering*, Dallas, TX, 4673-4682.

Henry, K. S., Clapp, J., Davids, W., Humphrey, D., and Barna, L. (2009). "Structural improvements of flexible pavements using geosynthetics for base course reinforcement." Final Report No. ERDC/CRREL TR-09-11. United States Army Cold Regions Research and Engineering Laboratory, Hanover, NH.

Holder, W. H., and Andreae, J. (2004). "Geogrid reinforcement to reduce pavement section thickness: a case study." *Geotechnical Special Publication No. 126, GeoTrans 2004: Geotechnical Engineering for Transportation Projects*, American Society of Civil Engineers, Reston, VA.

Huang, Y. H. (2004). *Pavement Analysis and Design*, Second Edition, Pearson Prentice Hall, Upper Saddle River, NJ.

Hufenus, R., Rueegger, R., Banjac, R., Mayor, P., Springman, S. M., and Brönnimann, R. (2006). "Full-scale field tests on geosynthetic reinforced unpaved roads on soft subgrade." *Geotextiles and Geomembranes*, 24(1), 21-37.

Huntington, G., and Ksaibati, K. (2000). "Evaluation of geogrid-reinforced granular base." *Geotechnical Fabrics Report*, 18(1), 22-28.

Joshi, R. V. (2010). "Field performance of geogrid reinforced low-volume pavements." M.S. thesis, Department of Civil, Architectural and Environmental Engineering, University of Texas, Austin, TX.

Joshi, R. V., and Zornberg, J. G. (2011). "Use of falling weight deflectometer data to quantify the relative performance of reinforced pavement sections. *Proceedings of Geo-Frontiers: Advances in Geotechnical Engineering,* Dallas, TX, 4713-4722.

Knighton, J. T. (2015). "Investigation of laboratory test procedures for assessing the structural capacity of geogrid-reinforced aggregate base materials." M.S. thesis, Department of Civil and Environmental Engineering, Brigham Young University, Provo, UT.

Kwon, J., and Tutumluer, E. (2009). "Geogrid base reinforcement with aggregate interlock and modeling of associated stiffness enhancement in mechanistic pavement analysis." *Transportation Research Record: Journal of the Transportation Research Board*, 2116, 85-95.

Kwon, J., Tutumluer, E., Al-Qadi, I., and Dessouky, S. (2008). "Effectiveness of geogrid base-reinforcement in low-volume flexible pavements." *Proceedings of GeoCongress 2008: Geosustainability and Geohazard Mitigation*, American Society of Civil Engineers, Reston, VA.

Mamlouk, M. S., and Zaniewski, J. P. (2011). *Materials for Civil and Construction Engineers*, Third Edition, Prentice Hall, Upper Saddle River, NJ.

Marshall, T. J., and Holmes, J. W. (1988). *Soil Physics*, Second Edition, Cambridge University Press, Cambridge, Great Britain.

Maubeuge, K., and Klompmaker, J. (2011). "New developments for geogrid reinforced base courses." *Proceedings of Geo-Frontiers: Advances in Geotechnical Engineering*, Dallas, TX, 4624-4634.

Moayedi, H., Kazemian, S., Prasad, A., and Huat, B. B. K. (2009). "Effect of geogrid reinforcement location in paved road improvement." *Electronic Journal of Geotechnical Engineering*, 14.

Moghaddas-Nejad, F., and Small, J. C. (1996). "Effect of geogrid reinforcement in model track tests on pavements." *Journal of Transportation Engineering*, 122(6), 468-474.

National Oceanic and Atmospheric Administration (NOAA). (2016). "Climate data online." NOAA, <https://www.ncdc.noaa.gov/cdo-web/> (March 27, 2016).

Perkins, S. W. (1999). "Geosynthetic reinforcement of flexible pavements: laboratory based pavement test sections." Report No. FHWA/MT-99-001/8138. Federal Highway Administration, United States Department of Transportation, Washington, DC.

Perkins, S. W., Christoper, B. R., Cuelho, E. L., Eiksund, G. R., Hoff, I., Schwartz, C. W., Svano, G., and Watn, A. (2004). "Development of design methods for geosynthetic-reinforced flexible pavements." Report No. DTFH61-01-X-00068. Federal Highway Administration, United States Department of Transportation, Washington, DC.

Reck, N. C. (2009). "Mechanistic empirical design of geogrid reinforced paved flexible pavements." *Proceedings of Jubilee Symposium on Polymer Geogrid Reinforcement*, Institute of Civil Engineers, London, England.

Rogers, M. A. (2013). "Water vapor movement in freezing aggregate base materials." Ph.D. dissertation, Department of Civil and Environmental Engineering, Brigham Young University, Provo, UT.

Schuettpelz, C., Fratta, D., and Edil, T. B. (2009). "Evaluation of the zone of influence and stiffness improvement from geogrid reinforcement in granular materials." *Transportation Research Record: Journal of the Transportation Research Board*, 2116, 76-84.

Tensar International Corporation. (2015). "Biaxial (BX) geogrid product specification sheet." <http://www.tensarcorp.com/Systems-and-Products/Tensar-geogrids/Tensar-Biaxial-BX-geogrids> (December 15, 2015).

Tingle, J. S., and Jersey, S. R. (2009). "Full-scale evaluation of geosynthetic-reinforced aggregate roads." *Transportation Research Record: Journal of the Transportation Research Board*, 2116, 96-107.

Tutumluer, E., Huang, H., and Bian, X. (2009). "Research on the behaviour of geogrids in stabilisation applications." *Proceedings of Jubilee Symposium on Polymer Geogrid Reinforcement*, Institute of Civil Engineers, London, England.

Utah Department of Transportation (UDOT). (2012). “Geogrid – base reduction.” UDOT Standards and Specifications: Materials Special Provision 02073S. UDOT, Salt Lake City, UT, <http://www.udot.utah.gov/main/f?p=100:pg:0:::1:T,V:3707,> (July 1, 2014).

Utah Department of Transportation (UDOT). (2014). “Traffic on Utah highways.” Traffic Analysis Section, Program Development Division, UDOT, Salt Lake City, UT, <http://www.udot.utah.gov/main/uconowner.gf?n=23660530071927911> (May 25, 2016).

United States Climate Data (USCD). (2016). “Climate Pleasant Grove – Utah.” USCD. <http://www.usclimatedata.com/climate/pleasant-grove/utah/united-states/usut0202/2015/1> (April 17, 2016).

APPENDIX A ADDITIONAL SPRINGVILLE FIELD SITE

During construction of the main Springville field site established for this study, the researchers were presented with an opportunity to establish an additional field site in the same parking lot. Although the experimental design applied to the main field sites in this research was not applied to the additional site, the inclusion of a geotextile at the additional site was not within the scope of the original research, and information about the geogrid product used at the additional site was not available to the researchers, the data collected at the additional site were nonetheless useful for addressing the research objective.

The additional Springville field site comprised an area on the south side of the meetinghouse and consisted of a 72-ft by 13-ft pavement area, as shown in Figure A-1. The pavement design applied to the reconstruction included 3 in. of fiber-reinforced HMA as the surface course and 15 in. of crushed aggregate as the base course, as shown in Figure A-2. The thicker layer of crushed aggregate as the base course compared to that used at the main Springville field site was a result of the contractor choosing to over-excavate the additional field site due to high moisture levels in the subgrade material observed during construction. A single layer of woven geotextile was also installed by the contractor at the base-subgrade interface of the pavement structure in this area.

Six 12-ft by 13-ft test sections were established within the additional field site. While only a geotextile was present in the eastern three test sections, a geogrid was placed immediately on top of the geotextile in the western three test sections as shown in Figure A-3. The base layer

was then compacted in a single 15-in. lift with a smooth-drum vibratory roller. The HMA lift was compacted using both a double-drum vibratory roller and a finish roller. The same base and

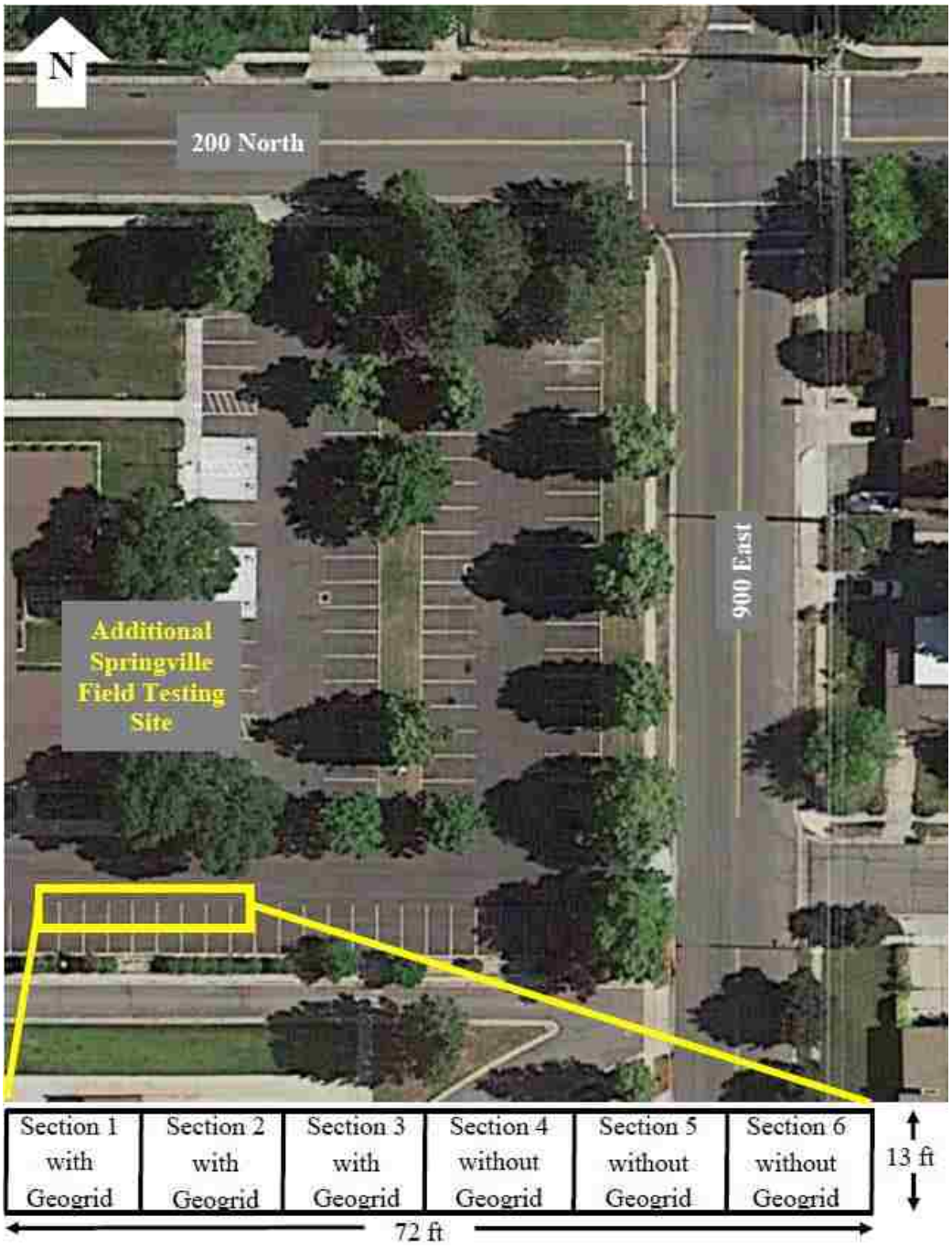

Figure A-1: Layout of additional Springville site.

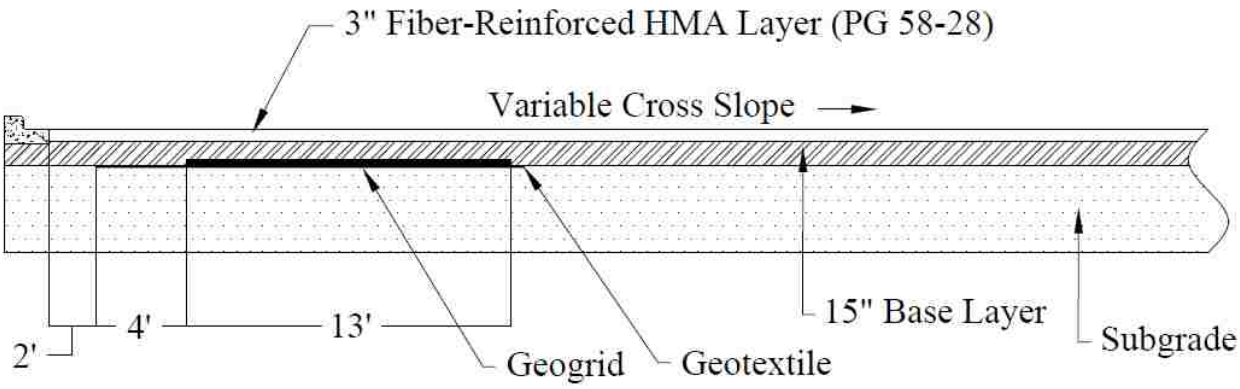

Figure A-2: Typical pavement cross section for additional Springville site.

Figure A-3: Installation of geogrid reinforcement at additional Springville site.

HMA materials used to construct the main Springville field site were also used to construct the additional Springville field site. Numerical values for the particle-size distributions are provided in Appendix B.

Field testing was performed between October 2014 and May 2015 for this additional field site to characterize the in-situ structural properties of the subgrade, base, and HMA layers of each geogrid-reinforced and unreinforced test section. A testing pattern was established that included six testing locations for NDG, SSG, CIST, PFWD and FWD testing in each test section and three locations for DCP testing. This pattern, shown in Figure A-4, was consistently followed at each of the two test sections at the field site. To facilitate repeated PFWD testing over time, survey nails were hammered into the surface of the HMA layer to mark the PFWD testing locations. Testing of the subgrade with the NDG, SSG, and CIST was not possible due to the accelerated construction schedule at this site. Testing of the HMA and base layers occurred as shown in Table A-1.

Field results included measurements obtained using the NDG, SSG, CIST, DCP, PFWD, and FWD. Individual test values are provided in Appendix C and were the basis for statistical analyses performed to compare the geogrid-reinforced section and accompanying unreinforced control section evaluated in this research. Detailed inputs as well as example BAKFAA screen shots showing the two-step process that applied to the PFWD and FWD data analyses are presented in Appendix D.

An ANOCOVA was conducted on the results of each field test performed on the subgrade, base, and HMA materials at the additional Springville field site. The statistical analyses were performed to determine if the structural capacity of the geogrid-reinforced sections was different than that of the accompanying unreinforced control sections. The independent variable of geogrid presence, as well as all covariates considered in each ANOCOVA model, are shown in Tables A-2 and A-3 for each given measurement of structural capacity. A hyphen in the tables indicates that the given covariate had a *p*-value exceeding 0.15 and was therefore

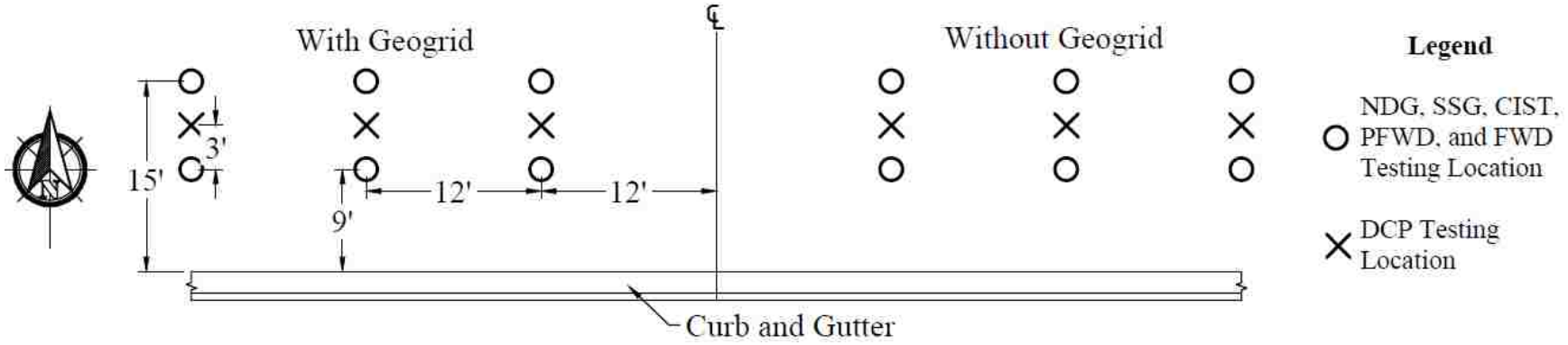

Figure A-4: Typical testing locations for additional Springville site.

Table A-1: Testing Schedule for Additional Springville Site

Date	Type of Testing					
	NDG	SSG	CIST	DCP	PFWD	FWD
October 18, 2014	x	x	x	x		
November 21, 2014	x				x	
December 10, 2014						x
May 5, 2015					x	

Table A-2: ANOCOVA Results for SSG, CIST, and DCP Testing at Additional Springville Site

Factor	*p* -value				
	SSG Base Modulus	CIST Base CIV	CIST Base Modulus	DCP Base CBR	DCP Base Modulus
Geogrid Presence	0.002	0.021	0.033	-	-
Subgrade CBR from DCP	0.003	0.047	0.072	-	-
Subgrade Modulus from DCP	0.003	0.046	0.070	-	-
Moisture Content of Base at Time of Construction	-	-	-	-	-
Dry Density of Base at Time of Construction	0.006	0.109	0.123	-	-
Wet Density of Base at Time of Construction	0.006	-	-	-	-
R^2	0.859	0.569	0.516	-	-

Table A-3: ANOCOVA Results for PFWD and FWD Testing at Additional Springville Site

Factor	*p* -value			
	PFWD Base Modulus for Varying Times		FWD Base Modulus for Varying Loads (lb)	
	Nov. 2014	May 2015	10,000	8,000
Geogrid Presence	0.045	0.007	0.022	0.004
Subgrade CBR from DCP	0.008	-	-	-
Subgrade Modulus from DCP	<0.001	0.010	0.012	0.002
Subgrade Modulus at Time of Testing	-	-	-	-
Dry Density of Base at Time of Construction	<0.001	-	-	-
HMA Thickness	<0.001	0.010	0.012	0.002
HMA Modulus at Time of Testing	<0.001	-	-	-
HMA Wet Density at Time of Construction	0.031	-	-	-
R^2	0.996	0.870	0.977	0.973

excluded in development of the reduced ANOCOVA model. A *p*-value less than or equal to 0.05 indicates that a given factor was statistically significant. While not all factors that potentially influenced geogrid performance could be measured and accounted for in this study, the inclusion of a high number of covariates produced comparatively high R^2 values for the reduced models. Thus, a high percentage of variation in the dependent variables is explained by variation in the independent variable and covariates included in the models.

Among the nine ANOCOVA models developed for the additional Springville site, seven indicated that geogrid presence was statistically significant. These included the models developed for base modulus from SSG testing, base CIV from CIST testing, base modulus from CIST testing, base modulus from PFWD testing in October 2014, base modulus from PFWD testing in May 2015, base modulus from FWD testing under an 10,000-lb load, and base modulus from FWD testing under a 8,000-lb load. Table A-4 displays the least squares means for the main effect of geogrid presence for the seven reduced ANOCOVA models in which geogrid presence was statistically significant and Figures A-5 through A-11 present graphs of the same data. The least squares means computed for two of the seven models indicate that the presence of geogrid reinforcement led to higher values of the given measurement of structural capacity compared to the unreinforced condition. These included the models developed for base modulus from SSG testing and base modulus from PFWD testing in November 2014. In those two models, the difference was practically important, which was defined in this research as greater than or equal to 2 ksi for modulus. The least squares means for the remaining five models indicate that the presence of geogrid reinforcement led to a lower value of the given measurement of structural capacity compared to the unreinforced condition, and the difference in modulus was

Table A-4: Least Squares Means for Main Effect of Geogrid Presence at Additional Springville Site

Factor	Level	SSG Base Modulus (ksi)	CIST Base CIV	Base Modulus (ksi)				
				CIST	PFWD Nov. 2014	PFWD May 2015	FWD at 10,000 lb	FWD at 8,000 lb
Geogrid Presence	With Geogrid	10.6	8.1	0.9	51.2	22.3	26.2	26.8
	Without Geogrid	5.2	22.4	15.9	45.2	26.3	28.8	30.8

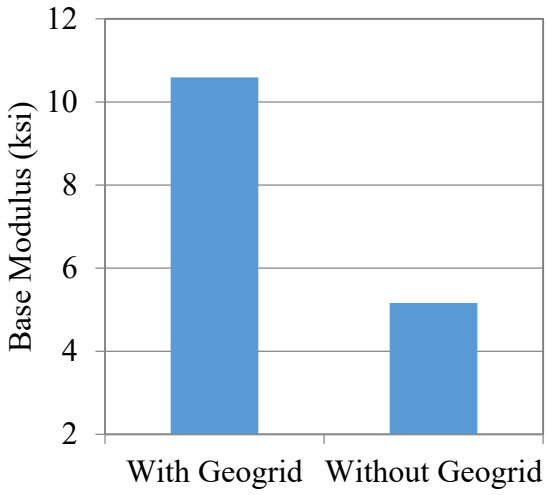

Figure A-5: Main effect of geogrid presence on base modulus measured with SSG at additional Springville site.

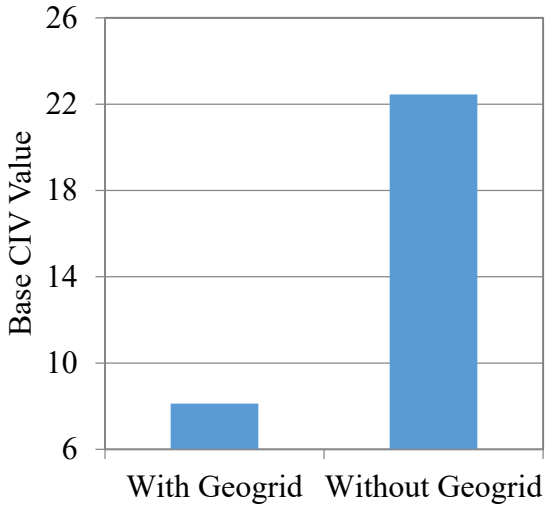

Figure A-6: Main effect of geogrid presence on base CIV measured with CIST at additional Springville site.

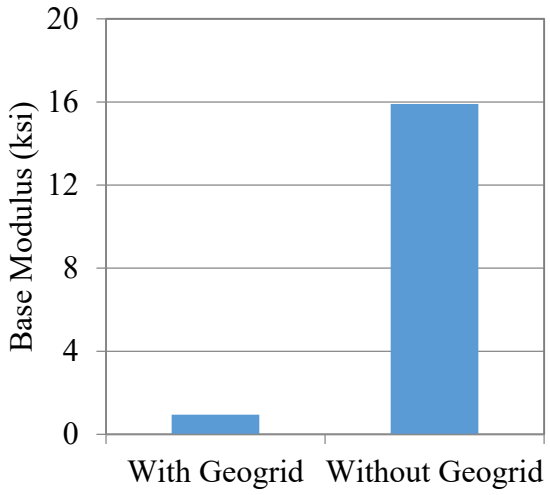

Figure A-7: Main effect of geogrid presence on base modulus measured with CIST at additional Springville site.

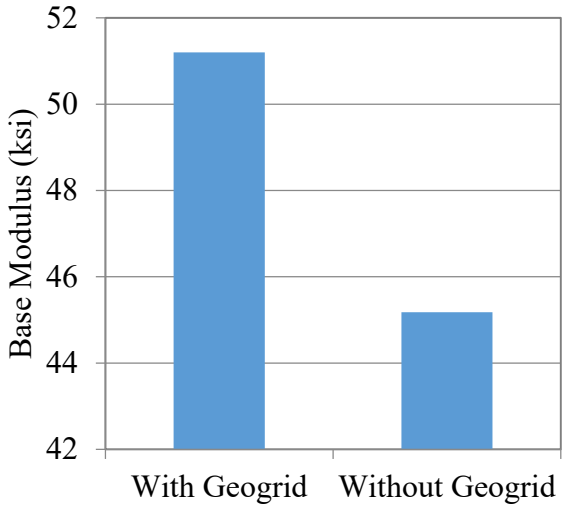

Figure A-8: Main effect of geogrid presence on base modulus measured with PFWD in November 2014 at additional Springville site.

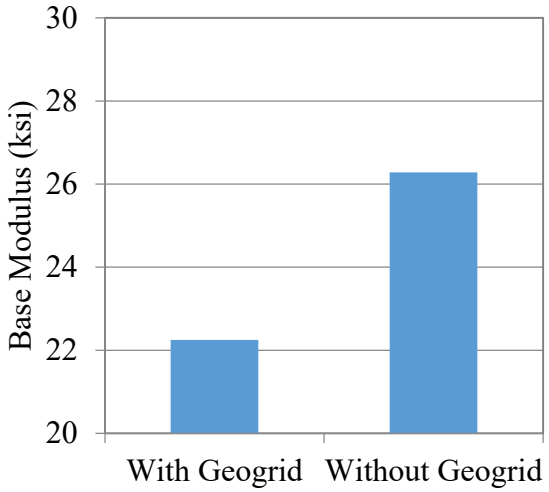

Figure A-9: Main effect of geogrid presence on base modulus measured with PFWD in May 2015 at additional Springville site.

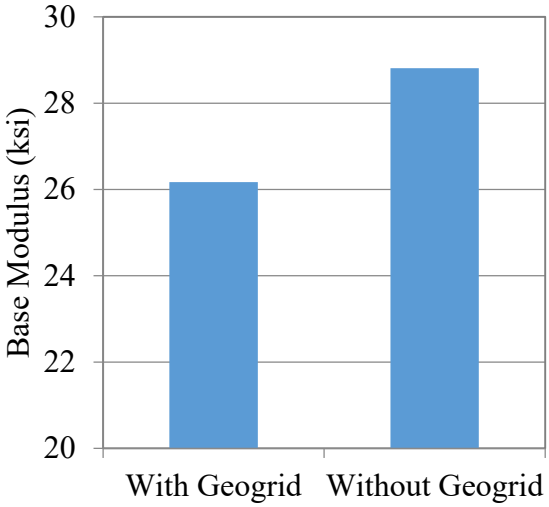

Figure A-10: Main effect of geogrid presence on base modulus measured with FWD at 10,000 lb at additional Springville site.

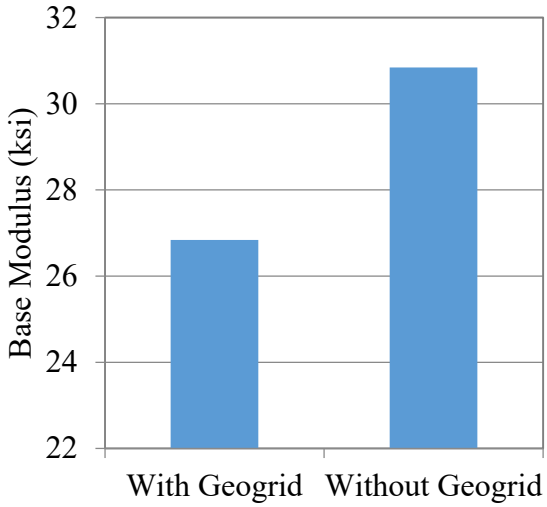

Figure A-11: Main effect of geogrid presence on base modulus measured with FWD at 8,000 lb at additional Springville site.

also considered to be practically important in all of these cases. A reason for these results was not identified.

Results from the investigation of the additional field site in Springville suggest that SSG and PFWD testing may also be useful for showing structural improvements associated with geogrid reinforcement in some cases. Results more favorable than those reported in this study may have been obtained after a longer conditioning period at each site. Also, to the extent that the benefit of geogrid reinforcement is limited to a zone of influence that extends only partially into the base layer, calculating average values of structural properties for the full depth of the tested base layers, as reported in this study, may have masked localized improvements associated with the use of geogrid reinforcement. All results presented in this appendix are limited in their application to the material types, pavement designs, construction techniques, environmental conditions, and trafficking levels associated with this study.

APPENDIX B LABORATORY DATA

This appendix presents laboratory test results for the Orem and Springville field sites. The test results for the Springville field site also apply to the additional Springville field site, as the same materials were used at both sites. Tables B-1 through B-4 present the results of washed sieve and hydrometer analyses for the base and subgrade materials at the Orem and Springville sites.

Table B-1: Results of Washed Sieve Analysis of Base Material for Orem Site

Sieve Size	Percent Passing (%)
3/4 in.	82
1/2 in.	68
3/8 in.	58
No. 4	37
No. 8	22
No. 16	15
No. 30	11
No. 50	8
No. 100	6
No. 200	4
Pan	0

Table B-2: Results of Washed Sieve and Hydrometer Analyses of Subgrade Material for Orem Site

Sieve/Particle Size (in.)	Percent Passing/Finer (%)
0.75000	92
0.50000	86
0.37500	84
0.18700	81
0.09290	78
0.04650	77
0.02360	75
0.01400	72
0.00590	70
0.00290	51
0.00186	47
0.00136	44
0.00101	41
0.00074	37
0.00054	34
0.00041	32
0.00030	27
0.00022	23
0.00016	20
0.00012	18
0.00008	17
0.00005	14

Table B-3: Results of Washed Sieve Analysis of Base Material for Springville Site

Sieve Size	Percent Passing (%)
3/4 in.	99
1/2 in.	86
3/8 in.	74
No. 4	50
No. 8	35
No. 16	26
No. 30	19
No. 50	14
No. 100	10
No. 200	6
Pan	0

Table B-4: Results of Washed Sieve and Hydrometer Analyses of Subgrade Material for Springville Site

Sieve/Particle Size (in.)	Percent Passing/Finer (%)
0.75000	96
0.50000	95
0.37500	95
0.18700	92
0.09290	89
0.04650	86
0.02360	84
0.01400	80
0.00590	75
0.00290	61
0.00186	53
0.00136	50
0.00101	46
0.00074	43
0.00054	39
0.00041	35
0.00030	31
0.00022	27
0.00016	25
0.00012	21
0.00008	18
0.00005	14

APPENDIX C FIELD DATA

This appendix presents field test results for the Orem, Springville, and additional Springville field sites. The presence of a hyphen in a table indicates that the given data were not measured.

C.1 Orem Field Site

The following Tables C-1 through C-11 present data recorded or calculated for the Orem field site.

Table C-1: NDG Results for Subgrade, Base, and HMA Layers at Orem Site

Layer	Location	Measurement	NDG Results									
			Section									
			1	2	3	4	5	6	7	8	9	10
			Without Geogrid	With Geogrid	Without Geogrid	With Geogrid	Without Geogrid	With Geogrid	Without Geogrid	With Geogrid	Without Geogrid	With Geogrid
Subgrade	East	Moisture (%)	11.8	12.3	12.9	9.0	13.9	9.9	9.2	9.5	8.1	7.6
		Wet Density (pcf)	128.4	131.3	133.7	136.7	131.4	130.7	133.9	137.3	137.6	137.2
		Dry Density (pcf)	114.8	116.9	118.4	125.4	115.4	118.9	122.6	125.4	127.4	127.5
	West	Moisture (%)	9.3	7.6	7.4	9.6	8.2	8.9	4.6	7.4	4.7	3.6
		Wet Density (pcf)	137.1	135.6	137.6	137.1	138.6	133.4	134.4	137.0	138.3	134.5
		Dry Density (pcf)	125.4	126.0	128.1	125.1	128.0	122.5	128.5	127.6	132.2	129.8
Base	East	Moisture (%)	3.5	3.1	3.3	3.2	3.4	3.5	3.2	3.5	3.6	3.6
		Wet Density (pcf)	134.3	134.4	133.1	131.1	133.8	133.2	136.1	135.7	132.7	132.6
		Dry Density (pcf)	129.8	130.3	128.8	127.0	129.4	128.7	131.9	131.2	128.0	128.0
	West	Moisture (%)	3.1	3.0	3.2	3.1	3.4	3.8	3.1	3.4	3.0	4.3
		Wet Density (pcf)	136.9	132.4	136.0	137.3	135.9	134.8	135.0	135.0	134.4	132.4
		Dry Density (pcf)	132.8	128.6	131.8	133.1	131.5	129.9	130.9	130.5	130.5	126.9
HMA	East	Oil Content (%)	4.6	4.8	4.5	4.1	3.8	4.8	4.5	5.4	4.4	4.9
		Wet Density (pcf)	141.9	142.1	142.7	141.6	142.8	140.5	138.4	133.7	138.6	140.9
	West	Oil Content (%)	5.5	5.5	4.9	5.2	5.4	4.9	5.6	5.6	5.2	5.9
		Wet Density (pcf)	134.4	136.0	137.9	137.8	135.5	133.8	132.1	134.7	136.5	135.1

Table C-2: SSG Results for Subgrade and Base Layers at Orem Site

Layer	Location	SSG Modulus (ksi)									
		Section									
		1	2	3	4	5	6	7	8	9	10
		Without Geogrid	With Geogrid	Without Geogrid	With Geogrid	Without Geogrid	With Geogrid	Without Geogrid	With Geogrid	Without Geogrid	With Geogrid
Subgrade	East	8.9	8.4	10.6	12.8	8.0	9.1	18.8	10.6	11.6	9.7
	West	11.5	8.1	14.7	14.8	12.3	9.0	12.0	7.3	14.5	9.7
Base	East	19.7	16.4	16.0	19.6	18.9	18.7	20.9	18.4	18.4	15.9
	West	15.2	16.4	17.0	15.9	15.9	16.0	16.9	16.2	15.4	15.8

Table C-3: CIST CIV Results for Subgrade and Base Layers at Orem Site

Layer	Location	CIST CIV									
		Section									
		1	2	3	4	5	6	7	8	9	10
		Without Geogrid	With Geogrid	Without Geogrid	With Geogrid	Without Geogrid	With Geogrid	Without Geogrid	With Geogrid	Without Geogrid	With Geogrid
Subgrade	East	5.3	4.7	3.0	9.3	3.3	5.8	6.9	1.5	4.2	5.0
	West	11.4	13.9	16.7	9.4	8.9	4.7	9.4	6.6	13.6	7.8
Base	East	21.7	22.6	31.1	29.0	28.0	24.4	18.7	28.0	21.9	31.9
	West	23.8	25.6	25.9	35.0	34.0	29.2	26.3	30.5	42.0	22.3

Table C-4: CIST Modulus Results for Subgrade and Base Layers at Orem Site

Layer	Location	CIST Modulus (ksi)									
		Section									
		1	2	3	4	5	6	7	8	9	10
		Without Geogrid	With Geogrid	Without Geogrid	With Geogrid	Without Geogrid	With Geogrid	Without Geogrid	With Geogrid	Without Geogrid	With Geogrid
Subgrade	East	0.9	0.7	0.3	2.9	0.4	1.1	1.6	0.1	0.6	0.8
	West	4.4	6.5	9.4	3.0	2.7	0.7	3.0	1.5	6.2	2.0
Base	East	15.8	17.1	22.5	28.2	26.3	20.0	11.7	26.3	16.1	34.2
	West	19.0	22.0	32.5	41.1	38.8	28.6	23.2	31.2	59.2	16.7

Table C-5: DCP Results for Subgrade and Base Layers at Orem Site

Layer	Measurement	DCP Results									
		Section									
		1	2	3	4	5	6	7	8	9	10
		Without Geogrid	With Geogrid	Without Geogrid	With Geogrid	Without Geogrid	With Geogrid	Without Geogrid	With Geogrid	Without Geogrid	With Geogrid
August 2014											
Subgrade	Penetration Rate (mm/blow)	5.0	4.6	4.7	4.7	4.6	4.6	4.3	4.3	4.8	4.7
	CBR (%)	47.9	53.0	52.1	52.2	53.5	53.5	56.9	57.3	50.0	51.6
	Modulus (ksi)	30.3	32.4	32.0	32.0	32.6	32.6	33.9	34.0	31.2	31.8
Base	Penetration Rate (mm/blow)	13.2	12.1	8.1	12.6	4.5	6.3	6.6	6.6	-	3.9
	CBR (%)	16.3	18.0	27.9	17.1	54.2	36.9	35.1	35.1	-	63.6
	Modulus (ksi)	15.2	16.2	21.5	15.7	32.8	25.7	24.9	24.9	-	36.4
October 2015											
Subgrade	Penetration Rate (mm/blow)	2.2	1.8	1.8	2.7	2.4	2.3	2.0	1.5	3.8	4.4
	CBR (%)	121.1	154.8	154.1	96.3	111.9	112.8	136.7	189.2	65.8	55.6
	Modulus (ksi)	54.9	64.3	64.1	47.4	52.2	52.5	59.4	73.1	37.2	33.4
Base	Penetration Rate (mm/blow)	1.3	1.1	1.0	1.3	1.5	1.1	0.8	1.3	2.4	2.0
	CBR (%)	209.6	268.5	301.4	220.0	181.5	260.7	386.5	226.1	109.3	136.4
	Modulus (ksi)	78.0	91.4	98.5	80.5	71.2	89.7	115.4	81.9	51.4	59.3

Table C-6: PFWD Results for HMA Layer at Orem Site

Location	Drop	PFWD HMA Modulus (ksi)									
		Section									
		1	2	3	4	5	6	7	8	9	10
		Without Geogrid	With Geogrid	Without Geogrid	With Geogrid	Without Geogrid	With Geogrid	Without Geogrid	With Geogrid	Without Geogrid	With Geogrid
September 2014											
East	1	185.9	175.5	206.4	205.7	189.1	183.3	198.7	182.1	197.1	176.7
	2	192.6	198.8	175.5	213.8	184.2	183.1	202.4	188.7	199.3	176.5
	3	198.3	187.9	176.9	193.8	197.6	180.0	198.2	189.6	194.3	179.0
West	1	186.2	365.7	186.4	223.6	152.6	163.2	148.4	136.7	146.0	155.5
	2	193.8	275.7	189.1	216.0	143.6	158.9	149.0	135.1	143.1	151.1
	3	192.5	277.2	195.1	222.0	150.9	159.5	152.5	135.7	133.0	154.1
November 2014											
East	1	678.7	657.7	774.3	940.5	795.7	621.8	716.5	697.4	923.3	628.7
	2	692.7	60.7	736.6	925.2	775.2	622.2	689.1	654.4	809.2	1049.8
	3	656.8	787.4	835.0	788.2	613.0	616.6	744.2	652.7	889.3	1267.7
West	1	829.9	1259.9	701.1	1086.7	546.1	645.6	636.2	1167.6	757.4	863.0
	2	869.7	1511.7	688.5	758.8	545.9	636.1	635.6	1321.5	636.7	928.0
	3	875.8	1006.1	721.0	627.7	568.4	599.7	593.6	945.2	635.0	711.6
May 2015											
East	1	432.1	450.0	371.0	532.1	530.3	351.0	401.6	313.5	486.3	285.5
	2	418.3	439.6	356.7	417.5	455.0	352.9	382.7	314.4	463.4	354.6
	3	426.8	422.6	357.4	393.0	509.0	347.5	392.3	298.5	473.4	332.0
West	1	435.8	556.3	640.5	441.5	312.7	287.8	351.7	314.2	309.9	371.4
	2	446.9	708.4	395.0	399.4	313.6	310.5	342.1	311.9	305.6	363.0
	3	420.5	473.7	405.5	376.7	299.3	325.2	329.7	317.2	313.3	385.1

Table C-7: PFWD Results for Base Layer at Orem Site

Location	Drop	PFWD Base Modulus (ksi)									
		Section									
		1	2	3	4	5	6	7	8	9	10
		Without Geogrid	With Geogrid	Without Geogrid	With Geogrid	Without Geogrid	With Geogrid	Without Geogrid	With Geogrid	Without Geogrid	With Geogrid
September 2014											
East	1	49.3	55.8	50.1	64.9	59.2	58.6	63.2	58.3	62.2	57.2
	2	49.4	51.8	54.7	60.6	58.3	57.3	64.5	60.1	62.7	56.4
	3	49.6	58.8	56.9	61.4	56.7	57.6	64.4	59.7	61.6	56.9
West	1	74.1	72.0	69.1	68.9	50.5	53.5	60.5	53.7	48.2	51.4
	2	76.9	67.8	67.4	67.6	54.4	53.0	58.9	53.5	47.1	50.0
	3	75.6	67.7	63.2	69.1	50.0	52.7	59.1	54.7	51.2	50.7
November 2014											
East	1	185.6	181.0	154.9	184.7	221.5	177.7	198.6	188.8	178.2	149.6
	2	178.7	183.4	181.6	178.2	215.3	177.5	204.3	196.7	198.5	201.6
	3	172.8	156.4	165.8	210.6	205.5	179.4	207.9	191.3	175.4	236.0
West	1	256.9	236.0	192.5	208.3	147.9	167.1	189.7	217.2	151.5	169.5
	2	257.5	277.9	199.3	214.2	157.2	159.4	194.0	244.4	162.1	178.6
	3	255.6	246.1	201.6	189.4	152.9	170.6	194.1	183.1	165.8	184.8
May 2015											
East	1	94.9	99.2	102.0	115.3	114.5	103.2	117.8	110.3	106.4	91.0
	2	91.7	98.1	98.3	123.6	122.3	102.2	116.9	110.6	101.5	92.4
	3	93.5	92.2	100.0	115.0	111.7	97.4	123.1	115.2	103.9	96.1
West	1	171.7	143.2	135.6	118.7	89.9	90.3	108.8	99.0	102.1	103.8
	2	179.6	148.4	113.6	115.9	94.0	94.2	109.7	98.8	95.5	104.7
	3	170.4	135.3	114.9	116.2	94.0	89.7	108.0	98.6	94.2	101.9

Table C-8: PFWD Results for Subgrade Layer at Orem Site

Location	Drop	PFWD Subgrade Modulus (ksi)									
		Section									
		1	2	3	4	5	6	7	8	9	10
		Without Geogrid	With Geogrid	Without Geogrid	With Geogrid	Without Geogrid	With Geogrid	Without Geogrid	With Geogrid	Without Geogrid	With Geogrid
September 2014											
East	1	11.7	10.9	11.7	15.2	18.6	17.2	17.4	15.4	15.4	14.5
	2	11.7	10.7	11.6	15.4	18.4	17.0	17.0	15.1	15.0	14.6
	3	11.8	10.6	11.5	15.4	18.5	17.1	17.0	15.0	15.2	14.5
West	1	17.5	13.4	16.4	17.4	22.3	20.8	20.5	18.5	16.7	17.9
	2	17.7	13.9	16.5	17.5	22.3	20.8	20.4	18.2	16.4	18.1
	3	18.0	13.9	16.4	17.5	22.4	20.5	20.3	18.2	16.5	18.1
November 2014											
East	1	14.7	13.5	12.8	16.2	21.8	19.5	19.9	17.1	14.9	16.0
	2	14.6	13.9	13.4	15.5	22.2	19.4	20.1	16.8	14.8	14.2
	3	14.7	13.3	13.4	16.2	22.8	19.6	19.8	16.9	14.9	13.3
West	1	19.1	16.1	16.6	17.6	22.9	21.0	20.7	15.6	15.1	17.3
	2	19.1	15.3	16.7	18.5	23.1	21.3	20.8	15.2	15.3	17.1
	3	18.8	16.5	16.5	19.4	23.1	21.2	20.8	16.5	15.4	17.5
May 2015											
East	1	12.5	11.5	12.0	14.3	18.3	16.3	17.7	15.4	13.8	14.3
	2	12.5	11.3	12.1	14.4	18.1	16.5	17.5	15.1	13.9	13.3
	3	12.5	11.6	12.0	14.6	18.3	16.7	17.8	15.2	14.0	14.1
West	1	19.6	16.2	14.6	17.1	20.3	19.6	19.9	17.2	15.1	16.3
	2	19.4	15.7	16.2	17.4	20.1	19.2	19.8	17.1	15.2	16.3
	3	19.7	16.4	16.3	17.5	20.4	19.5	18.6	17.1	15.3	16.3

Table C-9: FWD Results for HMA Layer at Orem Site

Applied Load (lb)	Drop	FWD HMA Modulus (ksi)									
		Section									
		1	2	3	4	5	6	7	8	9	10
		Without Geogrid	With Geogrid	Without Geogrid	With Geogrid	Without Geogrid	With Geogrid	Without Geogrid	With Geogrid	Without Geogrid	With Geogrid
8,000	1	1205.7	1152.0	941.6	1018.4	1155.8	984.6	997.8	799.2	1142.5	1028.8
	2	1188.0	1198.7	949.7	1060.2	1220.2	967.1	987.1	843.1	1096.1	1060.7
	3	1251.1	1227.7	949.7	1054.9	1208.8	1005.2	1013.5	857.8	1159.1	1055.5
10,000	1	1267.0	1293.6	991.4	1126.3	1257.8	978.6	1017.1	864.2	1307.7	1085.4
	2	1194.0	1304.6	1002.5	1170.6	1256.0	1027.1	1053.5	867.1	1155.1	1079.8
	3	1193.8	1262.3	1001.7	1095.7	1252.8	1020.9	985.4	863.8	1081.2	1107.7
12,000	1	1339.2	1316.2	1023.1	1136.2	1335.7	1045.7	1064.6	938.3	1154.4	1129.1
	2	1325.0	1310.7	1083.1	1198.5	1328.7	1164.8	1055.9	938.3	1199.6	1156.0
	3	1289.1	1268.0	1079.2	1174.4	1300.9	1030.2	1073.4	963.4	1203.5	1103.9
14,000	1	1321.3	1309.5	1127.1	1214.1	1333.5	1112.6	1086.3	935.1	1151.3	1158.4
	2	1302.8	1324.1	1129.2	1167.1	1328.3	1050.1	1018.0	933.1	1121.0	1115.5
	3	1255.6	1285.9	1115.8	1220.1	1371.8	1081.8	1082.6	925.3	1165.3	1133.5
16,000	1	1292.4	1409.7	1063.5	1295.7	1512.5	1051.7	1029.7	896.3	1259.7	1187.7
	2	1283.5	1364.7	1139.0	1144.2	1380.8	1065.9	1041.3	866.2	1204.1	1187.7
	3	994.7	1376.5	1053.7	1156.8	1369.6	1151.6	1050.4	957.7	1201.7	1158.4

Table C-10: FWD Results for Base Layer at Orem Site

Applied Load (lb)	Drop	FWD Base Modulus (ksi)									
		Section									
		1	2	3	4	5	6	7	8	9	10
		Without Geogrid	With Geogrid	Without Geogrid	With Geogrid	Without Geogrid	With Geogrid	Without Geogrid	With Geogrid	Without Geogrid	With Geogrid
8,000	1	75.2	79.3	77.3	85.9	97.9	90.9	98.6	83.5	69.0	78.6
	2	76.5	79.2	79.1	89.1	100.0	93.9	98.6	80.6	70.1	79.4
	3	78.4	79.3	79.1	89.5	98.7	90.6	96.9	80.5	67.5	78.7
10,000	1	77.9	79.7	78.8	89.7	101.0	94.1	97.2	80.0	64.0	80.4
	2	80.3	76.4	79.4	87.7	99.2	88.7	96.5	81.1	71.8	82.6
	3	81.1	77.8	76.9	89.9	104.2	90.1	101.3	79.7	75.7	80.4
12,000	1	59.2	78.7	79.9	87.6	102.9	92.5	97.3	81.1	68.7	78.3
	2	73.6	78.0	75.6	87.7	97.9	66.4	100.1	81.0	69.7	81.7
	3	78.0	78.8	74.0	88.5	102.3	94.5	95.6	76.1	68.1	82.6
14,000	1	74.2	81.3	73.5	88.0	103.7	87.9	97.8	78.4	72.0	78.1
	2	74.9	80.1	72.3	89.7	103.4	92.5	101.8	75.4	72.5	82.6
	3	78.7	82.1	70.9	84.8	102.1	91.5	93.1	77.2	69.1	79.8
16,000	1	76.4	74.7	74.3	78.5	96.2	91.2	98.4	79.4	64.2	76.2
	2	74.0	77.3	71.1	90.2	104.6	90.3	98.2	82.3	69.4	76.2
	3	75.7	76.8	74.7	90.5	105.6	84.3	96.8	78.1	70.2	80.9

Table C-11: FWD Results for Subgrade Layer at Orem Site

Applied Load (lb)	Drop	FWD Subgrade Modulus (ksi)									
		Section									
		1	2	3	4	5	6	7	8	9	10
		Without Geogrid	With Geogrid	Without Geogrid	With Geogrid	Without Geogrid	With Geogrid	Without Geogrid	With Geogrid	Without Geogrid	With Geogrid
8,000	1	18.0	16.0	15.6	21.6	27.4	26.4	27.0	21.4	18.0	19.4
	2	17.7	15.9	15.7	21.6	27.4	26.8	27.4	21.2	18.1	19.6
	3	17.8	16.0	15.8	21.6	27.4	27.1	27.5	21.1	18.1	19.8
10,000	1	17.6	15.8	15.5	21.3	27.4	26.7	27.5	21.2	17.9	19.8
	2	17.5	15.9	15.6	21.1	27.3	26.9	27.1	21.0	18.0	19.5
	3	17.7	15.9	15.6	21.2	27.3	27.1	27.0	21.0	17.9	19.7
12,000	1	18.4	15.8	15.3	21.2	27.1	26.7	27.2	20.8	17.8	19.7
	2	17.4	15.8	15.2	20.9	27.3	26.7	26.7	20.5	17.6	19.4
	3	17.2	15.8	15.3	21.0	27.1	26.5	26.7	20.9	17.9	19.3
14,000	1	17.2	15.6	15.1	20.8	27.3	26.9	26.6	20.6	17.6	19.4
	2	17.1	15.6	15.1	20.7	27.4	26.5	26.4	20.7	17.5	19.3
	3	17.0	15.6	15.3	20.8	27.2	26.4	26.6	20.4	17.6	19.5
16,000	1	17.1	15.9	15.1	20.8	27.6	26.7	26.4	20.6	17.8	19.5
	2	17.2	15.8	15.1	20.6	27.3	26.6	26.3	20.3	17.5	19.5
	3	17.4	15.7	15.0	20.3	27.3	26.5	26.1	20.3	17.5	19.2

C.2 Springville Field Site

The following Tables C-12 through C-22 present data recorded or calculated for the Springville field site.

Table C-12: NDG Results for Subgrade, Base, and HMA Layers at Springville Site

Layer	Location	Measurement	NDG Results									
			Section									
			1	2	3	4	5	6	7	8	9	10
			Without Geogrid	With Geogrid	Without Geogrid	With Geogrid	Without Geogrid	With Geogrid	Without Geogrid	With Geogrid	Without Geogrid	With Geogrid
Subgrade	East	Moisture (%)	5.6	8.8	6.6	13.9	6.6	8.1	8.4	8.8	8.5	8.0
		Wet Density (pcf)	135.6	137.1	132.1	126.7	137.7	142.3	141.1	144.6	140.9	140.0
		Dry Density (pcf)	128.4	126.0	124.0	111.3	129.2	131.7	130.2	132.9	129.9	129.6
	West	Moisture (%)	7.4	7.4	18.9	16.7	14.4	6.7	8.9	8.5	8.9	5.8
		Wet Density (pcf)	125.7	125.9	122.5	121.6	126.6	133.4	141.8	139.2	137.8	142.7
		Dry Density (pcf)	117.0	117.2	103.0	104.2	110.7	125.0	130.1	128.3	126.5	134.9
Base	East	Moisture (%)	4.0	3.5	3.2	4.7	3.6	4.8	3.3	3.7	4.9	3.5
		Wet Density (pcf)	128.0	130.2	131.1	128.5	129.4	130.4	130.6	132.4	127.5	128.2
		Dry Density (pcf)	123.0	125.8	127.1	122.8	125.0	124.4	126.3	127.7	121.5	123.9
	West	Moisture (%)	2.9	2.7	3.5	2.9	3.7	3.9	3.5	3.5	3.8	4.4
		Wet Density (pcf)	125.1	129.4	128.8	131.1	128.3	128.5	131.1	130.0	130.8	130.1
		Dry Density (pcf)	121.6	126.1	124.5	127.5	123.7	12.7	126.8	125.6	126.0	124.7
HMA	East	Wet Density (pcf)	128.6	131.4	135.1	135.4	132.7	132.9	131.7	131.5	131.8	132.1
	West	Wet Density (pcf)	130.1	134.3	133.0	131.4	132.5	132.0	132.1	134.1	137.9	132.5

Table C-13: SSG Results for Subgrade and Base Layers at Springville Site

Layer	Location	SSG Modulus (ksi)									
		Section									
		1	2	3	4	5	6	7	8	9	10
		Without Geogrid	With Geogrid	Without Geogrid	With Geogrid	Without Geogrid	With Geogrid	Without Geogrid	With Geogrid	Without Geogrid	With Geogrid
Subgrade	East	7.1	13.2	9.0	9.0	15.2	8.5	8.0	21.8	5.2	13.7
	West	12.8	14.2	13.3	13.7	13.2	8.8	9.9	9.0	19.1	18.0
Base	East	6.6	5.2	5.3	7.5	8.4	5.3	7.2	6.7	6.0	8.0
	West	5.6	7.1	7.0	6.7	6.3	6.4	5.5	4.8	5.1	6.3

Table C-14: CIST CIV Results for Subgrade and Base Layers at Springville Site

Layer	Location	CIST CIV									
		Section									
		1	2	3	4	5	6	7	8	9	10
		Without Geogrid	With Geogrid	Without Geogrid	With Geogrid	Without Geogrid	With Geogrid	Without Geogrid	With Geogrid	Without Geogrid	With Geogrid
Subgrade	East	8.4	6.6	3.8	9.2	4.7	4.3	4.8	7.6	9.0	7.7
	West	9.1	7.7	6.6	6.5	4.4	6.2	4.6	5.9	7.5	5.0
Base	East	13.0	14.2	19.0	14.6	16.4	11.9	13.4	13.3	10.7	10.5
	West	17.7	13.1	13.7	12.4	11.2	11.8	15.9	12.8	8.8	15.8

Table C-15: CIST Modulus Results for Subgrade and Base Layers at Springville Site

Layer	Location	CIST Modulus (ksi)									
		Section									
		1	2	3	4	5	6	7	8	9	10
		Without Geogrid	With Geogrid	Without Geogrid	With Geogrid	Without Geogrid	With Geogrid	Without Geogrid	With Geogrid	Without Geogrid	With Geogrid
Subgrade	East	2.4	1.5	0.5	2.8	0.7	0.6	0.8	1.9	2.7	2.0
	West	2.8	2.0	1.5	1.4	0.6	1.3	0.7	1.2	1.9	0.8
Base	East	5.7	6.8	12.1	7.2	9.0	4.8	6.0	5.9	3.8	3.7
	West	10.5	5.8	6.3	5.2	4.2	4.7	8.5	5.5	2.6	8.4

Table C-16: DCP Results for Subgrade and Base Layers at Springville Site

Layer	Measurement	DCP Results									
		Section									
		1	2	3	4	5	6	7	8	9	10
		Without Geogrid	With Geogrid	Without Geogrid	With Geogrid	Without Geogrid	With Geogrid	Without Geogrid	With Geogrid	Without Geogrid	With Geogrid
Subgrade	Penetration Rate (mm/blow)	11.7	12.9	13.3	17.5	25.5	16.0	17.5	37.0	27.8	13.3
	CBR (%)	18.6	16.7	16.2	11.8	7.8	13.1	11.8	5.1	7.0	16.1
	Modulus (ksi)	16.6	15.5	15.1	12.4	9.5	13.2	12.4	7.2	8.9	15.1
Base	Penetration Rate (mm/blow)	28.2	15.3	13.6	17.5	18.4	19.1	25.5	47.7	43.7	19.8
	CBR (%)	6.9	13.7	15.7	11.8	11.2	10.7	7.8	3.9	4.3	10.3
	Modulus (ksi)	8.8	13.6	14.8	12.4	12.0	11.6	9.5	6.0	6.4	11.4

Table C-17: PFWD Results for HMA Layer at Springville Site

Location	Drop	PFWD HMA Modulus (ksi)									
		Section									
		1	2	3	4	5	6	7	8	9	10
		Without Geogrid	With Geogrid	Without Geogrid	With Geogrid	Without Geogrid	With Geogrid	Without Geogrid	With Geogrid	Without Geogrid	With Geogrid
November 2014											
East	1	246.9	380.9	353.4	174.0	372.1	1088.4	450.1	791.3	375.8	881.0
	2	237.6	379.4	363.4	192.9	373.0	1134.3	446.8	828.5	389.5	898.4
	3	253.6	369.6	365.4	203.3	377.2	1146.4	455.8	823.2	373.2	921.7
West	1	383.4	436.0	186.2	222.6	237.7	648.4	476.9	546.3	642.1	356.9
	2	382.2	444.5	209.6	229.4	239.5	679.5	505.1	541.9	637.3	391.3
	3	388.1	436.3	210.9	237.1	240.3	651.0	501.9	557.7	637.6	383.2
May 2015											
East	1	176.3	293.0	329.2	180.0	181.0	331.6	176.6	186.3	152.4	256.7
	2	161.0	305.1	320.3	181.3	197.3	335.8	173.8	203.0	162.7	259.9
	3	183.9	271.8	313.5	178.7	179.6	315.6	165.7	195.4	162.8	256.5
West	1	191.6	341.0	222.1	140.8	111.1	230.5	146.0	193.7	463.8	218.0
	2	194.3	357.5	238.1	140.4	110.6	226.6	138.4	191.6	425.5	221.0
	3	203.1	358.9	235.2	151.8	112.7	231.1	149.2	199.0	434.3	221.2

Table C-18: PFWD Results for Base Layer at Springville Site

Location	Drop	PFWD Base Modulus (ksi)									
		Section									
		1	2	3	4	5	6	7	8	9	10
		Without Geogrid	With Geogrid	Without Geogrid	With Geogrid	Without Geogrid	With Geogrid	Without Geogrid	With Geogrid	Without Geogrid	With Geogrid
November 2014											
East	1	31.3	36.7	33.9	23.9	35.4	36.5	25.5	42.6	25.5	43.6
	2	36.3	35.9	34.2	24.5	35.5	37.2	26.1	41.9	25.2	43.0
	3	33.6	35.5	35.1	24.7	36.3	35.8	26.0	42.1	26.4	44.3
West	1	37.6	41.7	25.7	25.4	27.6	31.3	33.9	36.1	40.4	26.9
	2	37.9	43.2	27.0	25.5	27.7	30.7	34.8	37.2	40.5	27.5
	3	37.8	42.7	28.2	26.3	28.4	31.9	34.1	36.5	40.4	27.1
May 2015											
East	1	22.6	28.5	30.3	24.7	24.7	16.7	16.3	20.7	17.5	24.8
	2	23.0	29.5	30.3	25.4	25.0	16.5	16.3	21.3	17.2	25.4
	3	23.1	30.4	30.1	25.9	26.9	16.2	17.1	21.9	17.5	25.0
West	1	27.0	32.5	26.6	25.0	19.2	18.0	16.2	19.8	28.9	20.7
	2	28.0	33.8	27.0	24.9	19.9	17.7	17.0	21.7	28.6	21.1
	3	28.6	34.0	28.0	24.6	19.7	17.5	16.8	21.8	27.8	21.0

Table C-19: PFWD Results for Subgrade Layer at Springville Site

Location	Drop	PFWD Subgrade Modulus (ksi)									
		Section									
		1	2	3	4	5	6	7	8	9	10
		Without Geogrid	With Geogrid	Without Geogrid	With Geogrid	Without Geogrid	With Geogrid	Without Geogrid	With Geogrid	Without Geogrid	With Geogrid
November 2014											
East	1	13.6	11.4	10.4	9.4	11.7	13.3	10.6	13.8	12.7	15.0
	2	13.2	11.5	10.5	9.4	11.7	13.4	10.4	13.8	12.6	15.0
	3	13.5	11.6	10.3	9.3	11.7	13.5	10.4	13.9	12.5	14.8
West	1	12.7	11.7	12.4	10.5	11.5	10.8	13.0	14.2	16.2	14.5
	2	12.6	11.6	12.5	10.3	11.4	10.7	13.0	14.1	16.2	14.3
	3	12.9	11.6	12.4	10.3	11.4	10.7	13.0	13.9	16.0	14.3
May 2015											
East	1	10.6	11.9	11.1	11.0	12.6	10.4	11.1	14.5	13.8	15.1
	2	10.2	12.0	11.7	10.9	12.5	10.3	11.0	14.2	13.7	14.9
	3	10.6	12.0	11.6	11.0	12.4	10.2	10.9	14.1	13.7	14.8
West	1	10.9	11.0	11.9	12.4	11.5	10.7	12.4	14.3	15.5	15.1
	2	11.2	11.2	12.1	12.4	11.6	10.8	12.4	14.5	15.6	15.3
	3	11.1	11.3	12.1	12.4	11.6	10.8	12.6	14.3	15.5	15.2

Table C-20: FWD Results for HMA Layer at Springville Site

Applied Load (lb)	Drop	FWD HMA Modulus (ksi)									
		Section									
		1	2	3	4	5	6	7	8	9	10
		Without Geogrid	With Geogrid	Without Geogrid	With Geogrid	Without Geogrid	With Geogrid	Without Geogrid	With Geogrid	Without Geogrid	With Geogrid
8,000	1	1132.0	1285.8	1059.4	644.3	1206.6	2354.2	1624.8	2083.5	1571.9	1449.6
	2	1110.6	1308.2	1068.7	660.2	1266.4	2294.2	1679.0	2251.4	1692.6	1558.8
	3	1122.3	1317.8	1061.7	675.0	1329.0	2308.6	1649.0	2180.6	1632.4	1591.0
10,000	1	1087.4	1249.5	958.3	646.5	1159.5	2207.4	1624.8	2197.8	1558.7	1493.2
	2	1035.7	1321.6	1078.7	611.7	1173.0	2207.4	1699.1	2155.3	1574.3	1592.2
	3	1088.3	1295.6	1113.7	621.8	1210.9	2213.0	1621.1	2131.1	1603.9	1485.4

Table C-21: FWD Results for Base Layer at Springville Site

Applied Load (lb)	Drop	FWD Base Modulus (ksi)									
		Section									
		1	2	3	4	5	6	7	8	9	10
		Without Geogrid	With Geogrid	Without Geogrid	With Geogrid	Without Geogrid	With Geogrid	Without Geogrid	With Geogrid	Without Geogrid	With Geogrid
8,000	1	37.0	33.7	28.6	22.0	27.4	20.1	25.1	28.7	31.5	38.0
	2	38.8	34.8	28.9	22.1	28.1	22.1	25.4	27.6	29.9	36.8
	3	38.9	34.8	29.6	22.2	27.4	21.0	26.7	29.4	30.8	37.5
10,000	1	36.2	33.5	30.0	21.1	26.9	21.4	25.1	27.3	29.9	38.0
	2	38.5	32.9	28.7	21.4	26.3	21.4	23.7	26.8	30.8	36.2
	3	38.4	34.1	28.9	22.0	27.4	21.6	24.7	28.1	29.1	38.6

Table C-22: FWD Results for Subgrade Layer at Springville Site

Applied Load (lb)	Drop	FWD Subgrade Modulus (ksi)									
		Section									
		1	2	3	4	5	6	7	8	9	10
		Without Geogrid	With Geogrid	Without Geogrid	With Geogrid	Without Geogrid	With Geogrid	Without Geogrid	With Geogrid	Without Geogrid	With Geogrid
8,000	1	13.3	11.7	11.3	9.0	10.0	8.5	10.6	11.4	13.0	15.0
	2	13.2	12.0	11.3	9.2	10.0	8.6	10.6	11.4	13.2	15.0
	3	13.3	11.8	11.3	9.2	10.2	8.5	10.6	11.5	13.2	15.1
10,000	1	13.3	11.5	10.9	9.1	9.8	8.3	10.3	11.0	12.9	15.0
	2	13.0	11.5	11.0	9.0	9.9	8.2	10.2	10.9	12.6	15.0
	3	13.0	11.5	10.9	9.0	9.9	8.1	10.1	10.8	12.7	14.9

C.3 Additional Springville Field Site

The following Tables C-23 through C-33 present data recorded or calculated for the additional Springville site.

Table C-23: NDG Results for Base and HMA Layers at Additional Springville Site

Layer	Location	Measurement	NDG Results					
			Section					
			1	2	3	4	5	6
			With Geogrid	With Geogrid	With Geogrid	Without Geogrid	Without Geogrid	Without Geogrid
Base	North	Moisture (%)	3.5	2.9	3.9	3.1	3.8	3.8
		Wet Density (pcf)	126.8	125.0	126.1	127.1	122.7	126.9
		Dry Density (pcf)	122.9	121.5	121.4	123.2	118.1	122.3
	South	Moisture (%)	3.1	2.7	3.0	3.1	3.4	3.3
		Wet Density (pcf)	128.0	126.3	128.5	125.1	119.4	123.6
		Dry Density (pcf)	124.1	123.0	124.8	121.3	115.4	119.6
HMA	North	Wet Density (pcf)	126.1	125.6	129.6	122.0	126.9	127.8
	South	Wet Density (pcf)	126.6	126.4	128.6	125.4	126.6	127.6

Table C-24: SSG Results for Base Layer at Additional Springville Site

Layer	Location	SSG Modulus (ksi)					
		Section					
		1	2	3	4	5	6
		With Geogrid	With Geogrid	With Geogrid	Without Geogrid	Without Geogrid	Without Geogrid
Base	North	8.7	7.4	8.5	6.9	5.2	6.8
	South	8.2	7.4	10.5	8.8	8.4	7.6

Table C-25: CIST CIV Results for Base Layer at Additional Springville Site

Layer	Location	CIST CIV					
		Section					
		1	2	3	4	5	6
		With Geogrid	With Geogrid	With Geogrid	Without Geogrid	Without Geogrid	Without Geogrid
Base	North	14.6	13.9	10.8	15.2	15.9	20.4
	South	14.4	22.7	9.3	21.9	10.4	13.9

Table C-26: CIV Modulus Results for Base Layer at Additional Springville Site

Layer	Location	CIST Modulus (ksi)					
		Section					
		1	2	3	4	5	6
		With Geogrid	With Geogrid	With Geogrid	Without Geogrid	Without Geogrid	Without Geogrid
Base	North	7.2	6.5	3.9	7.8	8.5	14.0
	South	7.0	17.3	2.9	16.1	3.6	6.5

Table C-27: DCP Results for Subgrade and Base Layers at Additional Springville Site

Layer	Measurement	DCP Results					
		Section					
		1	2	3	4	5	6
		With Geogrid	With Geogrid	With Geogrid	Without Geogrid	Without Geogrid	Without Geogrid
Subgrade	Penetration Rate (mm/blow)	14.4	23.5	29.0	19.3	19.1	24.1
	CBR (%)	14.8	8.5	6.7	10.6	10.7	8.3
	Modulus (ksi)	14.3	10.0	8.6	11.6	11.6	9.9
Base	Penetration Rate (mm/blow)	8.1	18.7	12.7	22.4	23.9	9.0
	CBR (%)	28.3	11.0	17.0	9.0	8.4	24.8
	Modulus (ksi)	21.6	11.8	15.6	10.4	9.9	19.9

Table C-28: PFWD Results for HMA Layer at Additional Springville Site

Location	Drop	PFWD HMA Modulus (ksi)					
		Section					
		1	2	3	4	5	6
		With Geogrid	With Geogrid	With Geogrid	Without Geogrid	Without Geogrid	Without Geogrid
November 2014							
East	1	425.0	527.4	383.3	521.4	544.3	427.4
	2	432.3	511.8	382.5	491.0	544.4	426.0
	3	404.9	508.4	373.6	437.2	544.3	445.1
West	1	645.5	530.0	1036.0	1082.3	1135.9	699.2
	2	649.5	512.5	913.1	1081.8	1124.5	675.4
	3	676.8	517.8	962.2	957.1	1068.6	715.1
May 2015							
East	1	176.3	293.0	329.2	180.0	181.0	331.6
	2	161.0	305.1	320.3	181.3	197.3	335.8
	3	183.9	271.8	313.5	178.7	179.6	315.6
West	1	191.6	341.0	222.1	140.8	111.1	230.5
	2	194.3	357.5	238.1	140.4	110.6	226.6
	3	203.1	358.9	235.2	151.8	112.7	231.1

Table C-29 PFWD Results for Base Layer at Additional Springville Site

Location	Drop	PFWD Base Modulus (ksi)					
		Section					
		1	2	3	4	5	6
		With Geogrid	With Geogrid	With Geogrid	Without Geogrid	Without Geogrid	Without Geogrid
November 2014							
East	1	51.8	50.0	36.8	38.0	39.3	41.5
	2	50.8	49.3	36.5	39.2	39.1	41.3
	3	53.0	49.2	35.6	41.4	39.4	42.3
West	1	59.3	50.5	58.2	48.3	52.7	45.8
	2	63.7	48.4	59.5	51.1	53.4	47.6
	3	62.3	49.5	58.5	51.0	53.7	46.8
May 2015							
East	1	22.6	28.5	30.3	24.7	24.7	16.7
	2	23.0	29.5	30.3	25.4	25.0	16.5
	3	23.1	30.4	30.1	25.9	26.9	16.2
West	1	27.0	32.5	26.6	25.0	19.2	18.0
	2	28.0	33.8	27.0	24.9	19.9	17.7
	3	28.6	34.0	28.0	24.6	19.7	17.5

Table C-30: PFWD Results for Subgrade Layer at Additional Springville Site

Location	Drop	PFWD Subgrade Modulus (ksi)					
		Section					
		1	2	3	4	5	6
		With Geogrid	With Geogrid	With Geogrid	Without Geogrid	Without Geogrid	Without Geogrid
November 2014							
East	1	8.7	8.7	8.4	9.6	7.9	9.2
	2	8.6	8.8	8.4	9.8	7.9	9.2
	3	8.8	8.9	8.3	9.8	7.9	9.2
West	1	9.6	9.6	10.1	9.3	8.6	9.6
	2	9.5	9.7	10.2	9.3	8.6	9.6
	3	9.6	9.7	10.2	9.4	8.5	9.8
May 2015							
East	1	10.6	11.9	11.1	11.0	12.6	10.4
	2	10.2	12.0	11.7	10.9	12.5	10.3
	3	10.6	12.0	11.6	11.0	12.4	10.2
West	1	10.9	11.0	11.9	12.4	11.5	10.7
	2	11.2	11.2	12.1	12.4	11.6	10.8
	3	11.1	11.3	12.1	12.4	11.6	10.8

Table C-31: FWD Results for HMA Layer at Additional Springville Site

Applied Load (lb)	Location	Drop	FWD HMA Modulus (ksi)					
			Section					
			1	2	3	4	5	6
			With Geogrid	With Geogrid	With Geogrid	Without Geogrid	Without Geogrid	Without Geogrid
8,000	North	1	530.6	1203.7	480.5	727.4	976.0	564.7
		2	565.7	1246.0	504.5	727.5	1008.5	608.0
		3	601.6	1232.2	497.2	781.7	992.8	617.5
	South	1	673.0	682.1	436.9	962.1	992.1	628.0
		2	685.6	753.0	457.2	1003.8	972.6	705.0
		3	701.4	697.9	472.5	1029.8	1061.0	693.9
10,000	North	1	636.1	1158.0	518.4	869.9	1076.8	682.1
		2	630.8	1238.6	550.1	855.8	1162.3	677.7
		3	638.3	1307.2	574.7	848.1	1138.8	708.4
	South	1	757.7	709.6	517.4	1066.9	1042.6	728.3
		2	766.5	787.8	503.4	1100.1	1170.1	741.4
		3	781.4	775.6	508.2	986.0	1093.1	725.1

Table C-32: FWD Results for Base Layer at Additional Springville Site

Applied Load (lb)	Location	Drop	FWD Base Modulus (ksi)					
			Section					
			1	2	3	4	5	6
			With Geogrid	With Geogrid	With Geogrid	Without Geogrid	Without Geogrid	Without Geogrid
8,000	North	1	37.4	37.0	29.1	27.9	29.9	19.5
		2	36.7	36.7	29.0	28.9	30.6	19.7
		3	37.1	37.6	30.2	28.8	31.5	20.0
	South	1	30.7	31.7	19.3	28.5	25.5	25.4
		2	31.3	32.0	19.5	28.8	26.3	25.2
		3	31.9	33.4	19.5	29.2	26.3	25.9
10,000	North	1	36.0	37.3	27.7	26.8	28.6	18.9
		2	36.3	37.0	27.6	26.9	27.3	18.6
		3	36.7	36.3	26.7	27.1	28.2	18.3
	South	1	30.2	32.7	18.9	26.1	25.0	24.1
		2	30.3	31.7	18.5	25.2	24.3	24.5
		3	30.3	31.1	18.6	26.4	25.1	24.6

Table C-33: FWD Results for Subgrade Layer at Additional Springville Site

Applied Load (lb)	Location	Drop	FWD Subgrade Modulus (ksi)					
			Section					
			1	2	3	4	5	6
			With Geogrid	With Geogrid	With Geogrid	Without Geogrid	Without Geogrid	Without Geogrid
8,000	North	1	10.7	11.6	9.7	9.0	9.6	7.0
		2	10.5	11.4	9.5	8.8	9.6	7.0
		3	10.6	11.3	9.7	8.8	9.6	6.9
	South	1	9.5	9.4	7.8	8.6	8.7	8.4
		2	9.5	9.3	7.8	8.6	8.6	8.5
		3	9.5	9.2	7.7	8.7	8.5	8.4
10,000	North	1	10.2	11.1	9.2	8.7	9.2	6.7
		2	10.2	11.1	9.1	8.5	9.1	6.5
		3	10.2	11.1	9.1	8.5	8.9	6.5
	South	1	9.5	9.4	7.4	8.3	8.4	8.2
		2	9.4	9.3	7.3	8.1	8.3	8.0
		3	9.3	9.3	7.1	8.0	8.2	7.9

APPENDIX D BACKCALCULATION PROCESS

Example BAKFAA screen shots and detailed inputs for the two-step process applied to the PFWD and FWD data analyses are presented in this appendix. Example screen shots are presented in Figures D-1 through D-8, and detailed inputs for the Orem, Springville, and additional Springville field sites are provided in the following sections. Inputs that were not applicable (N/A) in specific cases are marked in the tables.

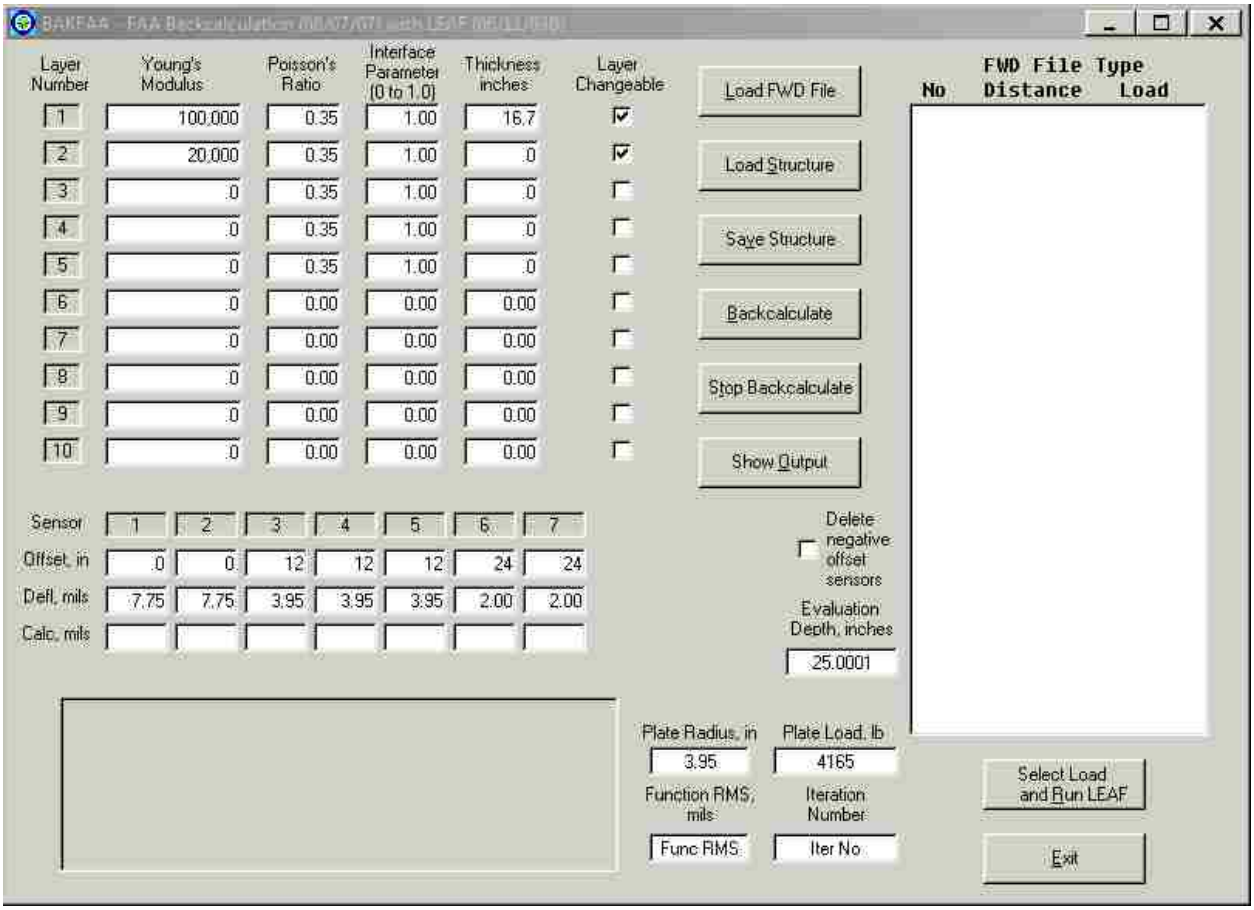

Figure D-1: Example seed modulus values for step one of the two-step backcalculation process for PFWD data.

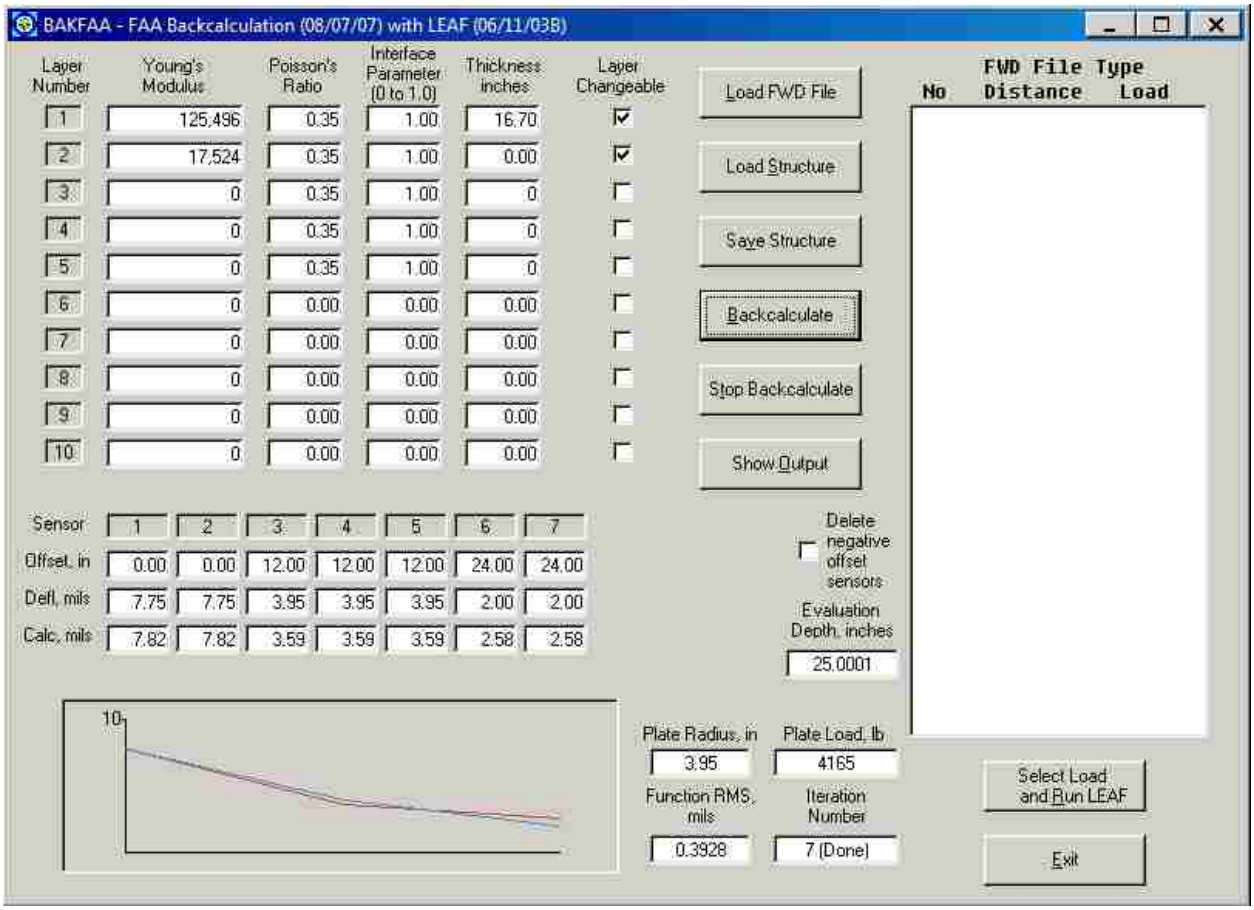

Figure D-2: Example calculated modulus values for step one of the two-step backcalculation process for PFWD data.

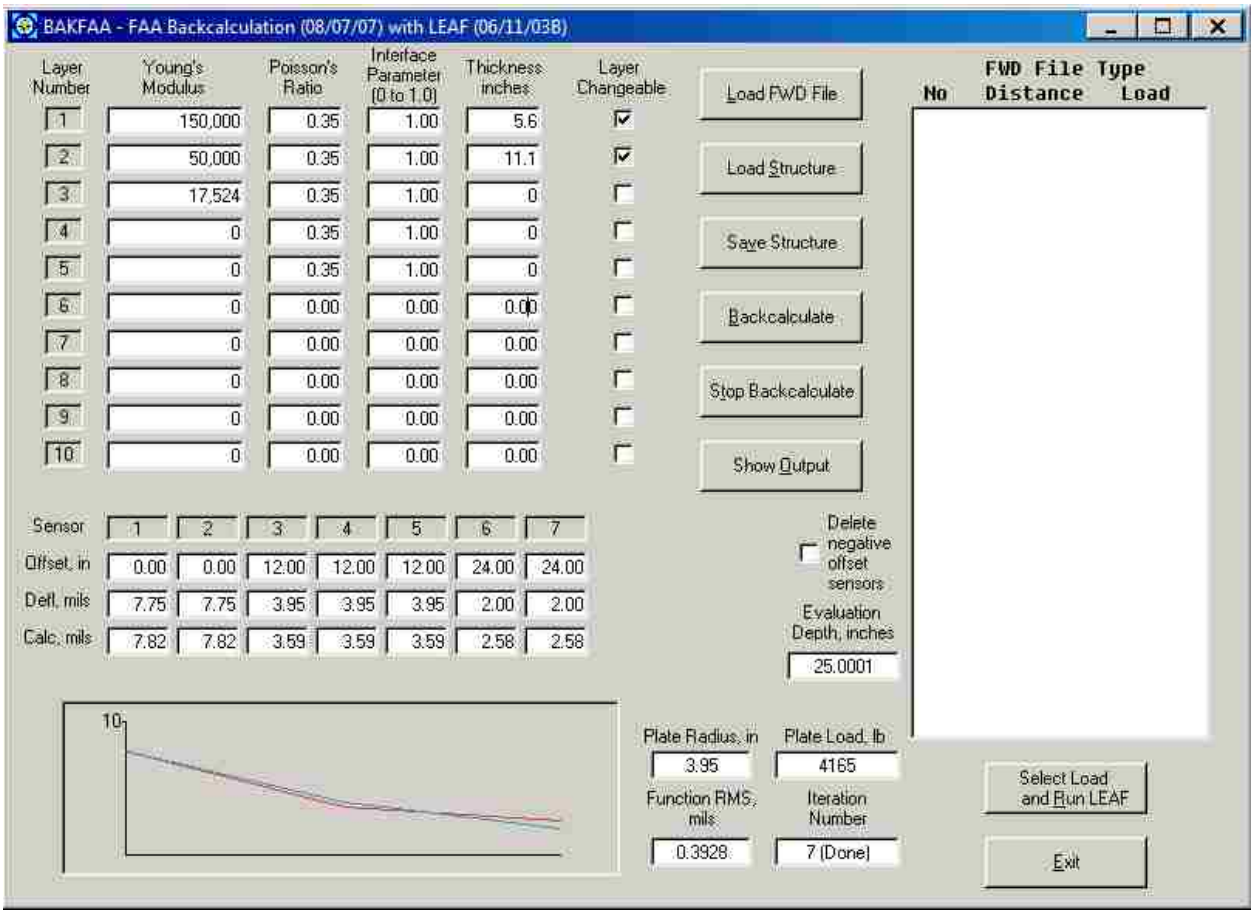

Figure D-3: Example seed modulus values for step two of the two-step backcalculation process for PFWD data.

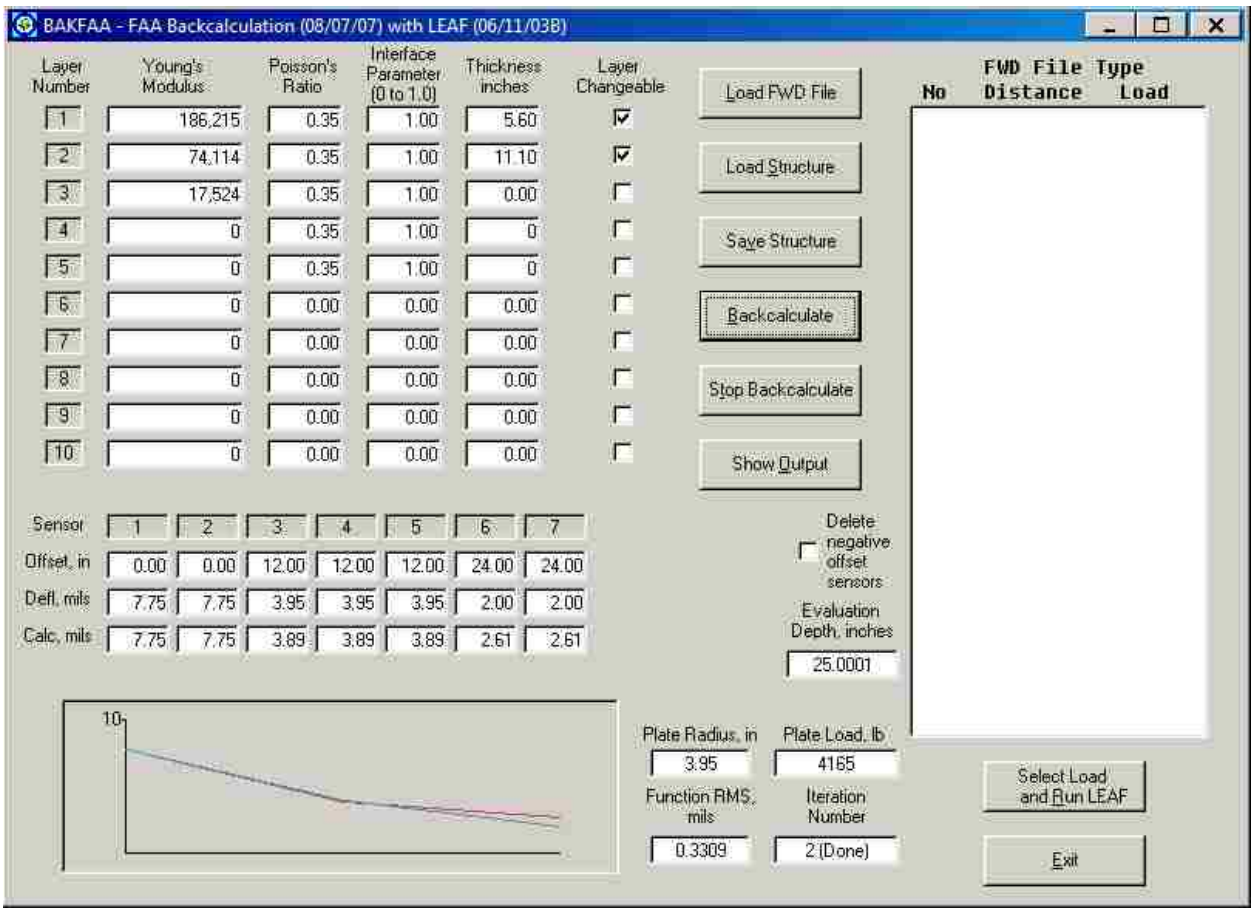

Figure D-4: Example calculated modulus values for step two of the two-step backcalculation process for PFWD data.

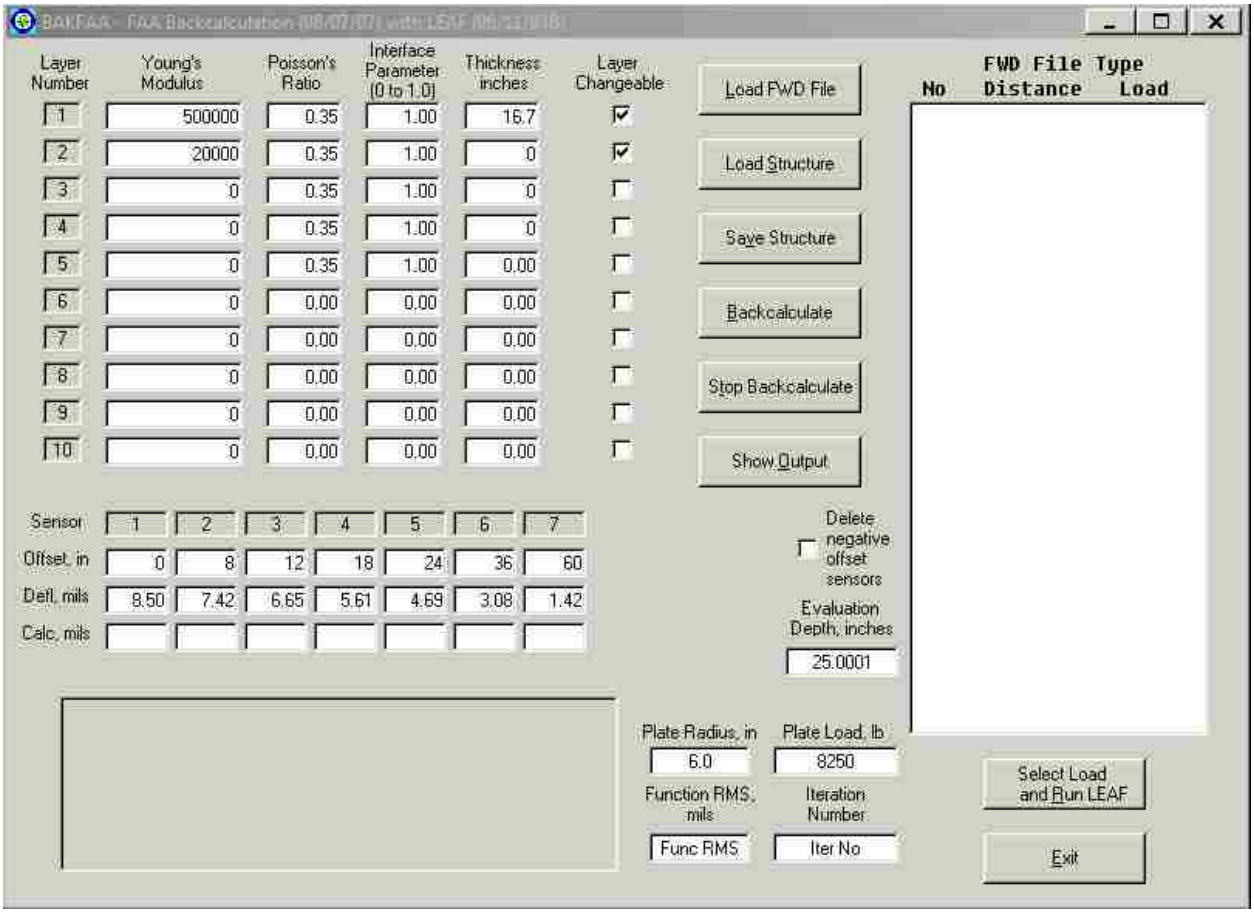

Figure D-5: Example seed modulus values for step one of the two-step backcalculation process for FWD data.

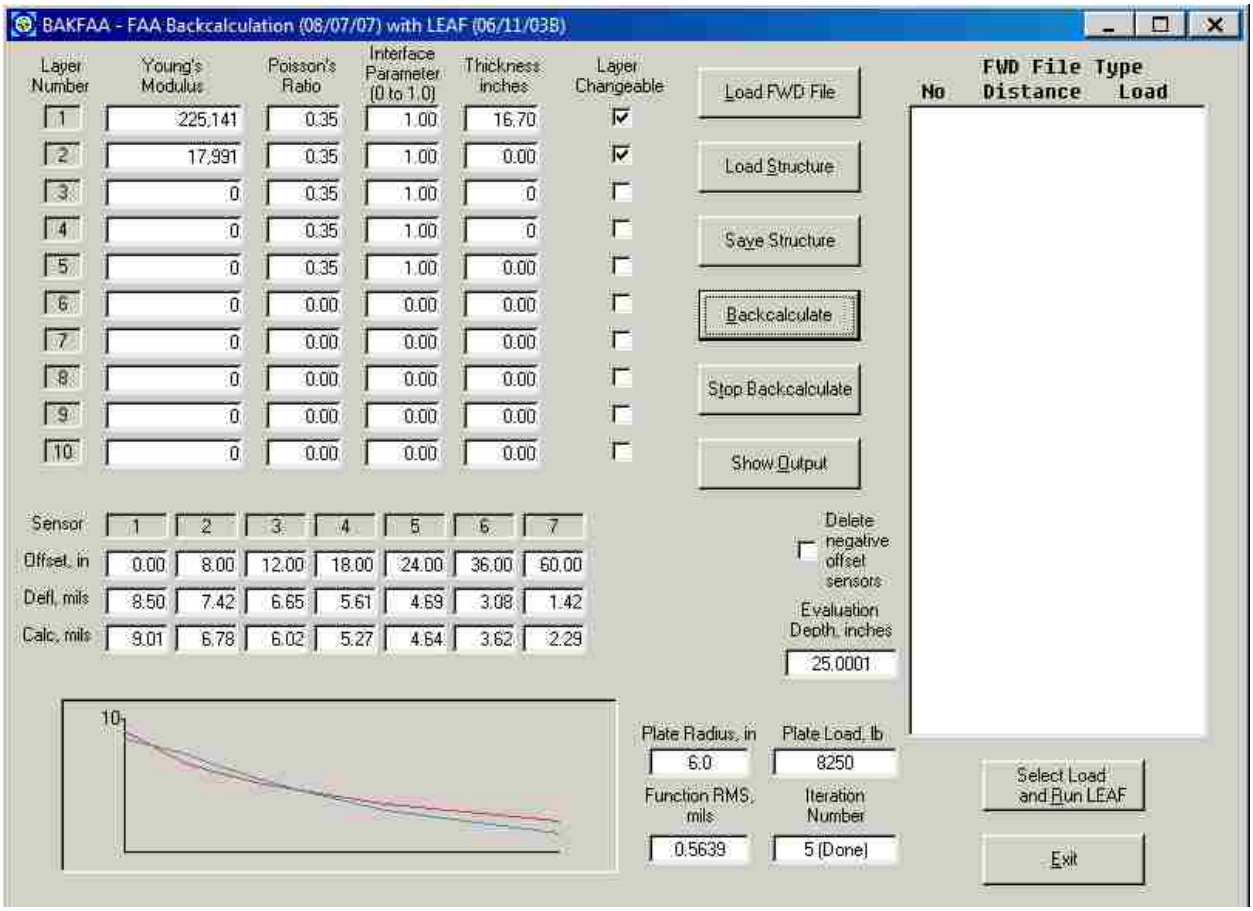

Figure D-6: Example calculated modulus values for step one of the two-step backcalculation process for FWD data.

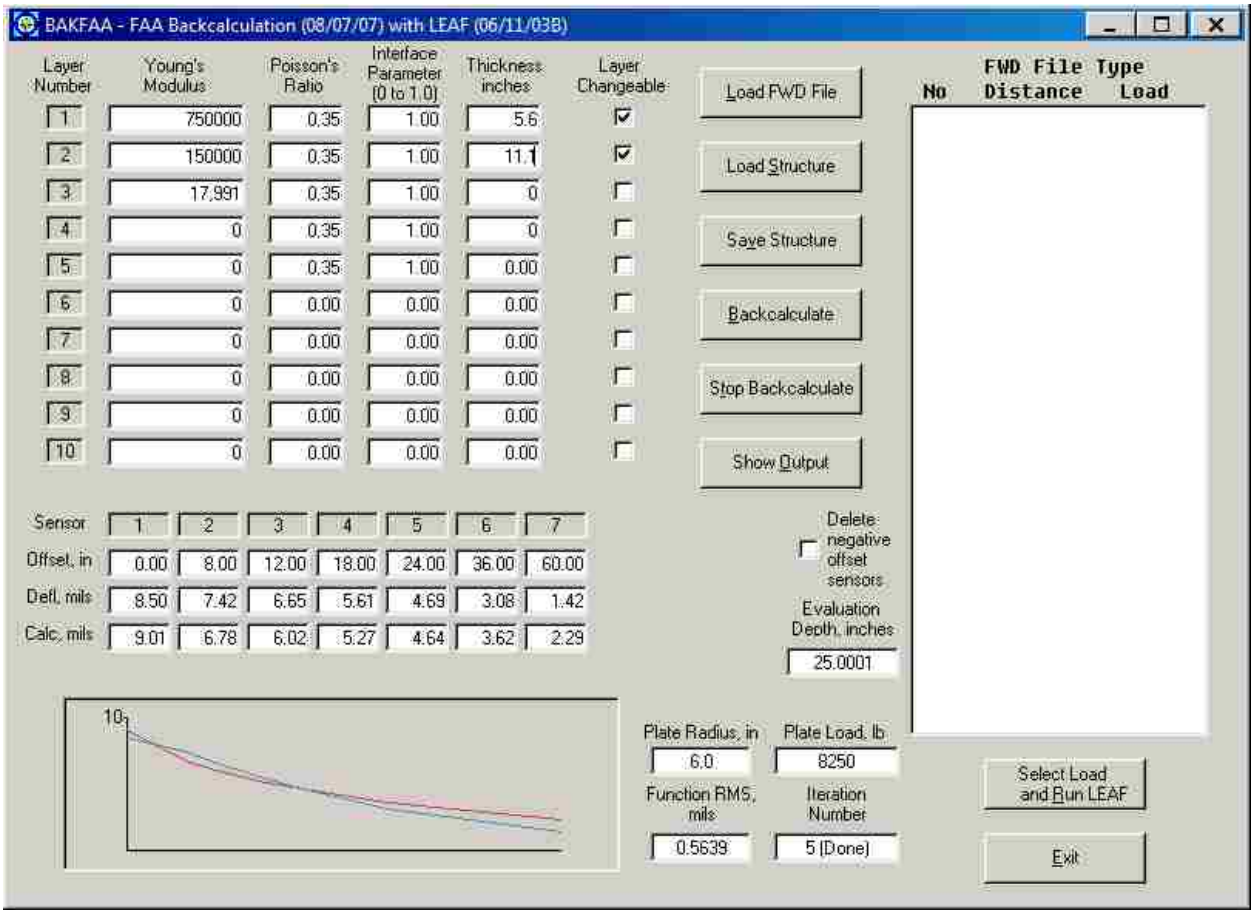

Figure D-7: Example seed modulus values for step two of the two-step backcalculation process for FWD data.

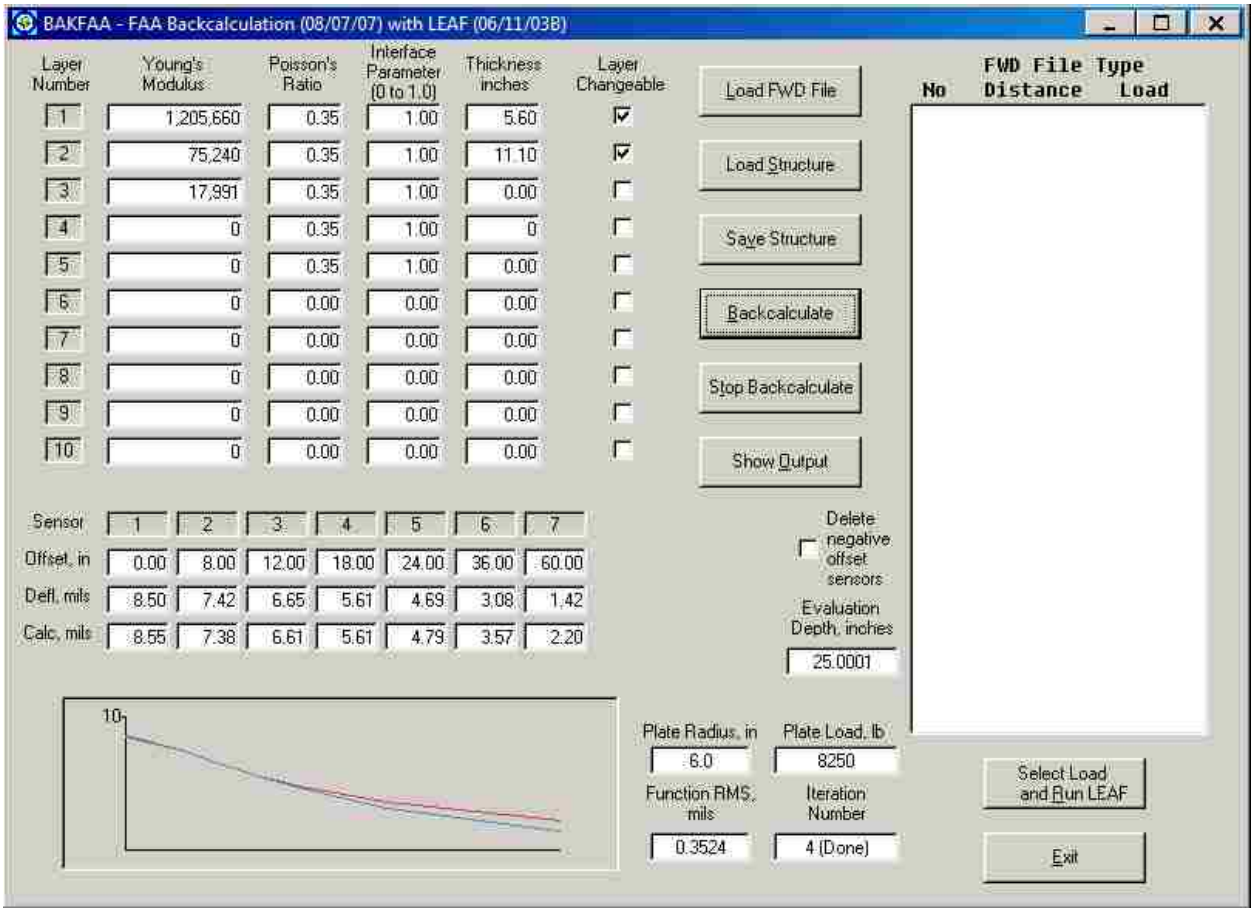

Figure D-8: Example calculated modulus values for step two of the two-step backcalculation process for FWD data.

D.1 Orem Field Site

This section presents the data used in the two-step backcalculation process for data obtained from the PFWD and FWD at the Orem field site. Tables D-1 and D-2 present seed modulus inputs for the PFWD and FWD for use in the backcalculation process. Tables D-3 through D-5 display layer thickness, deflection, and load data obtained from the PFWD for various testing times. Table D-6 displays layer thickness, deflection, and load data obtained from the FWD at the time of testing.

Table D-1: Seed Modulus Values for PFWD Testing at Orem Site

Site	Date	Layer	Seed Modulus (ksi)	
			For Step One	For Step Two
Orem	September 19, 2014	HMA	100	150
		Base		50
		Subgrade	20	Value from Step One
	November 26, 2014	HMA	500	750
		Base		150
		Subgrade	20	Value from Step One
	May 7, 2015	HMA	300	450
		Base		100
		Subgrade	20	Value from Step One
	September 24, 2015	HMA	200	300
		Base		75
		Subgrade	20	Value from Step One

Table D-2: Seed Modulus Values for FWD Testing at Orem Site

Site	Date	Layer	Seed Modulus (ksi)	
			For Step One	For Step Two
Orem	December 10, 2014	HMA	500	750
		Base		150
		Subgrade	20	Value from Step One

Table D-3: PFWD Data for September 19, 2014, at Orem Site

Section	Reinforcement	Location	HMA Thickness (in.)	Base Thickness (in.)	Drop 1				Drop 2				Drop 3			
					Deflection (mils)			Load (lb)	Deflection (mils)			Load (lb)	Deflection (mils)			Load (lb)
					0 in.	12 in.	24 in.		0 in.	12 in.	24 in.		0 in.	12 in.	24 in.	
1	No Geogrid	West	5.6	11.1	7.75	3.95	2.00	4165	7.56	3.86	2.02	4156	7.50	3.80	2.01	4140
		East			10.25	5.84	2.69	4165	10.07	5.81	2.68	4133	10.11	5.84	2.70	4183
2	Geogrid A	West	5.4	11.3	7.33	4.71	2.26	4154	7.94	4.74	2.28	4195	7.93	4.76	2.29	4200
		East			10.36	5.98	2.98	4127	10.33	6.07	2.98	4099	10.21	6.07	3.02	4129
3	No Geogrid	West	5.6	11.6	8.14	4.22	2.08	4216	8.11	4.20	2.06	4206	8.26	4.26	2.09	4238
		East			9.92	5.73	2.68	4188	10.09	5.78	2.72	4166	10.07	5.77	2.72	4198
4	Geogrid B	West	5.9	11.0	7.35	4.02	1.77	4177	7.47	4.03	1.78	4178	7.44	4.05	1.80	4223
		East			8.18	4.59	2.01	4193	8.21	4.57	2.01	4208	8.45	4.58	2.02	4211
5	No Geogrid	West	5.7	11.4	8.39	3.58	1.31	4178	8.53	3.63	1.34	4247	8.61	3.65	1.34	4245
		East			8.05	4.04	1.59	4219	8.12	4.06	1.59	4201	8.04	4.07	1.61	4226
6	Geogrid C	West	5.8	13.0	8.20	3.62	1.42	4228	8.31	3.68	1.44	4255	8.31	3.66	1.43	4212
		East			8.06	4.08	1.60	4193	8.19	4.15	1.63	4213	8.28	4.21	1.66	4253
7	No Geogrid	West	6.0	13.0	8.10	3.60	1.45	4223	8.16	3.62	1.47	4221	8.11	3.62	1.47	4222
		East			7.69	4.00	1.67	4242	7.70	4.02	1.70	4262	7.80	4.07	1.72	4295
8	Geogrid D	West	5.8	12.2	9.22	4.09	1.72	4255	9.29	4.13	1.74	4264	9.25	4.13	1.74	4261
		East			8.61	4.49	2.02	4205	8.55	4.54	2.05	4239	8.63	4.58	2.07	4248
9	No Geogrid	West	5.6	12.2	9.79	4.52	1.95	4270	9.80	4.51	1.94	4207	10.01	4.58	1.97	4306
		East			8.49	4.54	2.01	4270	8.49	4.61	2.04	4270	8.45	4.56	2.02	4226
10	Geogrid E	West	5.7	11.5	9.19	4.27	1.82	4287	9.38	4.31	1.84	4314	9.30	4.34	1.84	4333
		East			9.21	4.90	2.17	4265	9.22	4.93	2.19	4270	9.30	4.97	2.21	4297

Table D-4: PFWD Data for November 26, 2014, at Orem Site

Section	Reinforcement	Location	HMA Thickness (in.)	Base Thickness (in.)	Drop 1				Drop 2				Drop 3			
					Deflection (mils)			Load (lb)	Deflection (mils)			Load (lb)	Deflection (mils)			Load (lb)
					0 in.	12 in.	24 in.		0 in.	12 in.	24 in.		0 in.	12 in.	24 in.	
1	No Geogrid	West	5.6	11.1	3.43	2.48	1.64	3964	3.41	2.49	1.64	3988	3.38	2.48	1.64	3922
		East			4.39	3.21	2.05	3906	4.34	3.19	2.04	3835	4.44	3.21	2.06	3850
2	Geogrid A	West	5.4	11.3	3.56	2.76	1.83	3973	3.39	2.77	1.83	3987	3.68	2.80	1.85	4041
		East			4.64	3.39	2.22	3857	4.74	3.42	2.23	3946	4.78	3.54	2.25	3936
3	No Geogrid	West	5.6	11.6	4.09	2.93	1.86	4008	4.07	2.92	1.86	4012	4.05	2.92	1.87	4008
		East			4.58	3.45	2.17	3774	4.55	3.43	2.18	3975	4.54	3.44	2.18	3958
4	Geogrid B	West	5.9	11.0	3.53	2.72	1.63	3978	3.74	2.72	1.65	4053	3.87	2.68	1.62	3994
		East			3.95	2.98	1.84	4030	3.95	2.99	1.85	3860	3.96	2.98	1.85	4032
5	No Geogrid	West	5.7	11.4	3.95	2.52	1.34	3993	3.92	2.50	1.34	4027	3.95	2.53	1.35	4068
		East			3.38	2.38	1.40	4053	3.34	2.33	1.39	4001	3.54	2.35	1.39	4030
6	Geogrid C	West	5.8	13.0	3.71	2.50	1.33	4046	3.76	2.51	1.34	4064	3.74	2.49	1.34	4056
		East			3.81	2.60	1.45	4048	3.82	2.60	1.45	4040	3.81	2.59	1.46	4065
7	No Geogrid	West	6.0	13.0	3.57	2.42	1.38	4060	3.56	2.44	1.38	4099	3.56	2.39	1.37	4003
		East			3.45	2.43	1.40	4018	3.43	2.39	1.39	3987	3.39	2.40	1.39	4000
8	Geogrid D	West	5.8	12.2	3.66	2.92	1.70	4109	3.48	2.89	1.68	4089	3.82	2.88	1.67	4045
		East			4.03	2.88	1.75	4097	4.04	2.88	1.76	4073	4.05	2.87	1.75	4050
9	No Geogrid	West	5.6	12.2	4.55	3.27	1.96	4090	4.58	3.26	1.95	4077	4.54	3.25	1.95	4096
		East			4.09	3.09	1.91	3997	4.13	3.11	1.92	4045	4.14	3.12	1.92	4015
10	Geogrid E	West	5.7	11.5	4.07	2.97	1.78	4137	3.98	2.96	1.78	4138	4.07	2.92	1.76	4069
		East			4.57	3.26	1.89	4037	4.06	3.26	1.98	4064	3.90	3.27	1.98	4054

Table D-5: PFWD Data for May 7, 2015, at Orem Site

Section	Reinforcement	Location	HMA Thickness (in.)	Base Thickness (in.)	Drop 1				Drop 2				Drop 3			
					Deflection (mils)			Load (lb)	Deflection (mils)			Load (lb)	Deflection (mils)			Load (lb)
					0 in.	12 in.	24 in.		0 in.	12 in.	24 in.		0 in.	12 in.	24 in.	
1	No Geogrid	West	5.6	11.1	4.63	2.92	1.84	4200	4.61	2.93	1.88	4226	4.72	2.94	1.87	4226
		East			6.69	4.59	2.54	4150	6.82	4.63	2.57	4186	6.71	4.56	2.53	4113
2	Geogrid A	West	5.4	11.3	5.12	3.51	2.01	4236	4.81	3.50	2.00	4191	5.30	3.51	2.01	4177
		East			7.02	4.89	2.84	4205	7.01	4.87	2.83	4163	7.19	4.89	2.85	4191
3	No Geogrid	West	5.6	11.6	5.63	3.64	2.04	4131	5.75	3.66	2.05	4218	5.75	3.69	2.06	4270
		East			6.86	4.64	2.67	4160	6.97	4.64	2.67	4145	6.98	4.67	2.68	4170
4	Geogrid B	West	5.9	11.0	5.43	3.55	1.89	4258	5.52	3.53	1.88	4238	5.60	3.54	1.89	4244
		East			5.64	3.95	2.24	4202	5.81	3.94	2.24	4172	5.95	3.93	2.24	4178
5	No Geogrid	West	5.7	11.4	5.87	3.33	1.58	4210	5.86	3.33	1.59	4232	5.86	3.29	1.58	4207
		East			5.03	3.30	1.73	4213	4.99	3.24	1.69	4087	5.04	3.27	1.71	4145
6	Geogrid C	West	5.8	13.0	5.88	3.29	1.50	4189	5.68	3.30	1.51	4198	5.69	3.27	1.49	4191
		East			5.69	3.56	1.79	4143	5.69	3.53	1.76	4160	5.83	3.58	1.76	4211
7	No Geogrid	West	6.0	13.0	5.26	3.10	1.55	4278	5.22	3.07	1.54	4217	5.27	3.13	1.55	4089
		East			5.07	3.20	1.68	4176	5.12	3.20	1.67	4106	5.09	3.22	1.69	4233
8	Geogrid D	West	5.8	12.2	6.06	3.61	1.85	4235	5.99	3.57	1.84	4181	6.07	3.62	1.86	4255
		East			6.13	3.78	2.11	4214	6.16	3.80	2.15	4197	6.14	3.79	2.11	4194
9	No Geogrid	West	5.6	12.2	6.48	4.00	2.15	4263	6.44	3.92	2.11	4156	6.54	3.97	2.13	4215
		East			5.93	4.05	2.21	4230	5.98	4.02	2.20	4173	6.02	4.07	2.22	4265
10	Geogrid E	West	5.7	11.5	6.02	3.79	2.03	4277	6.03	3.79	2.04	4269	5.94	3.78	2.03	4238
		East			6.96	4.27	2.29	4177	6.56	4.27	2.31	4029	6.69	4.27	2.31	4215

Table D-6: FWD Data for December 10, 2014, at Orem Site

Section	HMA Thickness (in.)	Base Thickness (in.)	Drop	Load (1000 lb)	Deflection (mils)						
					0 in.	8 in.	12 in.	18 in.	24 in.	36 in.	60 in.
1	5.6	11.1	1	8.25	8.50	7.42	6.65	5.61	4.69	3.08	1.42
			2	8.01	8.34	7.28	6.53	5.51	4.59	2.98	1.37
			3	8.23	8.39	7.35	6.60	5.58	4.64	3.03	1.40
			1	10.03	10.27	9.00	8.11	6.87	5.74	3.78	1.77
			2	9.94	10.27	8.97	8.08	6.85	5.71	3.76	1.76
			3	10.11	10.33	9.04	8.16	6.89	5.73	3.80	1.75
			1	11.99	12.42	10.92	9.86	8.38	6.98	4.61	0.62
			2	11.96	12.36	10.88	9.81	8.34	6.94	4.58	2.13
			3	11.91	12.35	10.88	9.81	8.34	6.93	4.59	2.12
			1	13.96	14.56	12.83	11.58	9.86	8.19	5.44	2.38
			2	13.94	14.57	12.83	11.59	9.85	8.18	5.41	2.38
			3	14.01	14.59	12.86	11.61	9.89	8.22	5.43	2.52
			1	16.02	16.67	14.73	13.30	11.35	9.41	6.25	2.74
			2	16.04	16.75	14.76	13.30	11.38	9.44	6.28	2.75
			3	15.89	17.50	14.73	13.30	11.32	9.40	6.22	2.72
2	5.4	11.3	1	7.93	8.89	7.74	6.98	5.92	4.92	3.37	1.63
			2	8.03	8.97	7.83	7.06	6.01	4.97	3.38	1.66
			3	7.98	8.85	7.73	6.98	5.94	4.95	3.34	1.63
			1	9.99	11.03	9.67	8.74	7.46	6.22	4.23	2.10
			2	9.91	10.96	9.62	8.70	7.42	6.18	4.23	2.10
			3	9.96	10.99	9.66	8.73	7.44	6.19	4.23	2.07
			1	12.01	13.24	11.66	10.55	9.03	7.53	5.14	2.40
			2	12.01	13.27	11.70	10.59	9.05	7.54	5.18	2.53
			3	11.99	13.24	11.65	10.55	9.02	7.52	5.13	2.54
			1	13.99	15.40	13.58	12.30	10.56	8.81	6.06	2.98
			2	13.96	15.43	13.55	12.29	10.54	8.81	6.10	3.00
			3	13.87	15.35	13.45	12.19	10.49	8.76	6.08	2.96
			1	15.99	17.51	15.43	13.98	12.06	10.06	6.93	3.31
			2	15.94	17.49	15.42	13.98	12.04	10.05	6.94	3.26
			3	15.89	17.50	15.42	13.99	12.08	10.06	6.93	3.28

Table D-6 Continued

Section	HMA Thickness (in.)	Base Thickness (in.)	Drop	Load (1000 lb)	Deflection (mils)						
					D1	D2	D3	D4	D5	D6	D7
3	5.6	11.6	1	7.91	9.16	7.89	7.08	6.01	5.00	3.35	1.71
			2	8.01	9.19	7.95	7.13	6.05	5.01	3.37	1.72
			3	8.06	9.22	7.96	7.14	6.05	5.01	3.39	1.73
			1	9.99	11.43	9.92	8.91	7.58	6.29	4.29	2.20
			2	10.08	11.48	9.95	8.95	7.62	6.32	4.31	2.21
			3	9.96	11.37	9.87	8.88	7.54	6.27	4.26	2.18
			1	12.01	13.70	12.00	10.80	9.19	7.65	5.18	2.70
			2	11.91	13.67	11.98	10.79	9.20	7.66	5.17	2.54
			3	11.94	13.73	12.03	10.83	9.22	7.69	5.19	2.54
			1	13.94	16.08	14.13	12.71	10.88	9.03	6.17	2.99
			2	13.92	16.08	14.16	12.74	10.86	9.08	6.12	2.98
			3	14.09	16.19	14.26	12.85	10.98	9.15	6.15	3.03
			1	16.02	18.44	16.26	14.66	12.47	10.43	7.05	3.47
			2	15.97	18.44	16.28	14.66	12.49	10.42	7.04	3.46
			3	15.97	18.53	16.32	14.69	12.51	10.46	7.06	3.46
4	5.9	11.0	1	7.86	7.13	6.14	5.45	4.52	3.68	2.35	1.11
			2	7.98	7.14	6.14	5.47	4.55	3.70	2.37	1.14
			3	7.96	7.14	6.13	5.46	4.56	3.70	2.37	1.14
			1	10.01	8.93	7.71	6.89	5.76	4.70	3.06	1.42
			2	9.91	8.83	7.71	6.88	5.73	4.69	3.06	1.44
			3	9.94	8.93	7.70	6.87	5.75	4.69	3.05	1.44
			1	12.04	10.73	9.34	8.35	7.01	5.71	3.75	1.76
			2	11.99	10.69	9.32	8.34	7.01	5.71	3.75	1.76
			3	12.01	10.71	9.33	8.36	7.00	5.72	3.75	1.77
			1	14.09	12.50	10.95	9.81	8.22	6.74	4.39	2.08
			2	14.04	12.54	10.98	9.83	8.26	6.75	4.41	2.12
			3	13.99	12.57	10.97	9.83	8.26	6.77	4.42	2.11
			1	16.02	14.33	12.58	11.26	9.45	7.75	5.05	2.27
			2	15.99	14.36	12.57	11.25	9.45	7.74	5.06	2.28
			3	15.92	14.34	12.57	11.27	9.47	7.74	5.07	2.42

Table D-6 Continued

Section	HMA Thickness (in.)	Base Thickness (in.)	Drop	Load (1000 lb)	Deflection (mils)						
					D1	D2	D3	D4	D5	D6	D7
5	5.7	11.4	1	8.06	6.13	5.21	4.58	3.73	2.98	1.80	0.80
			2	8.08	6.07	5.18	4.57	3.72	2.96	1.79	0.81
			3	8.03	6.03	5.15	4.54	3.70	2.96	1.78	0.81
			1	9.96	7.40	6.34	5.60	4.58	3.66	2.23	1.01
			2	9.96	7.39	6.34	5.60	4.60	3.66	2.23	0.99
			3	10.01	7.38	6.33	5.58	4.58	3.66	2.24	1.02
			1	12.06	8.86	7.63	6.74	5.54	4.41	2.71	1.23
			2	11.96	8.81	7.58	6.72	5.51	4.37	2.70	1.23
			3	11.96	8.82	7.58	6.73	5.51	4.38	2.70	1.23
			1	14.06	10.22	8.84	7.83	6.41	5.13	3.18	1.43
			2	14.04	10.19	8.81	7.80	6.40	5.13	3.17	1.33
			3	13.99	10.18	8.81	7.80	6.40	5.11	3.18	1.43
			1	16.09	11.60	10.04	8.90	7.33	5.86	3.66	1.50
			2	16.09	11.58	10.04	8.90	7.31	5.86	3.66	1.64
			3	15.97	11.54	10.01	8.86	7.30	5.85	3.62	1.62
6	5.8	13.0	1	7.98	6.30	5.34	4.65	3.67	2.90	1.69	0.76
			2	8.08	6.28	5.34	4.65	3.66	2.89	1.70	0.79
			3	8.08	6.22	5.30	4.61	3.66	2.87	1.69	0.75
			1	9.96	7.71	6.57	5.72	4.53	3.57	2.12	0.95
			2	9.94	7.69	6.57	5.72	4.54	3.58	2.11	0.86
			3	10.06	7.72	6.59	5.73	4.55	3.59	2.10	0.94
			1	12.04	9.20	7.89	6.87	5.48	4.31	2.57	1.16
			2	12.06	9.22	7.90	6.89	5.49	4.33	2.59	1.15
			3	11.96	9.20	7.87	6.87	5.46	4.31	2.57	1.15
			1	13.94	10.68	9.17	7.98	6.37	5.02	3.00	1.24
			2	13.89	10.71	9.20	8.01	6.38	5.03	2.98	1.24
			3	13.92	10.72	9.19	8.01	6.40	5.03	3.00	1.24
			1	16.19	12.45	10.69	9.30	7.42	5.86	3.46	1.46
			2	16.14	12.43	10.65	9.28	7.42	5.85	3.50	1.45
			3	15.99	12.38	10.63	9.27	7.39	5.83	3.46	1.46

Table D-6 Continued

Section	HMA Thickness (in.)	Base Thickness (in.)	Drop	Load (1000 lb)	Deflection (mils)						
					D1	D2	D3	D4	D5	D6	D7
7	6.0	13.0	1	7.91	5.91	4.98	4.38	3.53	2.82	1.67	0.75
			2	7.96	5.91	5.00	4.39	3.53	2.83	1.71	0.74
			3	7.93	5.88	4.96	4.36	3.49	2.82	1.69	0.75
			1	10.08	7.42	6.27	5.51	4.44	3.58	2.14	0.96
			2	9.89	7.35	6.21	5.47	4.41	3.54	2.12	0.95
			3	10.01	7.40	6.25	5.51	4.44	3.58	2.15	0.98
			1	12.11	8.91	7.58	6.68	5.40	4.32	2.64	1.09
			2	12.01	8.89	7.58	6.65	5.38	4.31	2.65	1.15
			3	11.91	8.86	7.54	6.64	5.36	4.29	2.62	1.15
			1	14.04	10.38	8.84	7.80	6.31	5.07	3.10	1.37
			2	13.99	10.43	8.88	7.83	6.33	5.08	3.11	1.37
			3	13.89	10.39	8.84	7.79	6.32	5.05	3.10	1.36
			1	15.94	11.94	10.16	8.95	7.28	5.82	3.55	1.48
			2	15.99	11.99	10.23	9.01	7.31	5.85	3.58	1.47
			3	15.92	11.98	10.22	8.99	7.30	5.83	3.58	1.48
8	5.8	12.2	1	8.03	7.69	6.43	5.65	4.60	3.72	2.30	0.97
			2	7.89	7.57	6.38	5.61	4.58	3.69	2.31	0.98
			3	7.93	7.57	6.41	5.65	4.60	3.70	2.28	0.98
			1	9.91	9.52	8.00	7.04	5.78	4.63	2.89	1.26
			2	9.96	9.54	8.03	7.06	5.82	4.67	2.94	1.26
			3	9.89	9.50	8.01	7.07	5.81	4.67	2.92	1.26
			1	11.96	11.32	9.65	8.50	7.02	5.64	3.54	1.43
			2	11.89	11.34	9.69	8.55	7.02	5.64	3.58	1.53
			3	11.96	11.35	9.70	8.55	7.04	5.65	3.56	1.44
			1	13.89	13.29	11.36	10.03	8.24	6.66	4.22	1.67
			2	13.84	13.33	11.39	10.05	8.29	6.67	4.21	1.70
			3	13.87	13.33	11.43	10.08	8.29	6.68	4.24	1.81
			1	15.97	15.28	13.09	11.56	9.53	7.68	4.89	1.96
			2	16.02	15.36	13.15	11.61	9.57	7.70	4.87	1.95
			3	15.94	15.41	13.17	11.64	9.59	7.72	4.91	1.96

Table D-6 Continued

Section	HMA Thickness (in.)	Base Thickness (in.)	Drop	Load (1000 lb)	Deflection (mils)						
					D1	D2	D3	D4	D5	D6	D7
9	5.6	12.2	1	8.20	8.50	7.51	6.67	5.53	4.45	2.78	1.26
			2	8.03	8.30	7.34	6.53	5.39	4.37	2.71	1.23
			3	7.91	8.16	7.20	6.43	5.29	4.31	2.70	1.19
			1	10.16	10.44	9.22	8.25	6.83	5.52	3.48	1.57
			2	10.01	10.23	9.06	8.10	6.74	5.43	3.40	1.58
			3	10.01	10.24	9.07	8.09	6.72	5.44	3.42	1.56
			1	11.99	12.41	10.99	9.85	8.17	6.64	4.19	1.79
			2	11.94	12.35	10.96	9.83	8.17	6.60	4.15	1.90
			3	12.04	12.37	10.96	9.85	8.16	6.62	4.18	1.77
			1	14.06	14.46	12.86	11.55	9.58	7.78	4.93	2.10
			2	14.04	14.51	12.90	11.58	9.63	7.77	4.93	2.08
			3	14.01	14.53	12.91	11.58	9.65	7.81	4.93	2.24
			1	16.04	16.57	14.70	13.19	10.98	8.89	5.63	2.42
			2	15.99	16.56	14.70	13.20	10.99	8.88	5.64	2.40
			3	15.99	16.58	14.70	13.21	10.99	8.92	5.63	2.42
10	5.7	11.5	1	7.93	7.84	6.83	6.06	4.97	4.07	2.59	1.23
			2	8.06	7.87	6.87	6.09	5.01	4.11	2.59	1.23
			3	8.01	7.77	6.79	6.01	4.96	4.04	2.55	1.17
			1	10.06	9.69	8.46	7.52	6.21	5.07	3.24	1.43
			2	9.96	9.61	8.41	7.47	6.17	5.04	3.23	1.52
			3	9.99	9.59	8.39	7.46	6.18	5.03	3.21	1.53
			1	12.04	11.57	10.15	9.01	7.49	6.11	3.91	1.76
			2	12.06	11.58	10.17	9.06	7.50	6.13	3.94	1.87
			3	11.96	11.55	10.13	9.01	7.47	6.09	3.93	1.88
			1	14.01	13.54	11.89	10.59	8.78	7.18	4.63	2.07
			2	14.04	13.54	11.91	10.61	8.79	7.20	4.65	2.05
			3	14.09	13.53	11.92	10.61	8.81	7.21	4.63	2.06
			1	16.02	15.39	13.55	12.08	10.03	8.18	5.27	2.38
			2	16.09	15.46	13.60	12.13	10.07	8.23	5.30	2.38
			3	16.02	15.46	13.62	12.14	10.07	8.22	5.32	2.39

D.2 Springville Field Site

This section presents the data used in the two-step backcalculation process for data obtained from the PFWD and FWD at the Springville field site. Tables D-7 and D-8 present seed modulus inputs for the PFWD and FWD for use in the backcalculation process. Tables D-9 and D-10 display layer thickness, deflection, and load data obtained from the PFWD for various testing times. Table D-11 displays layer thickness, deflection, and load data obtained from the FWD at the time of testing.

Table D-7: Seed Modulus Values for PFWD Testing at Springville Field Site

Site	Date	Layer	Seed Modulus (ksi)	
			For Step One	For Step Two
Springville	November 26, 2014	HMA	200	400
		Base		40
		Subgrade	10	Value from Step One
	May 5, 2015	HMA	150	250
		Base		25
		Subgrade	10	Value from Step One

Table D-8: Seed Modulus Values for FWD Testing at Springville Field Site

Site	Date	Layer	Seed Modulus (ksi)	
			For Step One	For Step Two
Springville	December 10, 2014	HMA	200	400
		Base		40
		Subgrade	10	Value from Step One

Table D-9: PFWD Data for November 26, 2014, at Springville Site

Section	Reinforcement	Location	HMA Thickness (in.)	Base Thickness (in.)	Drop 1				Drop 2				Drop 3			
					Deflection (mils)			Load (lb)	Deflection (mils)			Load (lb)	Deflection (mils)			Load (lb)
					0 in.	12 in.	24 in.		0 in.	12 in.	24 in.		0 in.	12 in.	24 in.	
1	No Geogrid	West	3.7	10.1	12.48	6.04	2.30	4043	11.71	5.86	2.27	3902	11.97	5.91	2.30	4004
		East			10.81	6.06	2.47	4013	10.68	5.97	2.45	3959	10.83	6.00	2.47	4038
2	Geogrid A	West	3.3	11.3	12.01	6.61	2.64	4051	12.14	6.61	2.68	4062	12.28	6.63	2.71	4104
		East			11.05	6.24	2.80	4083	10.86	6.19	2.80	4032	11.04	6.21	2.82	4068
3	No Geogrid	West	3.2	11.7	12.98	7.03	2.96	3997	12.99	7.07	3.00	4052	12.99	7.13	3.04	4062
		East			15.65	6.61	2.57	4051	14.84	6.45	2.54	4017	14.74	6.51	2.59	4067
4	Geogrid B	West	3.3	11.4	17.88	8.30	3.41	4026	17.29	8.22	3.44	4007	17.09	8.26	3.46	4000
		East			16.01	7.60	2.97	4066	15.58	7.46	2.95	3952	15.45	7.48	2.99	4010
5	No Geogrid	West	3.4	9.5	12.43	6.78	2.94	4073	12.45	6.78	2.95	4078	12.19	6.67	2.94	4035
		East			14.88	7.13	2.99	4033	14.66	7.07	2.98	3971	14.59	7.06	2.99	4007
6	Geogrid C	West	2.6	8.0	11.23	6.39	2.70	4063	10.79	6.16	2.62	3974	11.14	6.35	2.70	4080
		East			14.39	7.68	3.59	4035	14.35	7.73	3.62	4026	14.20	7.68	3.61	3980
7	No Geogrid	West	2.9	7.8	15.79	8.22	3.42	4054	15.86	8.30	3.47	4070	15.86	8.33	3.51	4075
		East			12.67	6.44	2.94	3978	12.71	6.54	3.01	4081	12.79	6.57	3.02	4070
8	Geogrid D	West	2.9	7.5	10.78	6.11	2.81	4114	10.75	6.11	2.80	4101	10.71	6.12	2.81	4112
		East			11.98	6.12	2.78	4099	12.01	6.19	2.83	4120	11.88	6.12	2.82	4034
9	No Geogrid	West	3.0	7.7	14.89	7.14	2.71	4093	14.82	7.16	2.75	4080	14.83	7.21	2.78	4104
		East			10.34	5.42	2.27	4128	10.16	5.34	2.25	4059	10.32	5.43	2.29	4095
10	Geogrid E	West	2.9	9.0	9.69	5.49	2.32	4112	9.69	5.49	2.33	4104	9.61	5.54	2.36	4116
		East			14.02	6.23	2.27	4114	13.68	6.25	2.30	4124	13.72	6.23	2.29	4100

Table D-10: PFWD Data for May 5, 2015, at Springville Site

Section	Reinforcement	Location	HMA Thickness (in)	Base Thickness (in.)	Drop 1				Drop 2				Drop 3			
					Deflection (mils)			Load (lb)	Deflection (mils)			Load (lb)	Deflection (mils)			Load (lb)
					0 in.	12 in.	24 in.		0 in.	12 in.	24 in.		0 in.	12 in.	24 in.	
1	No Geogrid	West	3.7	10.1	16.92	7.94	2.94	4072	17.03	7.99	2.95	3992	16.76	7.96	2.97	4105
		East			15.24	7.39	2.99	4053	15.11	7.31	2.97	4103	14.86	7.28	2.97	4098
2	Geogrid A	West	3.3	11.3	13.95	6.76	2.64	4125	13.73	6.70	2.66	4140	13.80	6.68	2.65	4121
		East			13.14	6.97	2.89	4098	12.90	6.86	2.87	4131	12.87	6.87	2.87	4152
3	No Geogrid	West	3.2	11.7	13.73	7.14	2.68	4133	13.77	6.88	2.71	4175	13.94	6.88	2.71	4171
		East			15.40	6.90	2.65	4137	15.14	6.84	2.66	4178	14.92	6.80	2.66	4154
4	Geogrid B	West	3.3	11.4	17.11	7.55	3.00	4174	16.87	7.53	3.04	4154	16.64	7.41	3.03	4146
		East			17.12	6.83	2.72	4146	17.09	6.85	2.74	4142	16.89	6.82	2.78	4145
5	No Geogrid	West	3.4	9.5	16.38	7.05	2.67	4167	15.90	7.00	2.69	4143	15.78	7.00	2.71	4131
		East			20.36	7.72	2.87	4066	20.31	7.71	2.92	4108	20.24	7.69	2.93	4097
6	Geogrid C	West	2.6	8.0	21.20	9.23	3.11	4146	20.96	9.16	3.08	4098	21.50	9.27	3.08	4111
		East			21.87	8.72	3.47	4133	22.15	8.74	3.42	4155	21.93	8.65	3.42	4124
7	No Geogrid	West	2.9	7.8	22.31	8.63	3.20	4132	22.60	8.67	3.17	4148	22.40	8.66	3.21	4131
		East			22.47	7.86	2.74	4160	22.03	7.70	2.68	4108	21.74	7.67	2.69	4127
8	Geogrid D	West	2.9	7.5	18.28	6.67	2.51	4169	17.98	6.77	2.57	4183	17.85	6.76	2.58	4151
		East			18.42	6.75	2.54	4136	17.96	6.64	2.53	4183	17.77	6.69	2.56	4168
9	No Geogrid	West	3.0	7.7	20.13	7.06	2.31	4117	20.19	7.15	2.33	4156	20.05	7.17	2.35	4152
		East			12.71	6.08	2.13	4205	12.99	6.05	2.14	4194	13.07	6.09	2.13	4185
10	Geogrid E	West	2.9	9.0	15.38	6.25	2.10	4166	15.29	6.28	2.12	4165	15.36	6.27	2.13	4139
		East			17.26	6.42	1.97	4181	16.93	6.33	1.98	4171	17.01	6.35	2.00	4184

Table D-11: FWD Data for December 10, 2014, at Springville Site

Section	HMA Thickness (in.)	Base Thickness (in.)	Drop	Load (1000 lb.)	Deflection (mils)						
					0 in.	8 in.	12 in.	18 in.	24 in.	36 in.	60 in.
1	3.7	10.1	1	8.12	15.50	13.38	11.21	8.42	6.31	3.54	1.64
			2	8.02	15.31	13.23	11.10	8.35	6.28	3.53	1.66
			3	8.00	15.15	13.10	10.99	8.29	6.24	3.53	1.66
			1	10.16	19.69	16.84	14.13	10.69	8.01	4.50	1.90
			2	9.98	19.46	16.66	13.99	10.60	7.99	4.52	1.90
			3	9.98	19.40	16.63	13.97	10.61	8.00	4.54	1.91
2	3.3	11.3	1	8.00	17.35	14.57	12.32	9.36	7.08	4.10	1.67
			2	8.17	17.22	14.50	12.28	9.37	7.08	4.11	1.64
			3	8.00	17.01	14.34	12.15	9.28	7.02	4.08	1.64
			1	10.25	22.50	18.89	16.03	12.27	9.26	5.26	2.48
			2	10.13	22.23	18.70	15.88	12.19	9.21	5.27	2.15
			3	10.20	22.13	18.63	15.85	12.18	9.22	5.27	2.15
3	3.2	11.7	1	7.85	19.02	15.82	13.09	9.64	7.02	3.74	1.53
			2	7.87	18.93	15.79	13.08	9.67	7.06	3.78	1.54
			3	7.97	19.00	15.87	13.17	9.77	7.14	3.82	1.56
			1	10.03	24.69	20.54	17.10	12.70	9.23	4.88	1.99
			2	10.18	24.84	20.69	17.25	12.86	9.41	5.00	2.02
			3	9.98	24.42	20.38	17.01	12.71	9.30	4.96	1.98
4	3.3	11.4	1	7.90	25.15	21.09	16.89	11.90	8.32	4.59	1.99
			2	7.90	24.84	20.72	16.65	11.77	8.31	4.60	2.16
			3	8.05	24.88	20.86	16.80	11.95	8.44	4.70	2.00
			1	9.86	31.63	26.08	21.03	14.98	10.50	5.65	2.35
			2	9.91	31.91	26.29	21.25	15.18	10.72	5.80	2.26
			3	9.98	31.96	26.38	21.32	15.29	10.80	5.86	2.30
5	3.4	9.5	1	8.10	20.38	17.97	15.25	11.47	8.48	4.68	2.07
			2	8.19	20.38	17.99	15.28	11.55	8.57	4.74	2.09
			3	8.12	19.96	17.63	14.97	11.31	8.40	4.67	2.07
			1	10.03	26.03	22.69	19.26	14.59	10.80	6.03	2.25
			2	10.11	26.11	22.73	19.34	14.69	10.89	6.11	2.43
			3	10.16	25.90	22.59	19.23	14.62	10.86	6.10	2.54

Table D-11 Continued

Section	HMA Thickness (in.)	Base Thickness (in.)	Drop	Load (1000 lb.)	Deflection (mils)						
					0 in.	8 in.	12 in.	18 in.	24 in.	36 in.	60 in.
6	2.6	8.0	1	7.80	24.79	21.29	18.16	13.96	10.53	5.59	2.37
			2	7.90	24.77	21.28	18.17	13.99	10.55	5.60	2.37
			3	7.80	24.80	21.31	18.20	14.04	10.59	5.64	2.37
			1	9.91	32.10	27.47	23.53	18.22	13.72	7.26	3.04
			2	9.91	32.29	27.64	23.68	18.40	13.86	7.34	3.07
			3	9.86	32.29	27.66	23.70	18.41	13.89	7.35	3.06
7	2.9	7.8	1	7.92	21.61	18.02	15.18	11.52	8.53	4.38	1.71
			2	8.07	21.68	18.14	15.28	11.62	8.62	4.43	1.72
			3	8.17	21.93	18.36	15.47	11.79	8.75	4.51	1.76
			1	10.08	27.88	23.26	19.66	15.01	11.12	5.67	2.18
			2	9.96	27.82	23.31	19.70	15.08	11.16	5.70	2.17
			3	9.96	27.92	23.40	19.82	15.14	11.22	5.73	2.19
8	2.9	7.5	1	8.00	19.20	16.48	14.05	10.65	7.97	4.36	1.87
			2	8.12	19.35	16.66	14.21	10.78	8.08	4.43	1.90
			3	8.07	19.01	16.36	13.95	10.60	7.94	4.38	1.88
			1	10.08	24.69	21.34	18.23	13.89	10.38	5.62	2.37
			2	9.91	24.61	21.29	18.18	13.86	10.38	5.65	2.37
			3	9.98	24.76	21.42	18.31	13.97	10.44	5.69	2.37
9	3.0	7.7	1	7.95	17.98	15.19	12.59	9.20	6.65	3.47	1.48
			2	8.07	18.03	15.27	12.67	9.27	6.70	3.53	1.53
			3	8.02	17.95	15.23	12.58	9.22	6.67	3.52	1.72
			1	10.08	23.23	19.53	16.18	11.88	8.55	4.45	1.87
			2	10.25	23.78	20.07	16.67	12.25	8.84	4.61	1.97
			3	10.08	23.34	19.72	16.38	12.04	8.72	4.56	1.95
10	2.9	9.0	1	8.05	16.35	13.31	10.89	7.79	5.65	3.17	1.57
			2	8.17	16.15	13.23	10.85	7.78	5.65	3.18	1.58
			3	8.02	15.99	13.13	10.80	7.75	5.62	3.17	1.57
			1	10.08	20.38	16.59	13.61	9.80	7.07	3.96	1.98
			2	10.06	20.32	16.55	13.62	9.83	7.12	3.97	1.98
			3	10.03	20.23	16.53	13.60	9.85	7.15	4.00	2.00

D.3 Additional Springville Field Site

This section presents the data used in the two-step backcalculation process for data obtained from the PFWD and FWD at the additional Springville field site. Tables D-12 and D-13 present seed modulus inputs for the PFWD and FWD for use in the backcalculation process. Tables D-14 and D-15 display layer thickness, deflection, and load data obtained from the PFWD for various testing times. Table D-16 displays layer thickness, deflection, and load data obtained from the FWD at the time of testing.

Table D-12: Seed Modulus Values for PFWD Testing at Additional Springville Site

Site	Date	Layer	Seed Modulus (ksi)	
			For Step One	For Step Two
Additional Springville	November 21, 2014	HMA	200	400
		Base		40
		Subgrade	10	Value from Step One
	May 5, 2015	HMA	150	250
		Base		25
		Subgrade	10	Value from Step One

Table D-13: Seed Modulus Values for FWD Testing at Additional Springville Site

Site	Date	Layer	Seed Modulus (ksi)	
			For Step One	For Step Two
Additional Springville	December 10, 2014	HMA	200	400
		Base		40
		Subgrade	10	Value from Step One

Table D-14: PFWD Data for November 21, 2014, at Additional Springville Site

Section	Reinforcement	Location	HMA Thickness (in.)	Base Thickness (in.)	Drop 1				Drop 2				Drop 3			
					Deflection (mils)				Deflection (mils)				Deflection (mils)			
					0 in.	12 in.	24 in.	Load (lb)	0 in.	12 in.	24 in.	Load (lb)	0 in.	12 in.	24 in.	Load (lb)
1	Geogrid	North	3.6	15.0	10.03	6.26	3.23	3914	10.04	6.26	3.22	3907	9.99	6.23	3.22	3924
		South			8.45	5.56	2.85	3926	8.34	5.54	2.87	3967	8.45	5.61	2.87	4010
2	Geogrid	North	3.4	15.0	10.22	6.40	3.31	3996	10.12	6.31	3.22	3936	10.27	6.39	3.25	4021
		South			9.71	6.00	2.87	3971	9.66	5.94	2.85	3935	9.78	6.01	2.89	3992
3	Geogrid	North	2.9	15.0	13.28	7.36	3.63	3979	13.53	7.49	3.68	4053	13.53	7.41	3.66	3985
		South			8.70	5.61	2.91	4039	8.78	5.58	2.90	4058	8.79	5.58	2.89	4039
4	No Geogrid	North	2.7	15.0	12.05	6.50	3.23	3946	12.14	6.46	3.28	4019	12.07	6.40	3.27	4012
		South			9.93	6.32	3.10	4019	9.82	6.32	3.11	4061	9.94	6.28	3.10	4045
5	No Geogrid	North	2.9	15.0	12.70	7.55	3.84	4056	12.59	7.51	3.83	4022	12.67	7.58	3.86	4057
		South			9.78	6.65	3.36	4130	9.76	6.60	3.34	4108	9.81	6.64	3.36	4122
6	No Geogrid	North	2.9	15.0	12.27	6.84	3.43	4098	12.20	6.80	3.43	4082	12.11	6.83	3.46	4102
		South			10.54	6.37	3.10	4070	10.57	6.36	3.12	4121	10.40	6.26	3.11	4086

Table D-15: PFWD Data for May 5, 2015, at Additional Springville Site

Section	Reinforcement	Location	HMA Thickness (in.)	Base Thickness (in.)	Drop 1				Drop 2				Drop 3			
					Deflection (mils)				Deflection (mils)				Deflection (mils)			
					0 in.	12 in.	24 in.	Load (lb)	0 in.	12 in.	24 in.	Load (lb)	0 in.	12 in.	24 in.	Load (lb)
1	Geogrid	North	3.6	15.0	17.67	6.79	2.58	4211	17.46	6.71	2.59	4184	17.56	6.79	2.62	4187
		South			20.08	7.37	2.89	4161	19.54	7.29	2.91	4153	19.29	7.20	2.94	4136
2	Geogrid	North	3.4	15.0	18.09	6.21	2.41	4189	17.78	6.26	2.46	4216	17.65	6.22	2.44	4157
		South			18.97	7.47	2.77	4098	18.27	7.24	2.75	4090	18.59	7.33	2.82	4150
3	Geogrid	North	2.9	15.0	16.99	5.93	2.41	4206	17.05	5.97	2.43	4182	16.91	6.03	2.45	4186
		South			23.53	7.75	2.98	4133	23.25	7.76	3.00	4134	23.10	7.81	3.01	4120
4	No Geogrid	North	2.7	15.0	18.78	6.90	2.76	4198	18.71	6.97	2.80	4202	18.60	7.00	2.81	4125
		South			19.72	6.76	3.01	4186	19.40	6.72	3.03	4143	19.43	6.79	3.07	4195
5	No Geogrid	North	2.9	15.0	18.27	7.55	2.64	4169	18.17	7.49	2.62	4159	18.27	7.55	2.63	4173
		South			21.83	7.90	3.18	4150	21.63	7.85	3.15	4093	21.44	7.88	3.15	4126
6	No Geogrid	North	2.9	15.0	17.36	5.95	2.79	4188	16.98	5.96	2.82	4154	17.04	6.00	2.90	4174
		South			17.47	6.20	2.89	4162	17.12	6.28	2.93	4141	16.98	6.29	2.97	4170

Table D-16: FWD Data for December 10, 2014, at Additional Springville Site

Section	Reinforcement	Location	Drop	Asphalt Thickness (in.)	Base Thickness (in.)	Load (1000 lb)	Deflection (mils)						
							D1	D2	D3	D4	D5	D6	D7
1	Geogrid	North	1	3.6	15	8.24	20.40	16.79	14.16	10.87	8.41	5.06	2.55
			2	3.6	15	8.32	20.26	16.75	14.20	10.93	8.48	5.08	2.59
			3	3.6	15	8.22	20.04	16.61	14.06	10.85	8.42	5.06	2.94
			1	3.6	15	10.23	24.74	20.42	17.32	13.37	10.33	6.11	3.11
			2	3.6	15	10.16	24.70	20.47	17.39	13.44	10.42	6.19	3.13
			3	3.6	15	10.13	24.50	20.39	17.34	13.43	10.42	6.21	3.14
	Geogrid	South	1	3.6	15	8.14	18.74	14.57	12.23	9.48	7.42	4.54	2.46
			2	3.6	15	8.07	18.63	14.54	12.26	9.46	7.43	4.56	2.48
			3	3.6	15	8.12	18.38	14.41	12.16	9.43	7.39	4.55	2.47
			1	3.6	15	10.01	23.10	18.32	15.50	12.12	9.46	5.69	3.06
			2	3.6	15	9.94	22.87	18.17	15.38	12.04	9.40	5.67	3.05
			3	3.6	15	9.98	22.83	18.21	15.41	12.04	9.44	5.68	3.06
2	Geogrid	North	1	3.4	15	7.95	21.97	16.96	13.94	10.30	7.79	4.61	2.88
			2	3.4	15	7.87	21.80	16.93	13.96	10.36	7.83	4.63	2.59
			3	3.4	15	8.02	21.68	16.93	13.99	10.39	7.88	4.66	2.95
			1	3.4	15	9.59	27.17	21.47	17.73	13.16	9.88	5.71	3.14
			2	3.4	15	9.74	27.60	21.90	18.13	13.48	10.10	5.83	3.20
			3	3.4	15	9.76	27.72	22.07	18.28	13.59	10.19	5.88	3.23
	Geogrid	South	1	3.4	15	8.00	20.45	16.61	13.75	10.34	7.97	4.85	2.56
			2	3.4	15	8.07	20.44	16.67	13.84	10.41	8.04	4.89	2.57
			3	3.4	15	8.14	20.36	16.66	13.84	10.44	8.08	4.92	2.60
			1	3.4	15	10.38	26.17	21.58	17.96	13.57	10.35	6.17	3.22
			2	3.4	15	10.25	25.95	21.46	17.92	13.53	10.39	6.23	3.24
			3	3.4	15	10.18	25.88	21.41	17.89	13.56	10.39	6.23	3.24
3	Geogrid	North	1	2.9	15	7.65	30.15	22.39	18.03	12.96	9.49	5.24	2.59
			2	2.9	15	7.73	29.98	22.38	18.05	13.01	9.55	5.29	2.62
			3	2.9	15	7.60	29.71	22.28	18.01	13.02	9.50	5.28	2.58
			1	2.9	15	9.59	38.05	29.10	23.53	16.94	12.32	6.66	3.18
			2	2.9	15	9.54	38.41	29.50	23.90	17.22	12.49	6.76	3.20
			3	2.9	15	9.64	38.92	29.99	24.32	17.55	12.73	6.87	3.26
	Geogrid	South	1	2.9	15	8.07	17.45	13.96	11.68	8.83	6.75	4.13	2.20
			2	2.9	15	7.97	17.23	13.83	11.60	8.78	6.75	4.14	2.22
			3	2.9	15	8.00	17.25	13.88	11.65	8.84	6.79	4.17	2.22
			1	2.9	15	10.08	22.19	17.84	15.00	11.35	8.66	5.25	2.84
			2	2.9	15	10.18	22.27	18.01	15.17	11.54	8.80	5.33	2.86
			3	2.9	15	10.16	22.14	17.94	15.11	11.50	8.80	5.33	2.86

Table D-16 Continued

Section	Reinforcement	Location	Drop	HMA Thickness (in.)	Base Thickness (in.)	Load (1000 lb)	Deflection (mils)						
							D1	D2	D3	D4	D5	D6	D7
4	No Geogrid	North	1	2.7	15	8.05	26.80	20.19	16.47	12.25	9.51	5.81	2.96
			2	2.7	15	8.14	26.68	20.23	16.54	12.36	9.55	5.83	2.97
			3	2.7	15	8.07	26.35	20.07	16.43	12.32	9.51	5.82	2.97
			1	2.7	15	9.98	33.61	25.83	21.14	15.75	12.03	7.23	3.82
			2	2.7	15	10.06	33.89	26.17	21.49	16.03	12.24	7.36	3.66
			3	2.7	15	10.08	34.19	26.41	21.67	16.17	12.37	7.42	4.02
	No Geogrid	South	1	2.7	15	7.83	21.43	16.58	13.82	10.47	7.93	4.64	2.39
			2	2.7	15	7.85	21.24	16.52	13.80	10.48	7.93	4.65	2.81
			3	2.7	15	7.92	21.27	16.58	13.86	10.56	8.01	4.67	2.83
			1	2.7	15	9.71	27.12	21.33	17.87	13.60	10.23	6.05	2.94
			2	2.7	15	9.79	27.61	21.83	18.35	13.98	10.53	6.17	3.01
			3	2.7	15	9.79	27.70	22.02	18.50	14.15	10.68	6.61	3.03
5	No Geogrid	North	1	2.9	15	7.70	30.23	23.34	19.32	14.31	10.62	5.91	2.94
			2	2.9	15	7.75	30.19	23.53	19.53	14.50	10.73	5.97	2.94
			3	2.9	15	7.80	30.06	23.49	19.53	14.54	10.78	6.02	2.93
			1	2.9	15	9.64	37.83	30.22	25.16	18.62	13.70	7.50	3.58
			2	2.9	15	9.64	38.53	30.94	25.78	19.10	14.03	7.70	3.65
			3	2.9	15	9.67	38.72	31.28	26.13	19.40	14.28	7.85	3.66
	No Geogrid	South	1	2.9	15	8.07	22.83	18.29	15.44	11.79	8.96	5.24	3.13
			2	2.9	15	8.02	22.54	18.11	15.30	11.74	8.94	5.24	3.19
			3	2.9	15	8.17	22.50	18.17	15.36	11.80	9.01	5.26	3.20
			1	2.9	15	9.71	28.39	23.14	19.56	15.04	11.39	6.53	3.31
			2	2.9	15	9.74	28.86	23.59	19.99	15.44	11.68	6.70	3.35
			3	2.9	15	9.74	29.04	23.77	20.16	15.57	11.75	6.77	3.36
6	No Geogrid	North	1	2.9	15	8.07	23.54	19.05	15.87	11.94	8.97	5.11	2.56
			2	2.9	15	8.02	23.20	18.92	15.81	11.93	8.98	5.13	2.54
			3	2.9	15	8.17	23.40	19.17	16.08	12.14	9.13	5.20	2.66
			1	2.9	15	10.08	29.74	24.49	20.49	15.42	11.50	6.42	3.16
			2	2.9	15	10.11	29.78	24.60	20.65	15.57	11.63	6.51	3.20
			3	2.9	15	10.06	29.61	24.57	20.64	15.60	11.66	6.52	3.18
	No Geogrid	South	1	2.9	15	7.58	22.30	17.18	14.28	10.79	8.27	5.21	2.72
			2	2.9	15	7.63	22.25	17.28	14.41	10.92	8.39	5.26	2.73
			3	2.9	15	7.73	22.32	17.40	14.55	11.09	8.46	5.15	2.78
			1	2.9	15	9.44	27.79	21.96	18.33	13.88	10.49	6.23	3.31
			2	2.9	15	9.54	28.24	22.41	18.76	14.19	10.71	6.38	3.37
			3	2.9	15	9.59	28.39	22.59	18.93	14.35	10.83	6.43	3.39